SERVO CONTROLLED SWASH PLATE AXIAL PISTON PUMPS OPERATING UNDER VARIABLE LOAD DEMANDS WITH APPLICATION TO ROLLING MILLS

Deping Li

A Thesis in the

Department of Mechanical and Industrial Engineering

Presented in Partial Fulfillment of the Requirements

For the Degree of Master of Applied Science (Mechanical Engineering) at

Concordia University

Montreal, Quebec, Canada

October 2003

Your file Votre référence
ISBN: 0-612-83883-8
Our file Notre référence
ISBN: 0-612-83883-8

ABSTRACT

SERVO CONTROLLED SWASH PLATE AXIAL PISTON PUMPS OPERATING UNDER VARIABLE LOAD DEMANDS WITH APPLICATION TO ROLLING MILLS

Deping Li

Rolling mill automation systems started nearly in 1960s when the servo system was introduced to the metal forming industry. During the past decades, hydraulic control systems have found increased applications in rolling mills in an attempt to cope with the harsh environment conditions and the high power demands for metal forming. During the rolling process, both rolling speed and rolling load must be controlled in accordance with the independently varying torque that disturbs the control system.

This project is concerned with the development of an electro-hydraulic control system in order to control both rolling speed and rolling load with minimum number of components. A mathematical model of a pressure compensator is constructed and a simulation program based on Matlab-Simulink is developed to simulate both the static and the dynamic characteristics of the entire control system. The control system has very good flexibilities to various rolling mill requirements, and it is very convenient to adjust due to different variable load demands.

An experimental setup composed of real time control software and a hydraulic test bed is built in order to validate the compensator mathematical model and verify the control system simulation results. The simulation and experimental results are compared and discussed.

ACKNOWLEDGMENTS

This project was carried out in the Fluid Power Control and Simulation Laboratory of Concordia University, Montreal, Canada. It was an excellent opportunity for me to obtain experience in several new areas in my field. I am grateful to all those who have contributed to this thesis:

I would like to express my deepest appreciation to my supervisors, Prof. Rama Bhat and Prof. Jaroslav Svoboda for their continuous guidance, effective support and suggestions during the entire course of this research. Special thanks are due to Dr. Medhat Khalil for his advise, mentorship and guidance in this project. This project is essentially an extension of Dr. Medhat Khalil's doctoral thesis project on swash plate piston variable displacement pump with conical cylinder block. His help in the experiments and useful suggestions are very much appreciated.

I wish to thank Gilles Huard and Robert Oliver for their assistance in building the experimental set up for the project.

I also would like to express my warm love and sincere appreciation to my wife, Lihong Liang, my daughter, Suyue Li, my parents and parents-in-law for their understanding, continued encouragement and support.

TABLE OF CONTENTS

LIST OF FIGURES ix

LIST OF TABLES xvii

LIST OF SYMBOLS xviii

CHAPTER 1 INTRODUCTION AND LITERATURE REVIEW 1

1.1 Classification of Rolling Mills and Description of the Rolling Process 1

1.1.1 Classification of Rolling Mills 1

1.1.2 Description of the Flat Rolling Process 10

1.2 Survey of Previous Work 14

1.3 Thesis Objectives 20

1.4 Scope of Work 22

CHAPTER 2 DESCRIPTION AND MODELING OF PROPOSED ELECTRO-HYDRAULIC CONTROL SYSTEM 24

2.1 Description of the Hydraulic Control System 24

2.2 Modeling of the Variable Displacement Pump 28

2.2.1 Pump Kinematics 28

2.2.2 Piston Chamber Pressure and Flow Rate 34

2.2.3 Moments Acting on the Swash Plate 36

2.2.4 Mathematical Model of the Pump Control Unit 40

2.3 Modeling of the Electro-hydraulic Compensator 44

2.3.1 Analysis of Spool Motion 47

2.3.2 Transfer Function 48

2.3.3 Modeling of Compensator 49

2.4 Description and Modeling of the Electrical Control System 51

CHAPTER 3 SIMULATION AND PERFORMANCE INVESTIGATION OF THE CONTROL SCHEMES 54

3.1 Simulation of the Compensator Performance 54

3.1.1 Simulation of the Spool Motion 54

3.1.2 Simulation of the Compensator Performance 58

3.2 Simulation of the Variable Displacement Pump 71

3.2.1 Proposed Control Schemes 71

3.2.2 Simulation of the Pump Step Response at Constant Load 72

3.2.3 Simulation of the Pump Static Characteristics at Constant Load 82

3.2.4 Simulation of the Pump Frequency Response in Constant Power Operation 83

3.3 Simulation of the Hydraulic Control System 85

3.3.1 Simulation of the Hydraulic Control System to the Step Change in the Rolling Torque 87

3.3.2 Simulation of the Hydraulic Control System Static Characteristics 89

3.3.3 Frequency Response of the Hydraulic Control System 92

CHAPTER 4 MATHEMATICAL MODEL VALIDATION AND EXPERIMENTAL VERIFICATIONS 99

4.1 Description of the Hydraulic Test Bed 99

4.1.1 Hydraulic Test Pump Unit 101

4.1.2 Control Pressure Supply Unit 102

4.1.3 Load Disturbance Unit 103

4.1.4 Oil Conditioning Unit 104

4.2 Description of the Control and Data Acquisition System 105

4.2.1 Real Time Control and Data Acquisition Software 106

4.2.2 Hardware Part of the Control and Data Acquisition System 108

4.3 Test Preparations and Calibrations 110

4.3.1 Integration of the Hydraulic Test Bed 112

4.3.2 Interfacing with the Control and Data Acquisition System 116

4.3.3 Calibrations and Pretests 117

4.4 Testing of the Control System Performance 126

4.4.1 Measurement of the Step Response of the Hydraulic Control System due to the Step Change in the Rolling Torque 126

4.4.2 Measurement of the Static Response of the Hydraulic Control System due to the Ramp Change in the Rolling Torque 131

4.4.3 Measurement of the Frequency Response of the Hydraulic Control System due to the Harmonic Changes in the Rolling Torque 135

CHAPTER 5 CONCLUSIONS AND SUGGESTIONS FOR FUTURE WORK 140

5.1 Conclusions 140

5.2 Main Contributions 143

5.3 Suggestions for Future Work 144

REFERENCES 146

APPENDIX A CONSTRUCTIONAL AND OPERATIONAL PARAMETERS OFTHE TEST PUMP 155

APPENDIX B M-FILE FOR THE SIMULATION OF THE ELECTRO-HYDRAULIC CONTROL SYSTEM 157

LIST OF FIGURES

Figure No.	Name of the Figure	Page
Figure 1.1	Schematic illustration of various roll arrangements: (a) two-high; (b) three-high; (c) four-high;(d) cluster (Sendzimir) mill	3
Figure 1.2	A tandem rolling with 5-stand	4
Figure 1.3	A 48-inch, high-speed, five-stand tandem cold-reduction mill	4
Figure 1.4	A six-stand tandem cold mill for tinplate production	5
Figure 1.5	Schematic outline of various flat- and shape-rolling processes	6
Figure 1.6	Schematic illustration of the flat-rolling process	6
Figure 1.7	Stages in the shape rolling of an H-section part	7
Figure 1.8	(a) Schematic illustration of a ring-rolling operation. Thickness reduction results in an increase in the part diameter. (b) Examples of cross-sections that can be formed by ring rolling	8
Figure 1.9	Thread-rolling processes: (a) and (c) reciprocating flat dies; (b) two roller dies	9
Figure 1.10	Schematic illustration of various tube-rolling processes	9
Figure 1.11	Schematic diagram of a four-high mill stand with the hydraulic adjustment system acting on the upper backup roll	11
Figure 1.12	(a) Schematic illustration of the flat-rolling process. (b) Friction forces acting on strip surfaces. (c) The roll force, F, and the torque acting on the rolls	12

Figure 1.13	Increase in the width (spreading) of a strip in flat rolling	13
Figure 2.1	Symbolic representation of the electro-hydraulic control system	25
Figure 2.2	The connection of swash plate and control piston	26
Figure 2.3	Sectional view and essential dimensions of swash plate axial piston pump with conical cylinder block	28
Figure 2.4	Frames of reference for the piston motion	29
Figure 2.5	Variation of piston displacement, velocity, and acceleration, relative to the piston cylinder, with θ_k for the 40 cc/rev pump running at 1450 rpm	33
Figure 2.6	Piston chamber parameters and variable	34
Figure 2.7	Piston three-dimensional general space motion	36
Figure 2.8	Symbolic representation of the constant power control unit	43
Figure 2.9	Schematic representation of the hydro-mechanical part of the control system shown in Figure 2.8	44
Figure 2.10	The outer shape of the proportional valve	45
Figure 2.11	Symbolic representation of the proportional valve	45
Figure 2.12	Schematic of the pressure compensator (initial state)	46
Figure 2.13	Schematic of the pressure compensator (working state)	47
Figure 2.14	Analysis of the spool motion	48
Figure 2.15	Schematic of the pressure compensator	50
Figure 2.16	Block diagram of the control schemes and simulation subsystems	52
Figure 3.1	The open-loop block of the spool motion	55
Figure 3.2	The open-loop modeling of the spool motion	55

Figure 3.3	The simulation parameters of the spool motion for open loop	56
Figure 3.4	Open-loop step response of the spool motion	56
Figure 3.5	The closed-loop block of the spool motion	57
Figure 3.6	The closed-loop modeling of the spool motion	57
Figure 3.7	Closed-loop step response of the spool motion	57
Figure 3.8	The simulation modeling of the compensator	59
Figure 3.9	Reference command setting and parameters for static performance simulation of compensator	60
Figure 3.10	Simulation parameters for static performance of compensator	61
Figure 3.11	Reference command for static performance simulation of compensator	61
Figure 3.12	The static response of compensator	62
Figure 3.13	Reference command setting for simulation of step response of compensator	63
Figure 3.14	Reference command for step response simulation of compensator	64
Figure 3.15	The step response of compensator	64
Figure 3.16	Step response of compensator when the spool moves from zero position to different percentages of its full stroke	65
Figure 3.17	Step response of compensator when the spool moves from different percentages of its full stroke to zero position	65
Figure 3.18	Reference command setting for the simulation of harmonic response of compensator	66

Figure 3.19(a)	The reference command and the frequency response of compensator (Case 1 Frequency = 1 Hz, Amplitude = 25 %)	67
Figure 3.19(b)	The reference command and the frequency response of compensator (Case 2 Frequency = 10 Hz, Amplitude = 25 %)	68
Figure 3.19(c)	The reference command and the frequency response of compensator (Case 3 Frequency = 20 Hz, Amplitude = 25 %)	69
Figure 3.19(d)	The reference command and the frequency response of compensator (Case 4 Frequency = 30 Hz, Amplitude = 25 %)	70
Figure 3.20	Pump controlling using double feedback loops and PID controller	72
Figure 3.21	Pump controlling using single feedback loop and PD controller	73
Figure 3.22	Pump step response at constant load pressure using double feedback control loops with PID controller	75
Figure 3.23	Variation of swiveling angle with time using double feedback control loops with PID controller	76
Figure 3.24	Variation of swiveling angle with time using double feedback control loops with PID controller	77
Figure 3.25	Pump step response at constant load pressure using single feedback control loop with PD controller	79
Figure 3.26	Variation of swiveling angle with time using single feedback control loop with PD controller	80
Figure 3.27	Variation of swiveling angle with time using single feedback control loop with PD controller	81

Figure 3.28	Pump static characteristics at constant load pressure using double feedback control loops with PID controller	82
Figure 3.29	Pump static characteristics at constant load pressure using single feedback control loop with PD controller	83
Figure 3.30	Pump constant power operation using double feedback control loops with PID controller	84
Figure 3.31	The modeling of entire electro-hydraulic control system	86
Figure 3.32	Simulation parameters for the hydraulic control system	86
Figure 3.33	Reference command setting for simulation of the hydraulic control system to the step change in the rolling torque	87
Figure 3.34	The reference command – rolling torque (step signal)	88
Figure 3.35	The step response of the hydraulic control system	89
Figure 3.36	Reference command setting and parameters for static performance simulation of the hydraulic control system to the gradual change in the rolling torque	90
Figure 3.37	The reference command – rolling torque (ramp signal)	91
Figure 3.38	The static response of the hydraulic control system	91
Figure 3.39	Reference command setting and parameters for frequency response of the hydraulic control system	93
Figure 3.40	The reference command – 0.1 Hz sinusoidal rolling torque	94
Figure 3.41	The frequency response of the hydraulic control system (0.1 Hz)	94
Figure 3.42	The reference command – 0.5 Hz sinusoidal rolling torque	95
Figure 3.43	The frequency response of the hydraulic control system (0.5 Hz)	95

Figure 3.44	The reference command – 1 Hz sinusoidal rolling torque	96
Figure 3.45	The frequency response of the hydraulic control system (1 Hz)	96
Figure 3.46	The reference command – 2 Hz sinusoidal rolling torque	97
Figure 3.47	The frequency response of the hydraulic control system (2 Hz)	97
Figure 3.48	The reference command – 3 Hz sinusoidal rolling torque	98
Figure 3.49	The frequency response of the hydraulic control system (3 Hz)	98
Figure 4.1	Hydraulic test bed	100
Figure 4.2	Outer shape of the test pump	101
Figure 4.3	The test pump connection configuration with the original amplifier card (A)	107
Figure 4.4	Block diagram of control and data acquisition system	109
Figure 4.5	Block diagram of the integrated experimental setup	111
Figure 4.6	Schematic layout of the integrated experimental setup	113
Figure 4.7	Photographic view of the experimental setup. (a) A view of the pump loading unit and real time controller interface; (b) A view of the pump with the integrated control unit and set	114
Figure 4.8	Conditioning of the pressure compensator spool displacement in an open loop	118
Figure 4.9	Connection scheme of real time control	119
Figure 4.10	Measurement of open loop static characteristics of the compensator	120

Figure 4.11	Conditioning of the pressure compensator spool displacement in a closed loop	121
Figure 4.12	Measurement of closed loop static characteristics of the compensator	122
Figure 4.13	Measurement of the step response of the compensator	123
Figure 4.14	Measurement of the step response of the compensator moving from zero position to a different percentage of its full stroke	124
Figure 4.15	Measurement of the step response of the compensator moving from different percentage of its full stroke to zero position	124
Figure 4.16	A real time control software module for testing the characteristics of the hydraulic control system	125
Figure 4.17	Measured rolling torque step response as compared with the simulation result	127
Figure 4.18	Measured rolling force step response as compared with the simulation result	128
Figure 4.19	Measured rolling speed step response as compared with the simulation result	129
Figure 4.20	Measured displacement of spool step response as compared with the simulation result	130
Figure 4.21	Measured rolling torque static response as compared with the simulation result	131

Figure 4.22	Measured rolling force static response as compared with the simulation result	132
Figure 4.23	Measured rolling speed static response as compared with the simulation result	133
Figure 4.24	Measured displacement of spool static response as compared with the simulation result	134
Figure 4.25	Measured frequency response as compared with the simulation result (0.1 Hz)	135
Figure 4.26	Measured frequency response as compared with the simulation result (0.5 Hz)	136
Figure 4.27	Measured frequency response as compared with the simulation result (1 Hz)	137
Figure 4.28	Measured frequency response as compared with the simulation result (2 Hz)	138
Figure 4.29	Measured frequency response as compared with the simulation result (3 Hz)	139

LIST OF TABLES

Table No.	Name of the Table	Page
Table 2.1	The main technical data of 4WRE10EA75-2X/G24K4/V	45
Table 3.1	Parameters for step inputs	62
Table 3.2	Parameters for step inputs	88

LIST OF SYMBOLS

Symbol	Description	Units
$A_d(A_s)$	Area of the openings that connect the piston chamber to the delivery (suction) port on the port plate	m^2
A_{cp}	Area of the control piston	m^2
A_f	Compensator area coefficient	-
A_p	Piston cross-section area	m^2
$[a_{ck}]_0$	k^{th} piston absolute acceleration	m/s^2
B	Effective bulk modulus	Pa
C_d	Coefficient of discharge	-
D_1/R_1	Pitch circle diameter/radius of the cylinder arrangement at the base of the cylinder block	m
D_2/R_2	Pitch circle diameter/radius of the cylinder arrangement at the top of the cylinder block	m
D_3	Pitch circle diameter of the port plate	m
d_p	Piston diameter	m
F_{dt}	Piston detaching force	N
F_r	Rolling force	%
$F_{xk, yk, zk}$	Components of the resultant force acting on the swash plate duo to the k^{th} piston	N
f	Compensator viscous friction coefficient	Ns/m
f_v	Proportional valve viscous friction coefficient	Ns/m
f_α	Equivalent angular viscous friction coefficient of the swash plate	Ns/m
I_e	Equivalent moment of inertia of the swash plate	$kg.m^2$

I_s	Current applying on the solenoid of proportional valve	A
I_x	Current applying on the solenoid of compensator	A
i_n	Half the maximum current given to the proportional valve solenoid	A
k	Piston number in the piston group arrangement	-
k_i	Proportional solenoid force-current constant	N/A
k_s	Compensator spring stiffness	N/m
k_v	Proportional valve spring stiffness	N/m
k_α	Equivalent torsional spring stiffness of the swash plate	Nm/rad
L_1/L_2	Lengths, referred in Figure 2.3	m
L_{3k}	Variable length	m
L_c	Cylinder length	m
L_p	Piston length	m
$[M_k]_0$	Moment acting on the swash plate in vector form	Nm
M_b	Moment acting on the swash plate bearing system	Nm
$M_{x, y, z}$	Components of the moment acting on the swash plate	Nm
M_{y0}	Average value of the moment acting on the swash plate	Nm
m	Compensator spool mass	kg
m_p	Piston mass	kg
m_v	Proportional valve spool mass	kg
N	Number of pistons	-
N	Pump speed	rpm
nof	Number of frequencies	-
nop	Number of points	-
p_c	Pressure difference across the control piston	Pa

$p_{c1,2}$	Pressure at the two sides of the control piston	Pa
P_D	Compensator downstream pressure	Pa
p_d	Pump delivery pressure	Pa
p_k	Piston chamber pressure	Pa
P_{max}	Static characteristic maximum pressure	Pa
P_S	Pump suction pressure	Pa
p_T	Tank line pressure	Pa
P_U	Compensator upstream pressure	Pa
p_v	Control pressure	Pa
P	Value of the controlled constant power	kW
Q	Pump instantaneous delivery flow rate	m^3/s
$Q_{a,b,c,d}$	Flow rate through proportional valve ports	m^3/s
Q_d	Delivery flow rate of one cylinder	m^3/s
Q_{max}	Static characteristic maximum flow rate	m^3/s
Q_{LK}	The total instantaneous leakage flow rate of piston chamber	m^3/s
Q_{RV}	Flow rate through relief valve	m^3/s
Q_{sk}	The flow rate drawn into one piston chamber from pump	m^3/s
Q_S	Flow rate of pump	m^3/s
R_L	Leakage resistance across piston	$Pa/(m^3/s)$
R_s	Radius of swash plate swing	m
r_{ck}	Radius of the trace of the piston center of gravity relative to the Z_0 axial	m
$[r_{ck}]_{0/5/6}$	Position vector indicates to the k^{th} piston center of mass	-

	relative to inertial/5^{th} /6^{th} frame of reference	
$[r_{5k}]_0$	Position vector indicates to the k^{th} piston spherical head center relative to inertial frame of reference	-
s_k, s_v	The k^{th} piston, valve spool displacement	m
$\dot{s}_k, \dot{x}_{cp}, \dot{s}_v$	Velocity of the k^{th} piston, control piston, valve spool	m/s
$\ddot{s}_k, \ddot{s}_v$	Acceleration of the k^{th} piston, valve spool	m/s^2
s_{sp}, (s_e)	Set point of the spool displacement (error value)	m
s_{vmax}	Maximum proportional valve spool displacement	m
T_r	Rolling torque	%
t	Time	s
V	Control volume of compensator	m^3
$V_{c1,2}$	Control volume on the two sides of the control piston	m^3
V_{ci}	Initial control volume	m^3
V_{ck}	Instantaneous cylinder volume of the k^{th} piston	m^3
V_0	Piston chamber clearance volume	m^3
V_r	Rolling speed	%
$v(\dot{X})$	Compensator spool velocity	m/s
w	Proportional valve port width	m
X	Displacement of compensator spool	m
X_0	Compensator displacement overlap	m
$\ddot{X}$	Acceleration of compensator spool	m^2/s
$x_{cp(min, max)}$	Control piston displacement (minimum, maximum)	m
x_{5k}, y_{5k}, z_{5k}	Cartesian coordinate of piston spherical head center relative to the inertial frame of reference	m
$\dot{\alpha}$	Swash plate angular velocity	s^{-1}

α, (α_{sp}), (α_e)	Swash plate angle of inclination, (set point), (error value)	rad
β	Cylinder block cone angle	rad
θ_k	Angular position of the k^{th} piston	rad
ρ	Oil density	kg/ m^3
ϕ	Silencing groove angle	rad
ω / $\dot{\omega}$	Pump angular speed/ acceleration	s^{-1}/ s^{-2}
ω_n	Natural frequency	rad/s
ζ	Damping ratio	-

CHAPTER 1

INTRODUCTION AND LITERATURE REVIEW

In this chapter, a classification of rolling mills and description of the rolling process will be presented to start with, and then a survey of previous work dealing with rolling mill automation systems in general and microprocessor controlled variable geometric volume swash plate pumps to meet the variable load demands, in particular, is presented. Finally, the thesis objectives are formulated and the scope of work is articulated.

1.1 Classification of Rolling Mills and Description of the Rolling Process

1.1.1 Classification of Rolling Mills

The rolling is a widely used primary metal working process accounting for about 90% of all steel, copper and aluminum produced annually in the world. The rolling process plays an important role because of its versatility, efficiency and its high production rate in the manufacture of various products with uniform cross-sectional area. The latter part of the 20^{th} century saw a dramatic advancement in rolling technology. Significant achievements were seen in the improvement of product quality through development of tandem mills and rolling of strip in coil form. Before describing the rolling process, a classification of rolling mills is given in the following. The types of rolling mills can be categorized in different ways.

Based on the temperature of the metal to be processed, rolling mills are classified into cold rolling mills and hot rolling mills. For cold rolling mills, the temperature should be maintained at less than 350°F to avoid creating an oxide film on metal's surface while for hot rolling mills, the optimum temperature depends upon the metal composition. Preferred temperatures for high-carbon steels reheated in oxidizing atmosphere are usually in the range of 1950°F to 2050°F; for medium-carbon steels, the range is from 2000°F to 2100°F while low-carbon steels that contain no alloying elements may be heated to 2350°F.

Based on the number of stands, rolling mills are categorized into single stand and multi-stand.

Single stand mills are usually classified on the basis of their roll arrangements, such as, two-high, three-high, four-high and cluster mill, as shown in Figure 1.1.

Tandem mills, as shown in Figure 1.2, in which the metal is rolled in successive stands, are similar in arrangement, regardless of the number of the stands. The stands are placed as close together as possible and the center line spacing of stands, which depends upon such factors as the physical size and arrangement of the mill drives, is generally in the range of 12-16 feet (3.66-4.88 meters). For the large volume production of sheet and strip products, tandem mills are now generally employed for primary and second cold reduction as well as for temper rolling. A high-speed, 5-stand tandem cold mill and a six-stand tandem cold mill are shown in Figure 1.3 and 1.4, respectively. Tandem mills can be categorized into tandem sheet and tandem tinplate mills according to the size and the thickness of the metals.

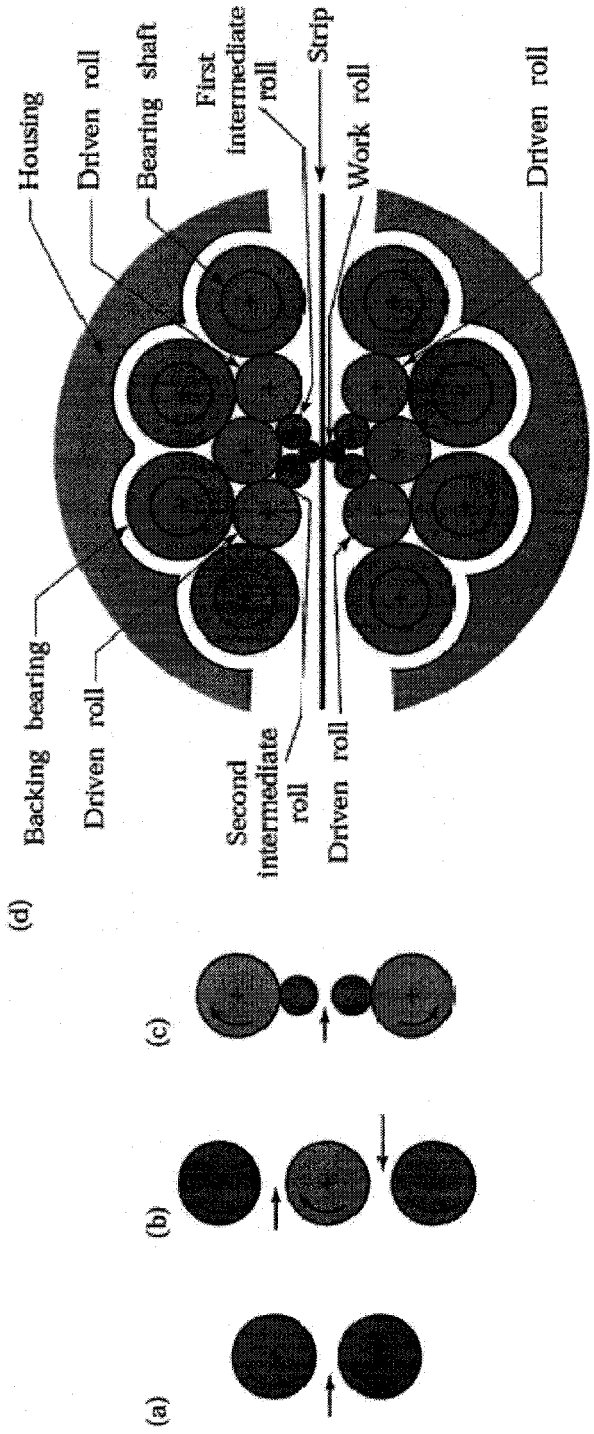

Figure 1.1 Schematic illustration of various roll arrangements: (a) two-high; (b) three-high; (c) four-high;(d) cluster (Sendzimir) mill [1]

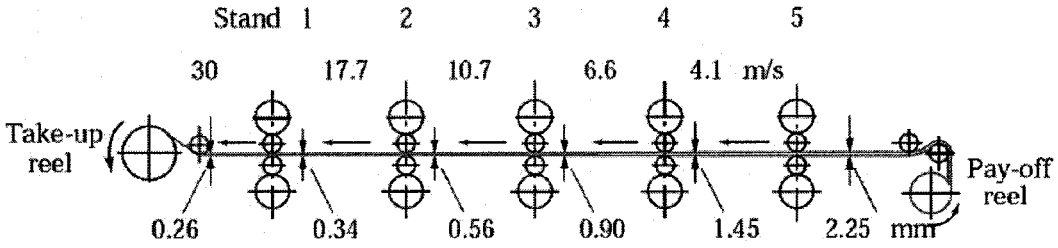

Figure 1.2 A tandem rolling with 5-stand [1]

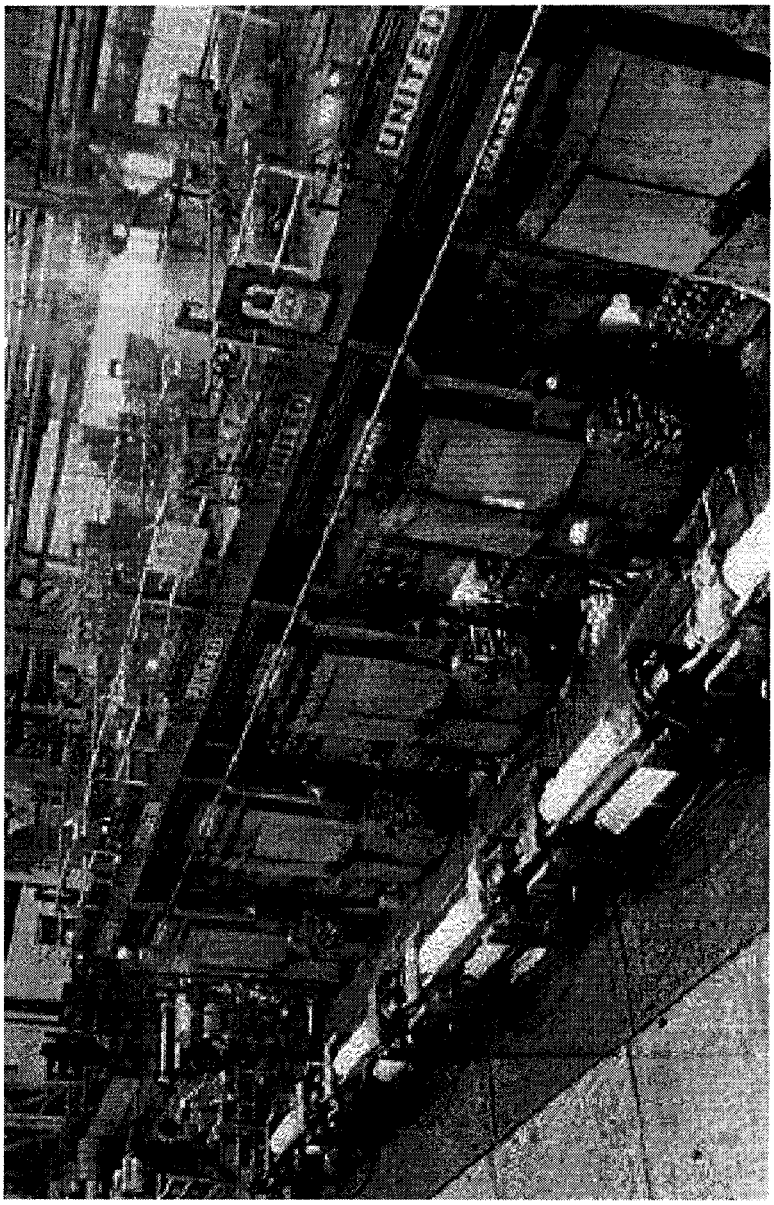

Figure 1.3 A 48-inch, high-speed, five-stand tandem cold-reduction mill [2]

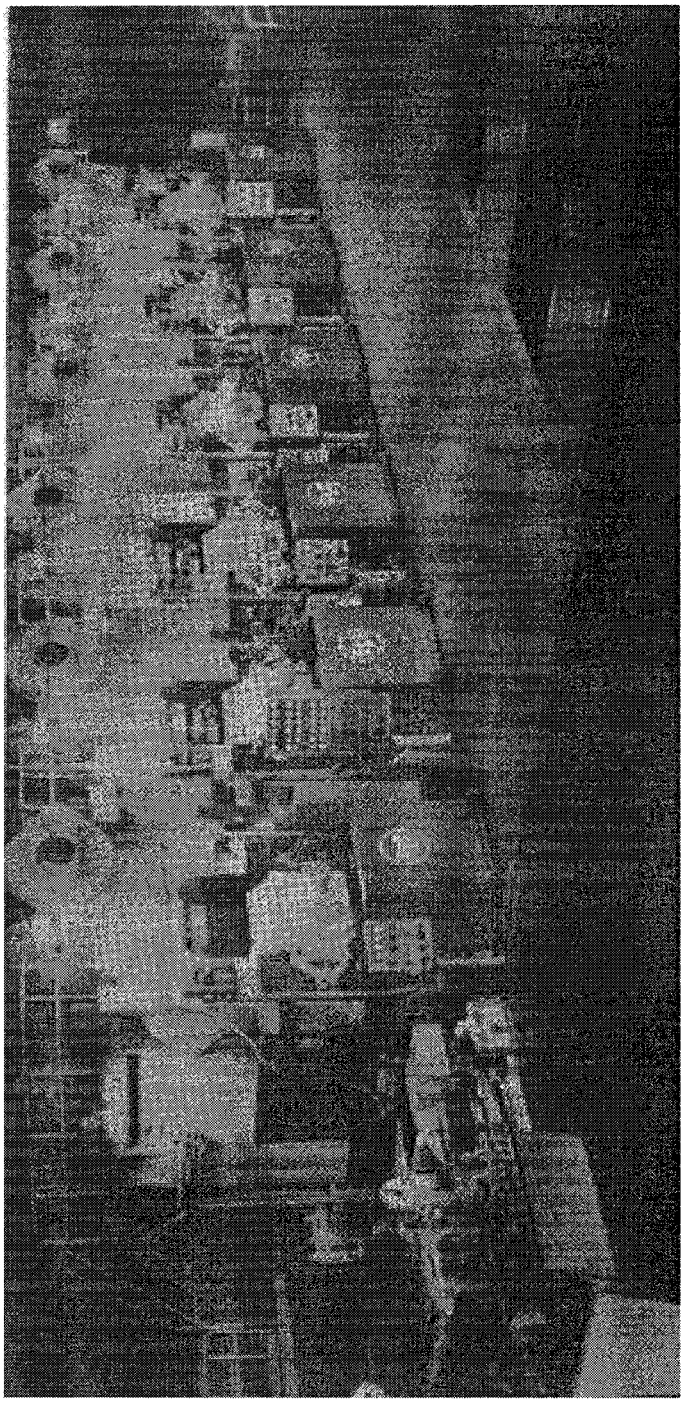

Figure 1.4 A six-stand tandem cold mill for tinplate production [2]

Rolling mills are usually identified by their functions, for example, flat rolling and shape rolling, as shown in Figure 1.5. Flat rolling, as shown in Figure 1.6, is the

process through which the incoming slab can be rolled to thin plate. Metals with various structural sections, such as channels, H-section and I-beams etc, can be rolled by shape rolling process, as shown in Figure 1.7.

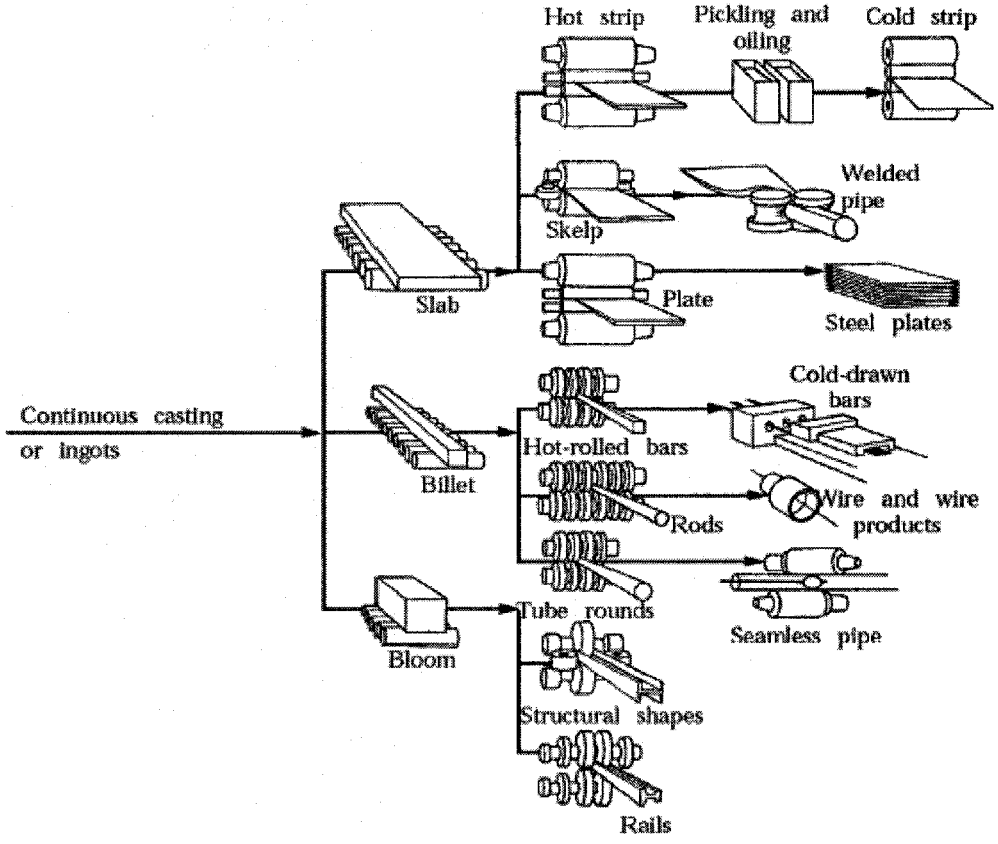

Figure 1.5 Schematic outline of various flat- and shape-rolling processes [1]

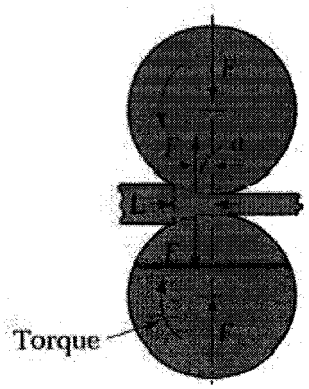

Figure 1.6 Schematic illustration of the flat-rolling process [1]

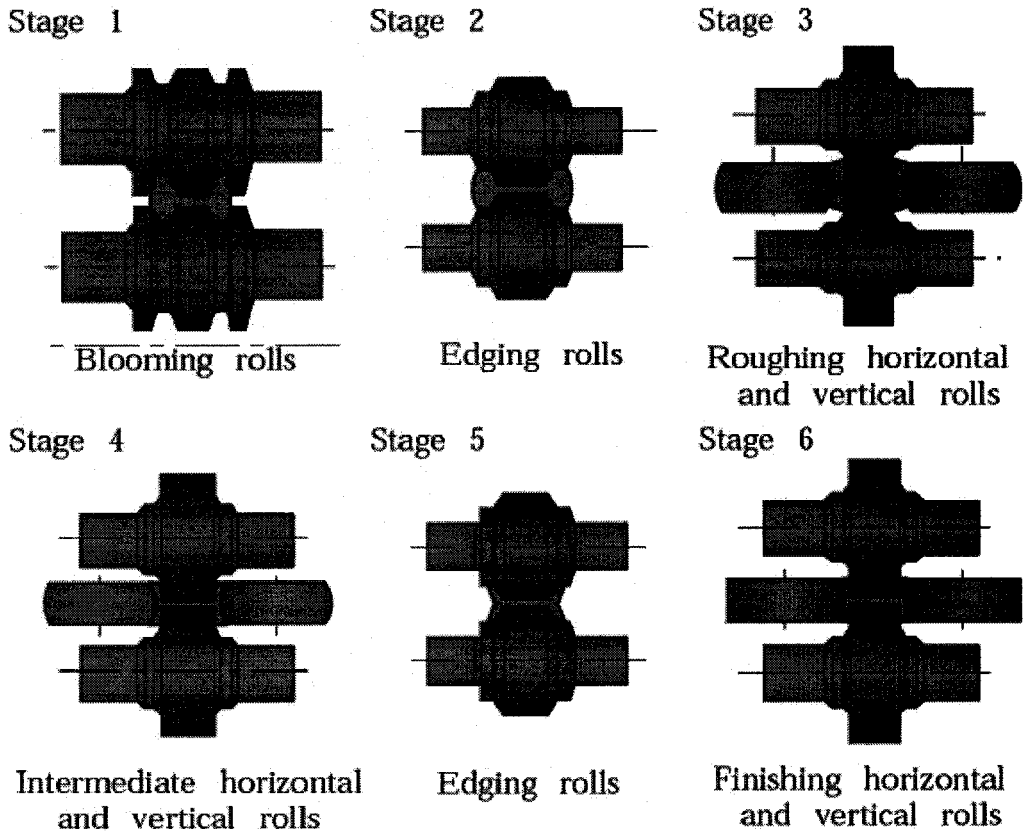

Figure1.7 Stages in the shape rolling of an H-section part [1]

Ring rolling is another rolling process, through which the metal can be rolled into ring, as shown in Figure 1.8. Threads can be made through the thread rolling process, as shown in Figure 1.9. Threaded fasteners, such as bolts, are made economically by these processes, at high rates of production. Through tube rolling technology, metal tube can be made also, as shown in Figure 1.10.

There are some other types of rolling mills, such as, temper or skin-pass mills, foil mills etc, but they have similar structures.

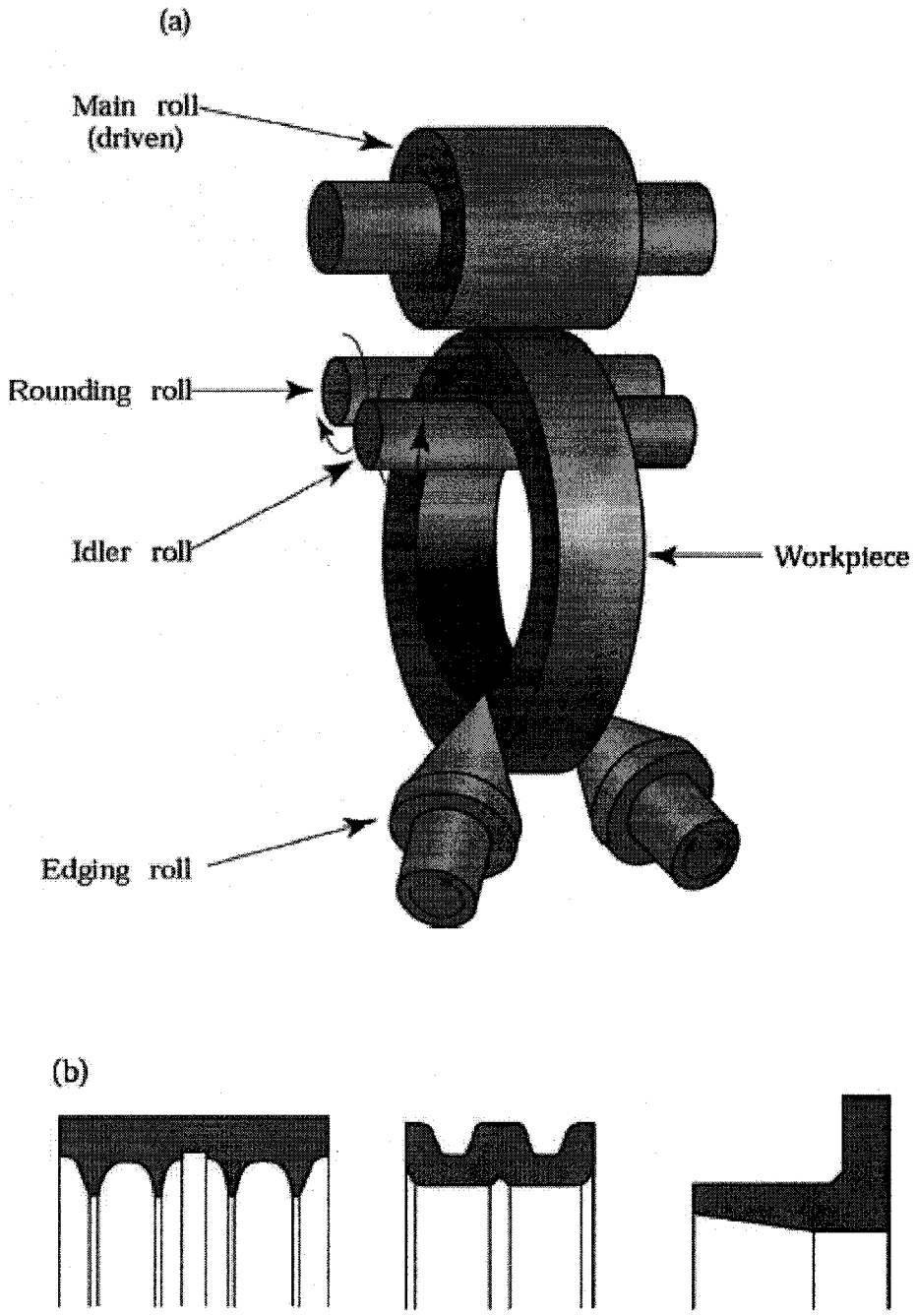

Figure 1.8 (a) Schematic illustration of a ring-rolling operation. Thickness reduction results in an increase in the part diameter. (b) Examples of cross-sections that can be formed by ring rolling [1]

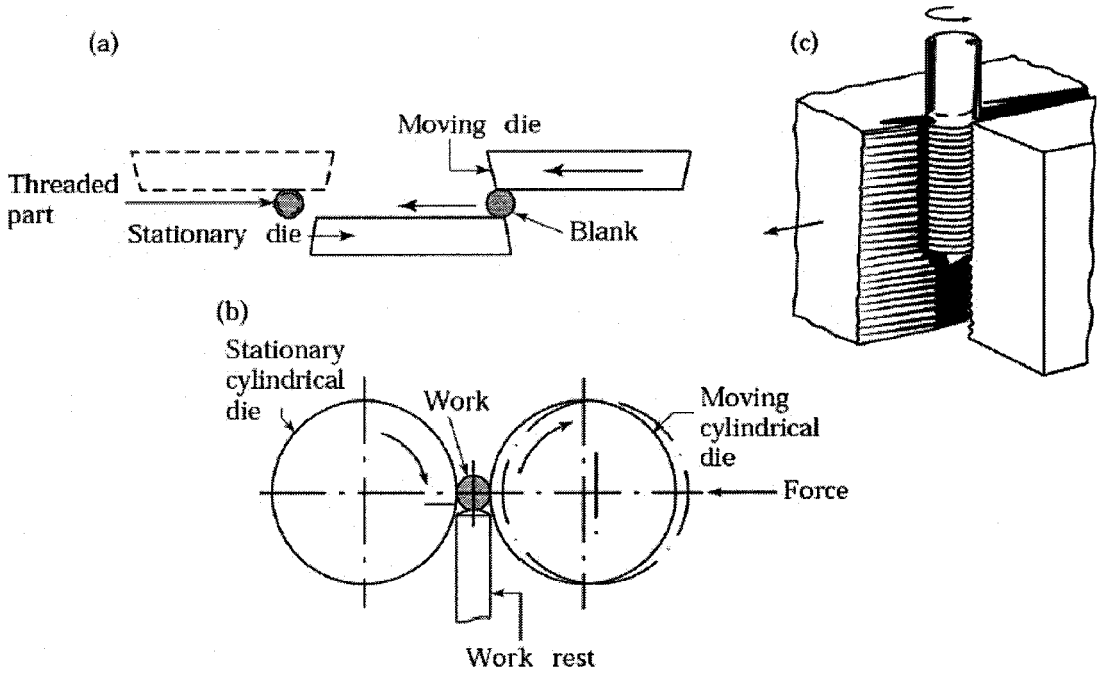

Figure 1.9 Thread-rolling processes: (a) and (c) reciprocating flat dies;

(b) two roller Dies [1]

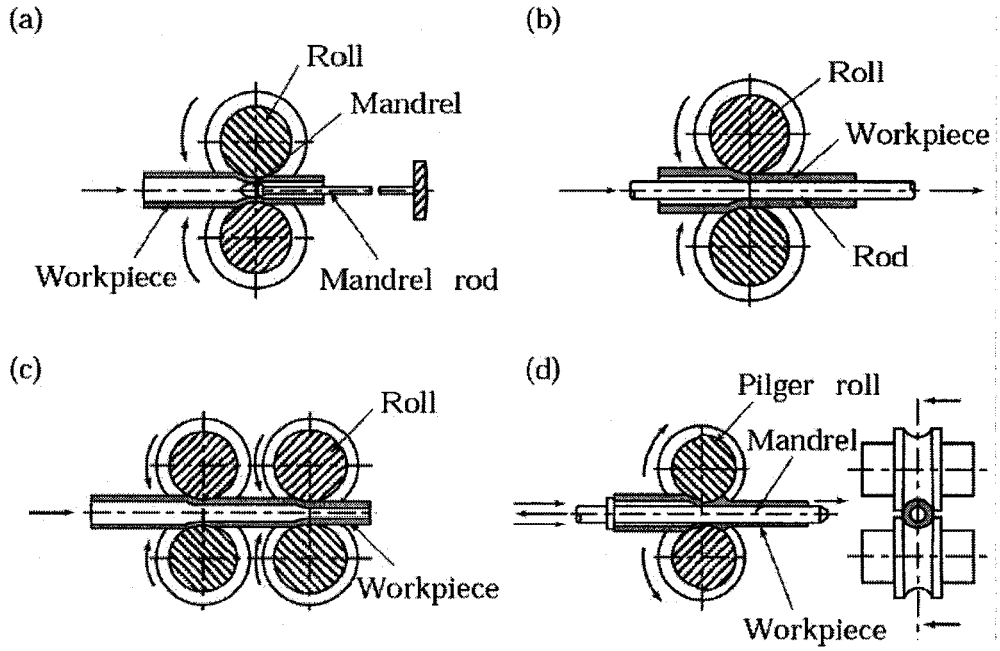

Figure 1.10 Schematic illustration of various tube-rolling processes [1]

1.1.2 Description of the Flat Rolling Process

There are many kinds of rolling mills depending on the various requirements, and hence it is impossible to describe all these rolling processes. This thesis focuses on the pressure compensation and electro-hydraulic control, applied to the flat rolling process. In the following the flat rolling process is described briefly.

The primary objective of the flat rolling process, as shown in Figure 1.6, is to reduce the cross-section of the incoming material while improving its properties resulting in the desired section at the exit from the rolls. The process can be carried out under hot, warm, or cold conditions, depending on the application and the material involved. The rolled products are flat plates and sheets. Rolling of blooms, slabs, billets, and plates is usually done at temperatures above the recrystallization temperature (hot rolling). Sheets and strips often are rolled cold in order to maintain close thickness tolerances.

For simplicity, a single-stand four-high rolling mill is considered. As shown in Figure 1.11, this flat rolling consists of the following components: (1) hydraulic cylinder; (2) mill housing; (3) upper back-up roll; (4) upper work roll; (5) lower work roll; (6) lower backup roll; (7) screw down drive; (8) load cell.

The mill housing (2) is employed to position and ensure the correct alignment of the rolls. Work rolls (4 and 5) are engaged to squeeze metals while the backup rolls (3 and 6) are intended to provide the rigid support required by the

the work rolls to prevent their flexure or bending under the rolling load. To control the relative positions of the rolls and the rolling forces that they exert on the workpiece during the rolling process, a rolling positioning system must be employed on the mill stand. Therefore, a hydraulic cylinder (1) and a screw drive (7) are employed. In order to detect the rolling force and feedback this signal to the control system, a load sensor (8) is used.

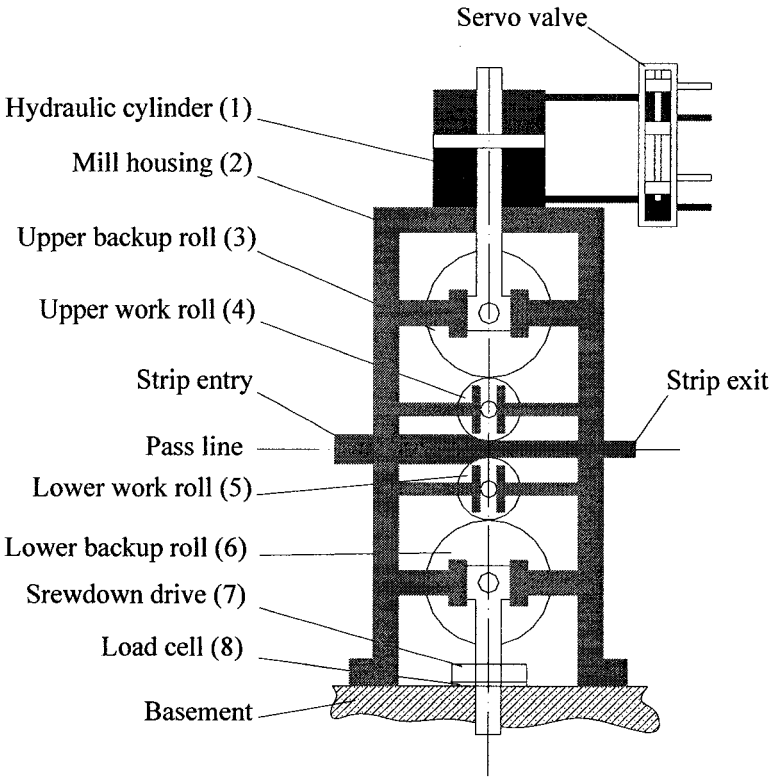

Figure 1.11 Schematic diagram of a four-high mill stand with the hydraulic adjustment system acting on the upper backup roll [3]

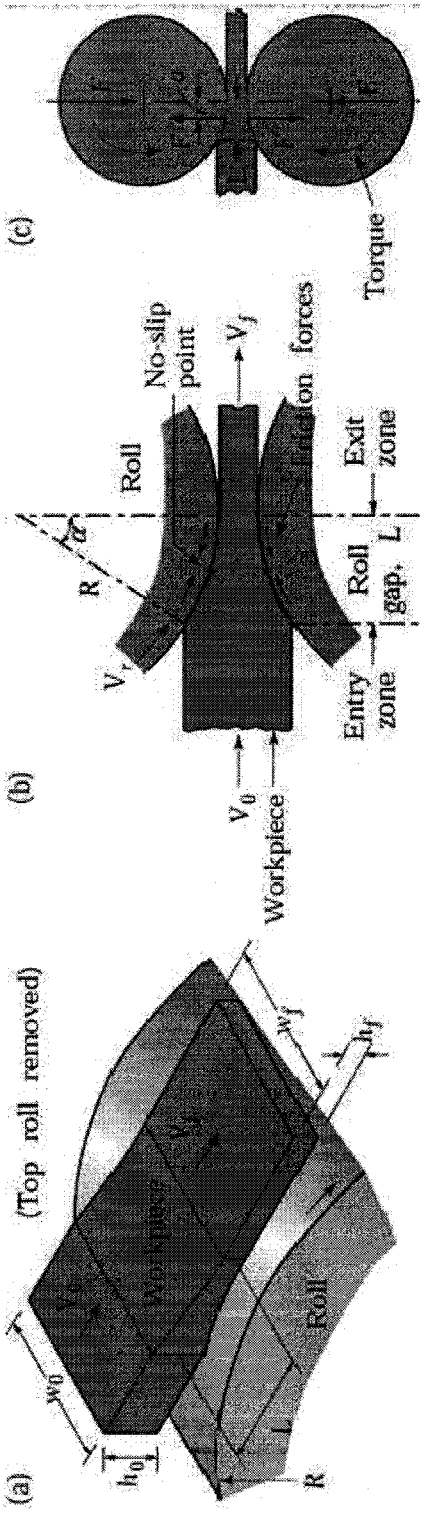

Figure 1.12 (a) Schematic illustration of the flat-rolling process. (b) Friction forces acting on strip surfaces. (c) The roll force, F, and the torque acting on the rolls [1]

As shown in Figure 1.12, the metal is fed forward to the rolling mill by delivery mechanism. Meanwhile, the two work rolls revolve in opposite directions driven by two motors, and the space between the rolls is less than the thickness of the entering metal. Because the work rolls rotate with a surface velocity exceeding the speed of the incoming metal, friction along the contact interface acts to propel the metal forward. The metal is then squeezed and elongated and usually changed in cross section, as shown in Figure 1.13. The thickness of the rolled metal is measured by the measurement device and sent to the AGC (Automatic Gauge Control) system. The AGC system can adjust the positioning system automatically according to the feedback signals, and the ultimate objective is to get the desired size flat. The quality of the rolled sheet, such as thickness, profile and shape, is determined by many factors, such as the rolling force, rolling speed, elastic deformation of mill housing, thermal expansion and wear of the work rolls, etc.

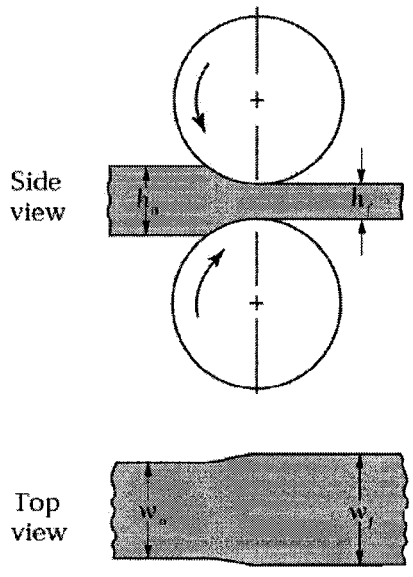

Figure 1.13 Increase in the width (spreading) of a strip in flat rolling [1]

From the above description it is clear that in order to reduce the thickness of a strip and get a desired value, the roll gap must be adjusted by an AGC system, a roll force must be applied to the strip while moving through the roll gap and the surface velocity must be kept at a constant value. Hence, the thickness of the rolled flat is controlled by the roll gap, the rolling speed and the rolling force. The rolling force is the dominant control factor when rolling hot strip and thick cold strip, whereas on thin strip and foil the tension and speed are dominant.

1.2 Survey of Previous Work

Rolling mill automation systems started in early 1960s when the servo system was introduced to the metal forming industry. With the rapid development of the measurement devices, computer technologies, modeling and simulation techniques, rolling mill automation has made significant progress in recent years. During the last decades, lot of studies on rolling process control have been carried out by the researchers and engineers. Some of them focused on the mathematical models, and some concentrated on the AGC system with hydraulic actuators for rolling mills; in addition, some of them emphasized on nonlinear control, etc. In the following survey, the relevant research studies are presented on the various stages of its development. Based on the previous work, the motivation for the present study and the thesis objectives will be presented.

F. W. Paul [4] described the development of a new mathematical model useful for evaluating the dynamics of four rolling stands when controlled with hydraulic drives. He also suggested a new control approach using roll gap rather than roll force

control. Qualitative comparisons of this study showed that the model predicted and described the fundamental model behavior of a roll mill stand when compared with the limited experimental data found in the literature at that time. The simulation results also revealed that cold rolling mills with hydraulic drives and inner loop gap control can have position response times of 50 to 200 milliseconds.

In order to describe the process dynamics and estimate the thickness of the strip, L. M. Pedersen [5] identified and derived two multivariable models for hot rolling mill. In this study, the basic model structures were derived using physical relations for the process and the input signals for the models were measured during normal operation. The study indicated that it was possible to estimate the low frequency behavior of the process using the static model and the physical model structure was reasonable.

An attempt was made by N. V. Reddy et al. [6] to develop a set-up model for tandem cold rolling mill in order to maximize the throughput. The results of this study indicated that the power consumed is minimum for the reduction schedule obtained by distributing the strip thickness in arithmetic, geometric, harmonic and quadratic series.

V. B. Ginzbury [7] applied Laplace transforms and control systems theory and developed a computer model to simulate the dynamic characteristics of the AGC (automatic gage control) system with hydraulic actuators for rolling mills. This study showed that the stability and accuracy of the AGC system can be evaluated as a function of engineering parameters, such as the material stiffness, hydraulic stiffness,

roll structural stiffness and roll separating force, etc. In addition, an algorithm was developed to provide adaptive optimization of the system during rolling.

In order to investigate the nonlinear effects of the hydraulic system and to compare the performance of various cylinder designs using both a position and pressure mode, R. M. Guo [8] also constructed a mathematical model and simulated the dynamic characteristics of the HAGC (Hydraulic Automatic Gage Control) system. In this research, six major dynamic components considered that form of a complete hydraulic system and ordinary differential equations were first derived to explain the physics of each hydraulic component; then characteristics of each component were discussed. The result of this study showed that the nonlinear effects of valve saturation and uneven pressure drop can be negated by using two servovalves and an additional gain amplifier for the damping process, and the return line did not provide the necessary damping effect, particularly for a long-stroke cylinder. The study also revealed that for a low-speed mill (less than 2 Hz), there were no significant differences between long or short-stroke, single or double-acting cylinders.

The design and implementation of a hot-strip steel mill thickness control system was discussed by I. J. Ferguson and R. F. De Tina in [9]. In this study, a thickness control system of world-class performance was developed by using structured design techniques and well-tuned control loops. The study showed that a high-level software design approach provided the ability to make quick and accurate modifications to both control loops and tuning constants. Moreover, the use of hydraulic cylinders to adjust the roll gap instead of electromechanical screws was available.

The deviation of thickness in hot-strip mill is mainly caused by skid marks and roll eccentricity. H. Katori et al. [10] developed an AGC system to remove or reduce the influence of such disturbances. This study indicated that the Automatic Gauge Control System with Two-degree-Freedom, not only rejected disturbances caused by skid marks but also reduced those by roll eccentricity.

S. G. Choi et al. [11] described the problem of Back-Up-Roll eccentricity variation in cold rolling steel mills and developed a new polynomial LQG controller to solve the problem. In this study, the authors initially introduced the gaugemeter principle, analyzed the characteristics of strip, roll-force and their interpretation and then constructed system and disturbance models. Finally, a new polynomial LQG controller was designed and simulation was carried out. The simulation results demonstrated the design flexibility and the robustness of the inferential controller.

A thickness controller for a hot rolling mill, which is a multivariable nonlinear process with time varying parameters, was designed by L. Malcolm et al. [12]. In order to improve the control of the cross-width thickness profile of the plates, a controller that makes independent thickness control possible at two sides of the rolling mill must be designed. Consequently, the authors divided the model for the rolling mill into a nonlinear model for the hydraulic systems and a linear multivariable model for the rolling stand in the study. For the hydraulic system, it was first linearized using feedback linearization and then eigenspace design was performed on the linear model. Moreover, integral control was included to ensure zero stationary error. Furthermore, the stability of the system was investigated using small gain theorem in order to ensure the stability of the design. The result of the simulation indicated that the new

controller not only yielded a more accurate control but also could handle asymmetric hardness conditions of the plates.

The design of LQG (Linear Quadratic Gaussian) multivariable controller for system with input and output transport delays was presented and an application to rolling mills was considered by M. J. Grimble and G. Hearns [13]. In this work, they designed LQG stochastic optimal tracking and regulating systems for continuous-time systems with different time delays in different paths and then applied this LQG system to the control of the thickness of strip in rolling mills. The study showed that the LQG solution provided an optimal regulating solution and a well defined structure that was easy to understand and motivate physically. Moreover, tuning the LQG controller was as straightforward as tuning a PID solution and hence the results provided a very practical thickness control option.

S. S. Garimella et al. [14] presented learning control structures for coil- to-coil gauge and tension control at a single stand cold rolling mill to help compensate for disturbance caused by the variation of roll bite friction during accelerating and decelerating the head end of the coil through the gap between work rolls. Mill acceleration simulation result indicated that this method could significantly reduce the mentioned disturbance.

A. Kugi et al. [15] presented a new strategy for the active compensation of the roll-eccentricity-induced periodic disturbances in the strip exit thickness of hot and cold rolling mills. In this study, on the basis of modern control theory, such as input-output exact linearization, the factorization approach, the projection theorem, etc.,

they developed a control concept. The key point of the control concept was that they took advantage of the special kind of eccentricity-induced disturbance, and then the solution of the eccentricity compensation was obtained by means of the projection theorem. The simulation results for a cold rolling mill and measurement results for a hot strip mill demonstrated the feasibility and the excellent performance of the design. Moreover, a big advantage of this compensation was that it could operate with the conventional control circuit for AGC systems without additional effort.

A new perspective for designing controllers in rolling mills was presented by A. Kugi et al. [16] in 2001. In this study, they applied the modern nonlinear control techniques to the thickness control in rolling mills. This study showed that the nonlinear controller had the ability to cope with the essential nonlinearities of the systems.

The control systems with variable load demands have been utilized in various industrial fields, not only in rolling mills but also in earth moving equipment, printing press and aerospace machinery, etc.

D. F. Zhang et al [17] investigated a four-roll reversal medium plate rolling mill under a condition of frequently changed loading. In order to ensure the operation safety of rolling device and improve the production technology, they analyzed the relationship between the rolling forces on both stands, the stress around the corner of stand and the pressure inside the cylinder of the hydraulic system. Their study showed that these three parameters possess good linear relation and conformity of performance condition.

The performance of an open-circuit hydraulic system of heavy earth moving equipment consisting of a pressure compensated variable displacement swash plate controlled axial piston pump has been analyzed by K. Dasgupta et al [18]. The effects of some critical parameters on the overall performance of the system have been studied also in their research.

High pressure and high power are the main development trends of aircraft hydraulic systems. Based on the traditional constant pressure variable flow pump system, the high pressure and high power of the system will lead to an increase of noneffective power, and its temperature will increase rapidly. This is a very difficult problem on the development of future aircraft hydraulic systems. High pressure, variable flow and variable pressure intelligent pump system is the best solution to this problem. B. Zhang et al [19] proposed a general scheme of a high pressure, variable flow and variable pressure aircraft intelligent hydraulic pump system. It is controlled by a microcomputer, and has four working modes including flow, pressure, power and integration.

1.3 Thesis Objectives

Microprocessor-controlled variable geometric volume swash plate pumps and electro-magnetic proportional directional valves with electrical position feedback have been employed in rolling mill automation systems. Based on the previous literature overview, the objectives of this thesis are formulated as follows:

The first objective of this thesis is to build the simulation model for the pressure compensator, through which the static and dynamic performance of compensator can be investigated.

The second objective is to build the simulation model for the electro-hydraulic control system. The electro-hydraulic system is composed of a servo-actuated variable displacement pump to supply the required controlled flow while an electro-hydraulic pressure compensator is used in order to control the supply pressure of the variable displacement pump in accordance with the independently varying rolling driving torque.

The third objective is to simulate the electro-hydraulic control system and to investigate the performance. The different responses of the system can be obtained by feeding corresponding reference commands, such as step signal, ramp signal and harmonic signal. The variations of rolling speed, rolling force and displacement of the compensator can be observed from the simulation results.

The last objective is to validate the mathematical models and to verify the simulation results through the experiments. Experimental setup consists of a hydraulic test bed interfaced with real time control software. The analytical results are compared with the experimental results in order to validate the hydraulic control system model. Moreover, it is impossible to verify the simulation of the electro-hydraulic control system in an actual rolling mill, and hence it is a good way to verify it through experiments.

1.4 Scope of Work

The first chapter of this thesis describes the classification of rolling mills and the rolling process, and then presents survey of previous work. At the end, it proposes the thesis objectives and the scope of work. The hydraulic control system is depicted in detail at the beginning of the second chapter, and then a mathematical model for the key component-variable displacement pump is formulated. Later on, the model of the electro-hydraulic compensator is established. Lastly, description and modeling of the electrical control system is presented.

The third chapter deals with the simulation of the pressure compensator and the electro-hydraulic control system in order to investigate the performance of the compensator and the control system. The compensator static and dynamic characteristics are simulated when a conventional PID controller is employed to control the displacement of the spool. Software based on Matlab-Simulink is described in order to simulate the performance of the hydraulic control system. Rolling mill operating conditions are assumed at very arbitrary steady state values, and rolling speed and rolling load reference values are assumed to be at 40% and 60%, respectively. The simulation results are compared with experimental results and then discussed.

An experimental setup composed of real time control software and a hydraulic test bed is prepared to test the static and dynamic performance of the control system. The components of the setup are fully depicted in Chapter 4. The steps that should be taken to prepare the test are also presented in this chapter. The setup is used to

validate the compensator mathematical model. The validity of the model is confirmed on the basis of the agreement between the simulation and experimental results.

Conclusions and suggestions for future work are presented in the fifth chapter.

CHAPTER 2

DESCRIPTION AND MODELING OF PROPOSED ELECTRO-HYDRAULIC CONTROL SYSTEM

In this chapter the hydraulic control system is described in detail, and mathematical models for the key components such as variable displacement pump, and electro-hydraulic pressure compensator are formulated. Finally, description and modeling of the electrical control system is presented.

2.1 Description of the Hydraulic Control System

Figure 2.1 illustrates schematically the proposed hydraulic control system, with the rolling mill demanding a variable load. Basically the entire system is composed of a hydraulic system and a control system. The hydraulic system is composed of four key components. A servo-actuated variable displacement pump "1" is employed to supply a controlled flow Q_S. An electro-hydraulic proportional compensator "2" is engaged to control its upstream pressure P_U. A hydraulic single acting cylinder "3" is used to provide the required rolling load F_r utilizing the compensator controlled upstream pressure P_U. A hydraulic motor "4" drives the strips with the required rolling speed V_r by means of the controlled flow Q_S. During the rolling process, the torque on the hydraulic motor is expected to vary within a range. Consequently, the compensator downstream pressure P_D is expected to vary accordingly. The pressure compensator is then employed to compensate the variation

of its downstream pressure P_D in order to keep its upstream pressure P_U controlled as required by the operation.

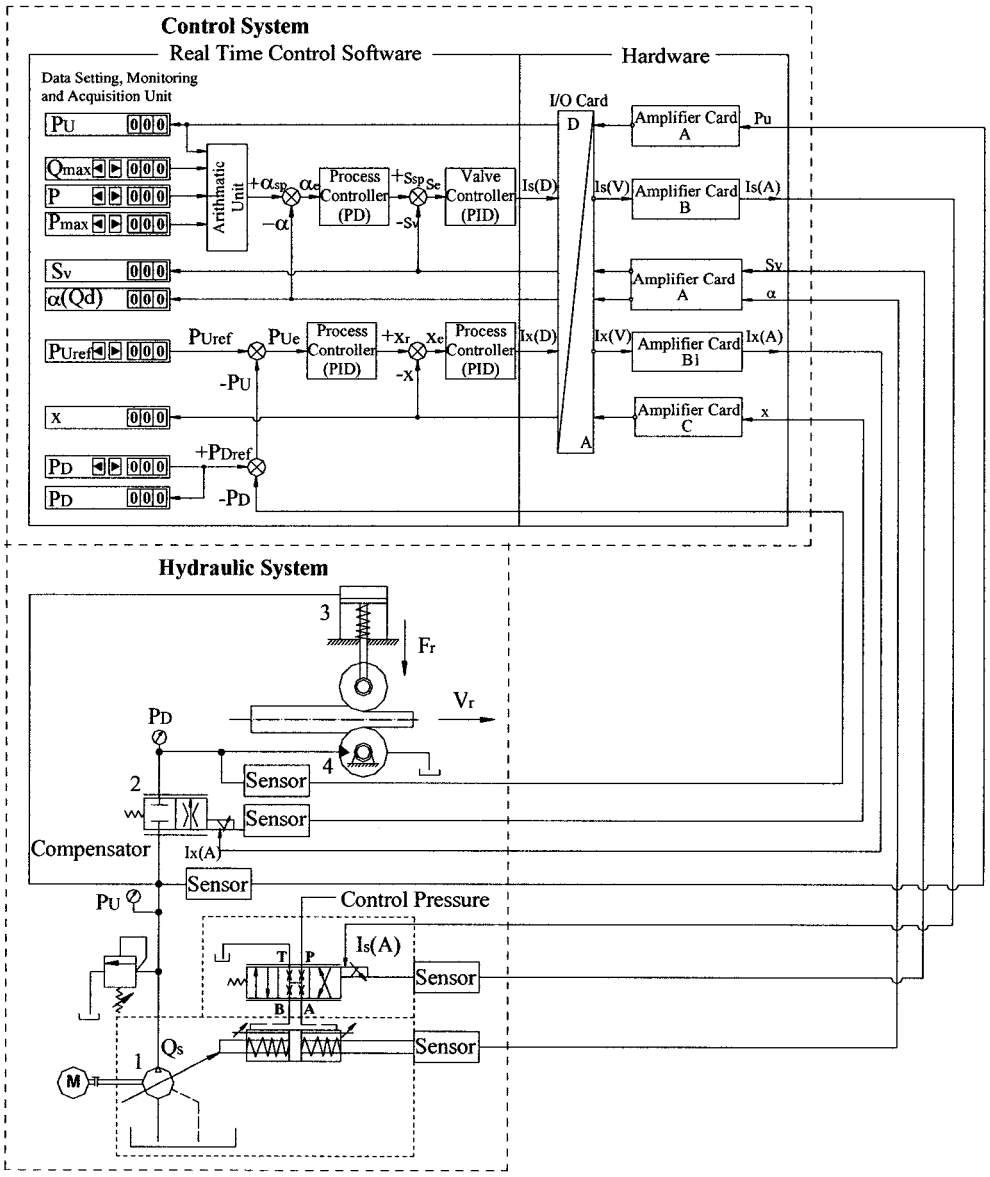

Figure 2.1 Symbolic representation of the electro-hydraulic control system

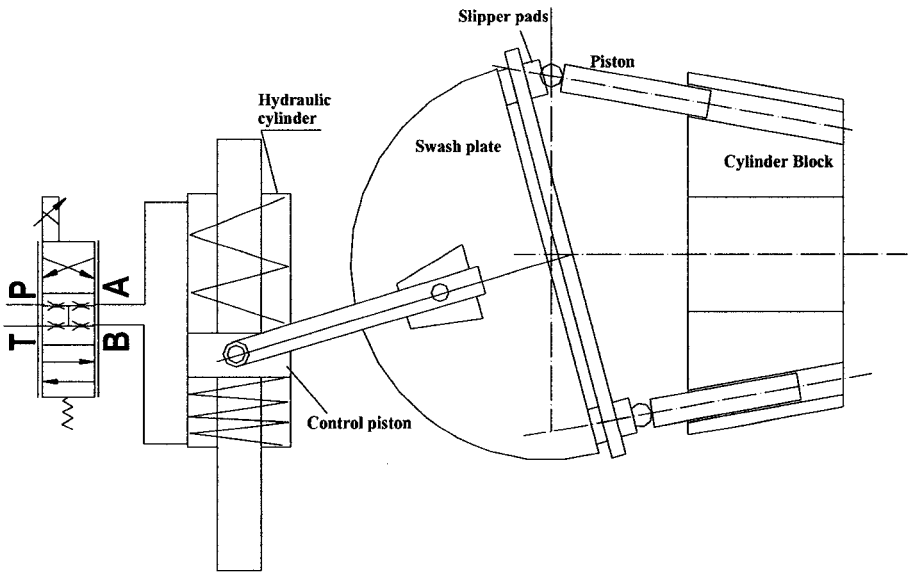

Figure 2.2 The connection of swash plate and control piston

The most suitable pump for the proposed system is one in which the flow rate could be electrically controlled via an input signal. The pump "1" shown in Figure 2.1 is a servo-actuated swash plate axial piston pump in which the swash plate inclination angle is linearly proportional to the pump flow rate. The pump should be driven by an adequately powered electric motor. As shown in the Figure 2.2, the pump swash plate is rigidly connected to a built-in symmetrical hydraulic cylinder, which drives the swash plate to change its inclination angle. Position of the piston of the symmetrical hydraulic cylinder is controlled by means of a hydraulic proportional valve that is integrated with the pump. A control pressure feeds the proportional valve from a secondary circuit, which is not shown in the figure. Two LVDT position sensors that sense the swash plate position and the proportional valve spool displacement are used to control the pump supply flow. The output signals from the sensors are fed back to the electrical control system of the pump, which consequently feeds the proportional valve solenoid with a corresponding electrical control input signal I_s(A).

The pressure compensator "2" is an electro-hydraulic proportional directional or throttle valve. Three sensors serve the control scheme of the pressure compensator. Two of them sense the upstream and downstream pressures of the compensator. The third one senses the compensator spool position. The output signals from the sensors are fed back to the electrical control system of the compensator, which consequently feeds the compensator solenoid with a corresponding electrical control input signal $I_x(A)$.

Pressure relief valve is located on the pump supply line. Maximum supply pressure is set at 15% to 25% more than the maximum required value of P_U (100 bar). The pump supply flow is then guaranteed to pass completely through the compensator.

The hydraulic system contains some other accessories that are necessary for its normal operation, such as oil conditioning elements, physical measuring components, and some safety accessories. These accessories are not shown in the Figure 2.1; however, similar accessories will be presented in chapter 4.

Both the hydraulic cylinder "3" and the hydraulic motor "4" should be adequately sized to meet the requirements of the rolling process such as rolling force F_r and rolling speed V_r, respectively. Hydraulic motor should also be able to provide the rolling torque.

The control system will be described in detail in Chapter 4.

2.2 Modeling of the Variable Displacement Pump

2.2.1 Pump Kinematics

Figure 2.3 shows a sectional view and essential dimensional parameters of the swash plate axial piston pump mechanism with a conical cylinder block [20]. The cone angle of the cylinder block is designated as β. This model can be applied to the general swash plate pumps including those with a circular arrangement of the pistons where the cone angle is zero.

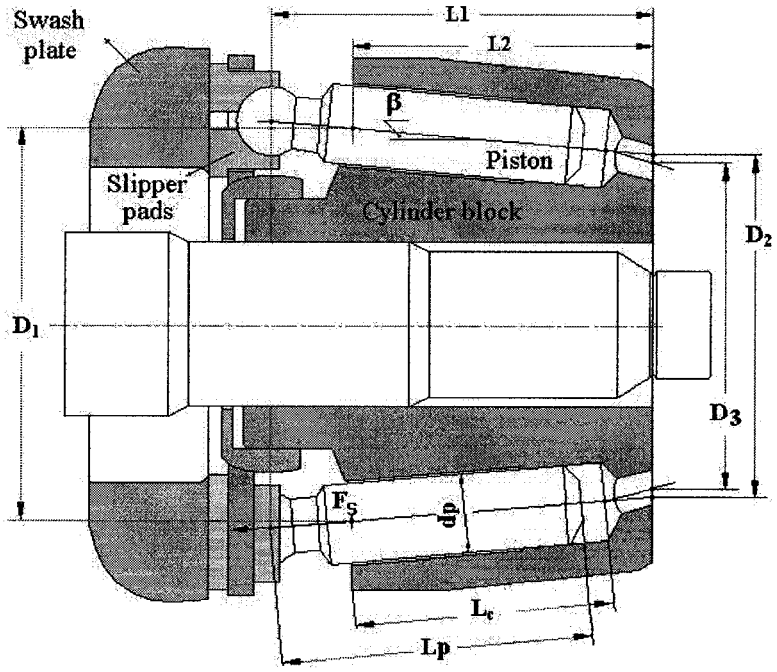

Figure 2.3 Sectional view and essential dimensions of swash plate axial piston pump with conical cylinder block [20]

In order to study pump kinematics, a relationship between the displacement $s_k(t)$ of the k^{th} piston, relative to the piston chamber, and piston angular position $\theta_k(t)$ is established. Figure 2.4 shows the frames of reference used to deduce this relationship. The initial frame of reference $X_0Y_0Z_0$ is chosen where its origin coincides with the swash plate pivoting point O_0, the axis Z_0 coincides with the pump driving shaft axis, and Y_0 coincides with the axis around which the swash plate is swinging. Following a coordinate transformation [21], five steps of frame transformations are then carried out beginning at $X_0Y_0Z_0$ and ending with $X_5Y_5Z_5$. The objective of the coordinate transformation is to obtain the coordinate of the k^{th} piston spherical head center at the angular position θ_k, relative to the initial frame of reference.

The first transformation is from the initial frame of reference $X_0Y_0Z_0$ to the

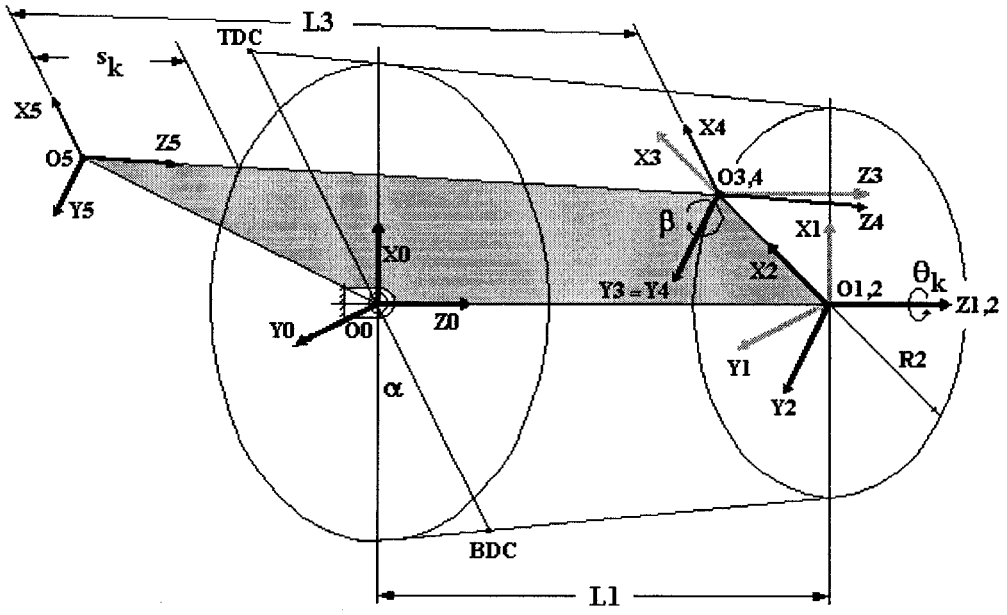

Figure 2.4 Frames of reference for the piston motion [20]

$X_1Y_1Z_1$ frame that represents a translation along the Z_0 axis through a distance L_1. The matrix T_{01} represents this translation and is given by:

$$T_{01} = \begin{bmatrix} 1 & 0 & 0 & 0 \\ 0 & 1 & 0 & 0 \\ 0 & 0 & 1 & L_1 \\ 0 & 0 & 0 & 1 \end{bmatrix}$$

The second transformation is taken from the frame $X_1Y_1Z_1$ to the $X_2Y_2Z_2$ frame. It represents a rotation around Z_1 by an angle θ_k. The matrix T_{12} represents this rotation and is given by:

$$T_{12} = \begin{bmatrix} \cos\theta & -\sin\theta & 0 & 0 \\ \sin\theta & \cos\theta & 0 & 0 \\ 0 & 0 & 1 & 0 \\ 0 & 0 & 0 & 1 \end{bmatrix}$$

The third transformation is carried out from the $X_2Y_2Z_2$ frame to the $X_3Y_3Z_3$ frame. This transformation represents a translation along the axis X_2 through a distance $R_2 = 0.5\ D_2$. Matrix T_{23} represents this transformation and is given by:

$$T_{23} = \begin{bmatrix} 1 & 0 & 0 & R_2 \\ 0 & 1 & 0 & 0 \\ 0 & 0 & 1 & 0 \\ 0 & 0 & 0 & 1 \end{bmatrix}$$

The transformation from the $X_3Y_3Z_3$ frame to the $X_4Y_4Z_4$ frame is carried out by a rotation around the Y_3 axis through an angle β. The transformation matrix T_{34} represents this rotation and is given by:

$$T_{34} = \begin{bmatrix} \cos\beta & 0 & -\sin\beta & 0 \\ 0 & 1 & 0 & 0 \\ \sin\beta & 0 & \cos\beta & 0 \\ 0 & 0 & 0 & 1 \end{bmatrix}$$

The final transformation from the $X_4Y_4Z_4$ frame to the $X_5Y_5Z_5$ frame represents a translation along the Z_4 axis through a distance $-L_3$. The transformation matrix T_{45} is given by:

$$T_{45} = \begin{bmatrix} 1 & 0 & 0 & 0 \\ 0 & 1 & 0 & 0 \\ 0 & 0 & 1 & -L_3 \\ 0 & 0 & 0 & 1 \end{bmatrix}$$

The resultant transformation matrix T_{05} is obtained by multiplying these five transformation matrices starting from the initial frame of reference $X_0Y_0Z_0$ to the final frame of reference $X_5Y_5Z_5$. Consequently, the final transformation matrix T_{05} is given by:

$$T_{05} = T_{01} \times T_{12} \times T_{23} \times T_{34} \times T_{45}$$

$$= \begin{bmatrix} \cos\theta_k\cos\beta & -\sin\beta & -\cos\theta_k\sin\beta & L_{3k}\cos\theta_k\sin\beta + R_2\cos\theta_k \\ \sin\theta_k\cos\beta & \cos\theta_k & -\sin\theta_k\sin\beta & L_{3k}\sin\theta_k\sin\beta + R_2\sin\theta_k \\ \sin\beta & 0 & \cos\beta & -L_{3k}\cos\beta + L_1 \\ 0 & 0 & 0 & 1 \end{bmatrix} \qquad (2.1)$$

Hence, the piston vector $[r_{5k}]_0$ that starts at the origin O_0 and points to the center of the k^{th} piston spherical head O_5 at any given angular position $\theta_k(t)$, relative to the initial frame of reference, has the following time dependent components:

$$X_{5k} = L_{3k}\cos\theta_k \sin\beta + R_2\cos\theta_k \tag{2.2}$$

$$Y_{5k} = L_{3k}\sin\theta_k \sin\beta + R_2\sin\theta_k \tag{2.3}$$

$$Z_{5k} = -L_{3k}\cos\beta + L_1 \tag{2.4}$$

The tip of the piston vector $[r_{5k}]_0$ is constrained by a plane parallel to the swash plate surface and passes through the swash plate pivoting point. As a consequence, the coordinate of the origin O_5 must satisfy the equation of that plane which is inclined at an angle α to the vertical plane, and is given by:

$$X_0 \tan\alpha + Z_0 = 0 \tag{2.5}$$

Inserting the values of X_{5k} and Z_{5k} from equation (2.2) and (2.4) into equation (2.5) results in:

$$L_{3K}(t) = (R_2 \cos\theta_k \tan\alpha + L_1)/(\cos\beta - \cos\theta_k \sin\beta \tan\alpha) \tag{2.6}$$

Knowing the value of L_{3k}, the k^{th} piston displacement s_k relative to the piston cylinder along Z_5 direction can be deduced, since it can be shown from the geometry that

$$s_k(t) = -(L_{3k} - L_1/\cos\beta) \tag{2.7}$$

where: $\theta_k(t) = \omega t + 2\pi(k-1)/N$ and $\beta = \tan^{-1}0.5(D_1 - D_2)/L_2$

For a pump running at constant speed of 1450 rpm, $\theta_k(t)$ is linearly dependent on the time taken for one complete revolution, which equals 0.0413793 second. Knowing that, the time variation of the piston displacement, velocity, and acceleration, relative to the piston cylinder, can be found.

Software based on the Matlab-Simulink simulation program has been developed to calculate and plot the k^{th} piston relative displacement, velocity and acceleration against the angle θ_k for any pump running speed [20]. A simulation was carried out for a 9-piston pump configuration of geometric volume 40 cc/rev, running at a constant speed of 1450 rpm. The various dimensions of this pump are shown in Figure 2.3 and the numerical values are included in Appendix A. The results are illustrated in Figure 2.5.

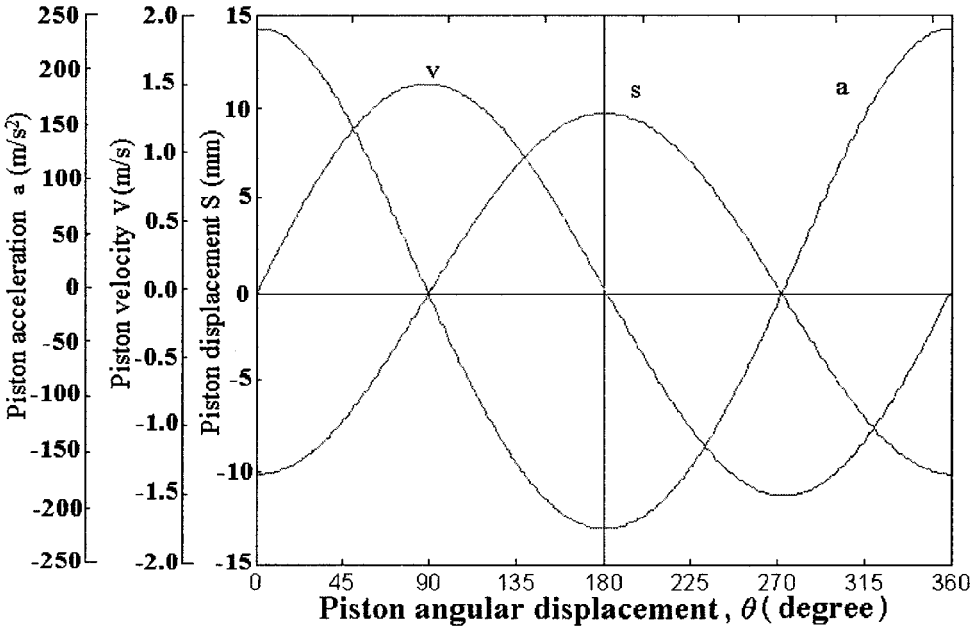

Figure 2.5 Variation of piston displacement, velocity, and acceleration, relative to the piston cylinder, with θ_k for the 40 cc/rev pump running at 1450 rpm [20]

2.2.2 Piston Chamber Pressure and Flow Rate

The variation of pressure in each piston chamber during one complete revolution of the pump is derived with the following assumptions:

i) The pump rotational speed is constant;

ii) The pump suction and delivery pressures are constant;

iii) The inertia effect of the oil column inside the piston chamber is negligible;

iv) The total instantaneous leakage flow rate out of the piston chamber Q_{LK} is proportional to the piston chamber instantaneous pressure p_k;

v) The coefficient of discharge is constant;

vi) The oil density and bulk modulus are constant.

The above are realistic assumptions normally used in similar situations.

Applying the continuity equation [22] to the control volume (C.V.) surrounding the interior volume of the piston chamber shown in Figure 2.6, results in the equation:

$$Q_{sk} + A_p \dot{S}_k = Q_{dk} + p_k/R_L + V_{ck}\dot{p}_k/B \tag{2.8}$$

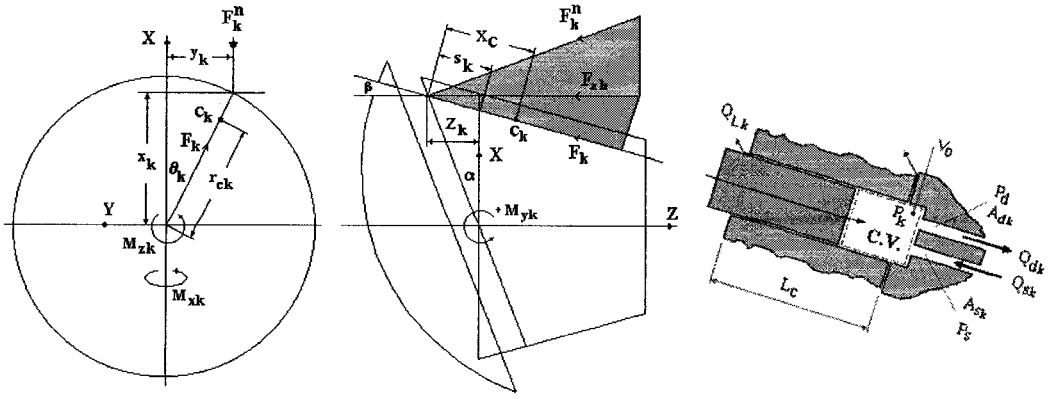

Figure 2.6 Piston chamber parameters and variable [20]

where Q_{sk} represents the oil flow rate drawn into the piston chamber from the pump suction line, and Q_{dk} is the flow rate delivered from the piston chamber to the pump delivery line at any angular position θ_k. A_p is the piston cross section area and V_{ck} is the piston chamber instantaneous volume. The instantaneous piston chamber pressure is p_k and the oil bulk modulus is B. The leakage flow rate out of the piston chamber to the pump housing Q_{Lk} is assumed to be linearly dependent on p_k and equals p_k/R_L.

The piston chamber instantaneous volume is given by:

$$V_{ck} = A_p(0.5L_c - s_k) + V_0 \tag{2.9}$$

where L_c is the cylinder block maximum length filled with oil, and V_0 is the piston chamber volume as shown in Figure 2.6. The following equations can be obtained that state the flow variables.

$$Q_{sk} = C_d A_{sk} \sqrt{\frac{2|p_s - p_k|}{\rho}} \operatorname{sgn}(p_s - p_k) \tag{2.10}$$

and

$$Q_{dk} = C_d A_{dk} \sqrt{\frac{2|p_k - p_d|}{\rho}} \operatorname{sgn}(p_k - p_d) \tag{2.11}$$

where C_d is the coefficient of discharge and ρ is the oil density. The areas A_{sk} and A_{dk} are the instantaneous cross sectional areas of the ports communicating the piston chamber to the suction and delivery ports, respectively. Evidently, the port plate design should be such that for any nonzero A_{sk} corresponding to any angular position θ_k, the value of A_{dk} should be zero, and vice-versa.

Knowing the values of A_{sk} and A_{dk} at each value of θ_k, and for given constructional and operation parameters, the values of each piston chamber pressure p_k and flow rate Q_{dk} can be calculated by solving equations (2.8) to (2.11) simultaneously, provided that the piston displacement and speed are determined. Superimposing Q_{sk} for the group of N pistons, the total pump delivery flow rate Q at any θ_k is given by:

$$Q = \sum_{k=1}^{N} Q_{dk} \tag{2.12}$$

2.2.3 Moments Acting on the Swash Plate

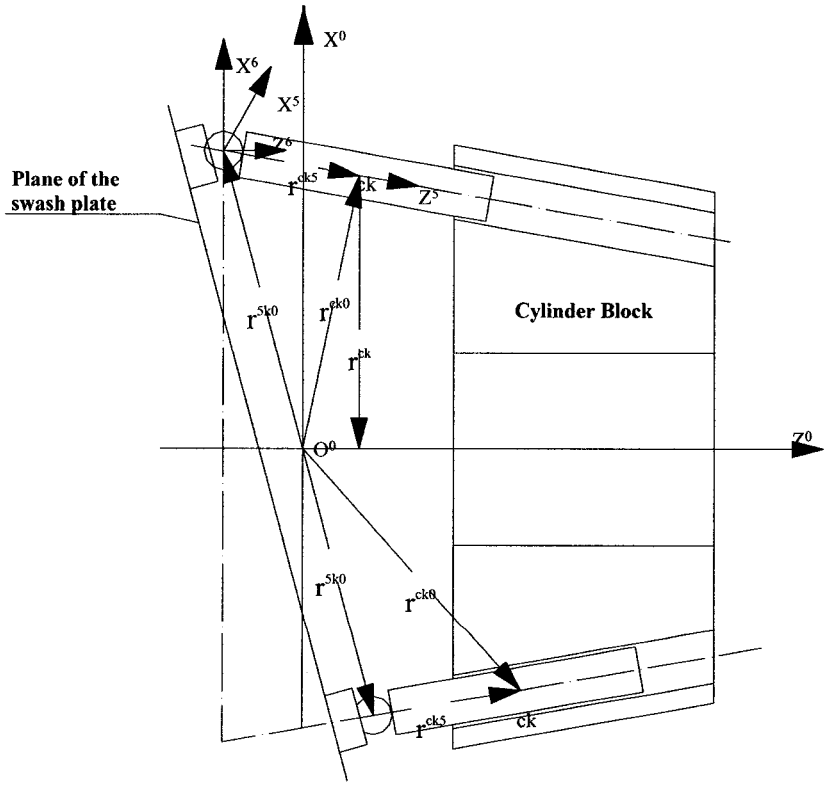

Figure 2.7 Piston three-dimensional general space motion [20]

As illustrated in Figure 2.7, the piston performs general three-dimensional motion relative to the initial frame of reference $(OXYZ)_0$, which is assumed to be inertial. At the same time, the piston movement $s_k(t)$ is constrained in the Z_5 direction of the 5^{th} frame of reference, which is attached to the piston spherical head center O_5. During the piston general motion, it acts on the swash plate by a resultant force $[F_k]_0$ with respect to the inertial frame of reference. This resultant force vector acts on the swash plate at the point O_5 that is indicated by the position vector $[r_{5k}]_0$. The position vector $[r_{5k}]_0$ has the previously calculated components, which are relative to the inertial frame of reference given by equations (2.2) to (2.4). Consequently, the moments acting on the swash plate relative to the inertial frame of reference, can be obtained by multiplying the resultant force vector $[F_k]_0$ by the position vector $[r_{5k}]_0$.

The resultant force $[F_k]_0$ that is exerted by the k^{th} piston on the swash plate during the piston general space motion is composed of the following:

1. The force resulting from the oil pressure inside the piston chamber.
2. The piston inertia due to its absolute acceleration.
3. The friction force between the piston and the cylinder block walls that can be represented as an equivalent viscous friction force.

An order of magnitude analysis of the values of these forces with constructional parameters shown in Figure 2.3 revealed that the equivalent viscous friction force is of the least and negligible amplitude. This force was disregarded during the following analysis.

The force resulting from the oil pressure inside the piston chamber equals $A_p p_k$ and acts along the Z_5 axis. Hence, it can be defined in vector form relative to the 5th frame of reference to be $[F_{pk}]_5$ that has the components 0, 0 and $A_p p_k$ along the unit vectors i_5, j_5 and k_5, respectively. This force can be redefined relative to the inertial frame of reference, using equation (2.1), as follows:

$$[F_{pk}]_0 = \begin{bmatrix} \cos\theta_k\cos\beta & -\sin\beta & -\cos\theta_k\sin\beta \\ \sin\theta_k\cos\beta & \cos\theta_k & -\sin\theta_k\sin\beta \\ \sin\beta & 0 & \cos\beta \end{bmatrix} \times [F_{pk}]_5 = A_p p_k \begin{bmatrix} -\cos\theta_k\sin\beta \\ -\sin\theta_k\sin\beta \\ \cos\beta \end{bmatrix} \tag{2.13}$$

In order to calculate the piston absolute acceleration, the point ck is defined as the center of mass of the k^{th} piston, as shown in Figure 2.7. The position vector $[r_{ck}]_0$ is calculated first as below:

$$[r_{ck}]_0 = [r_{5k}]_0 + [r_{ck}]_6 \tag{2.14}$$

where $[r_{ck}]_6$ is the fixed magnitude position vector $[r_{ck}]_5$ redefined relative to the 6th frame of reference that has its origin that coincides with the 5th frame origin, and axes parallel to those of the inertial frame of reference. It can be calculated using the transformation matrix in equation (2.1) as follows:

$$[r_{ck}]_6 = \begin{bmatrix} \cos\theta_k\cos\beta & -\sin\beta & -\cos\theta_k\sin\beta \\ \sin\theta_k\cos\beta & \cos\theta_k & -\sin\theta_k\sin\beta \\ \sin\beta & 0 & \cos\beta \end{bmatrix} \times [r_{ck}]_5 = \frac{L_p}{2} \begin{bmatrix} -\cos\theta_k\sin\beta \\ -\sin\theta_k\sin\beta \\ \cos\beta \end{bmatrix} \tag{2.15}$$

At any angle θ_k, the piston absolute acceleration due to its three-dimensional general motion relative to the inertial frame of reference is given by:

$$[a_{ck}]_0 = \dot{\omega} \times [r_{ck}]_0 + \omega \times (\omega \times [r_{ck}]_0) + 2\omega \times [\dot{r}_{ck}]_0 + [\ddot{r}_{ck}]_0 \tag{2.16}$$

The first two terms in equation (2.16) represent the piston acceleration due to its rotation, while the last two terms represent the piston acceleration due to its translation. The first term is the piston tangential acceleration that equals zero due to pump rotation with constant angular speed. The second term is the piston normal (centripetal) acceleration. The third term is the piston coriolis acceleration. The last one is the second derivative of the position vector $[r_{ck}]_0$.

The resultant force vector exerted by the k^{th} piston on the swash plate has the components F_{xk}, F_{yk} and F_{zk}. It can be calculated as follows:

$$[F_k]_0 = [F_{pk}]_0 + m_p[a_{ck}]_0 \tag{2.17}$$

where m_p is the piston mass.

The resultant force vector $[F_k]_0$ acts on the swash plate and causes a moment referred to the inertial frame of reference as follows:

$$[M_k]_0 = [r_{5k}]_0 \times [F_k]_0 = \begin{vmatrix} i_0 & j_0 & k_0 \\ x_{5k} & y_{5k} & z_{5k} \\ F_{xk} & F_{yk} & F_{zk} \end{vmatrix} \tag{2.18}$$

The moment acting on the swash plate from the k^{th} piston thus has the three components M_{xk}, M_{yk} and M_{zk} along the unit vector direction i_0, j_0 and k_0, respectively. The total moment components acting on the swash plate due to the whole piston group is given by:

$$M_x = \sum_{k=1}^{N} M_{xk} \tag{2.19}$$

$$M_y = \sum_{k=1}^{N} M_{yk} \tag{2.20}$$

$$M_z = \sum_{k=1}^{N} M_{zk} \tag{2.21}$$

The moment M_y tends to change the swash plate inclination angle, while the moment M_z equals the pump driving torque. The resultant of the two moment components M_x and M_z; namely M_b, acts on the swash plate bearing system and is given by:

$$M_b = \sqrt{M_x^{\,2} + M_z^{\,2}} \tag{2.22}$$

2.2.4 Mathematical Model of the Pump Control Unit

The circuit diagram of the pump control system is shown in Figure 2.8, while Figure 2.9 shows a schematic drawing of the hydro-mechanical part of the control system. The system consists of a symmetrical hydraulic cylinder that has a piston connected mechanically to the swash plate. The position of the control piston is controlled by means of a hydraulic proportional valve. In open hydraulic circuits, when the proportional valve is de-energized and the control pressure p_v exists, the pump swash plate swivels to an adjustable minimum value. When the proportional valve receives an actuating electrical signal from its electronic control card, its spool moves accordingly. Consequently, the control piston moves causing a change in the swash plate inclination angle and hence in the pump flow rate. The system incorporates three sensors. The first sensor senses the pump delivery pressure and

produces a voltage proportional to it, while the other two are position sensors, with one of them sensing the swash plate position, while the other senses the proportional valve spool displacement. The output signals of these sensors, as well as the setting values of the constant power and the limits of the pump static characteristic curve, are fed to the electronic card.

The equations governing the dynamics of the hydro-mechanical part of the control system, shown schematically in Figure 2.9, are derived below. When the proportional valve solenoid receives a control current i_v, a force proportional to this current, namely $k_i i_v$, acts on the valve spool and causes it to move. The equation of motion of the valve spool is:

$$m_v \ddot{s}_v + f_v \dot{s}_v + k_v s_v = k_i i_v \tag{2.23}$$

The proportional valve spool displacement throttles oil flow through the four control gaps of the valve since the valve is of the open center type. Assuming a constant discharge coefficient and negligible valve leakage, it can be verified that the flow rates through the four control gaps, shown in Figure 2.9, are given by the following equations:

$$Q_a = C_d w(s_{vmax} - s_v)\sqrt{\frac{2|p_{c1} - p_T|}{\rho}}\,\mathrm{sgn}(p_{c1} - p_T) \tag{2.24}$$

$$Q_b = C_d w s_v \sqrt{\frac{2|p_v - p_{c1}|}{\rho}}\,\mathrm{sgn}(p_v - p_{c1}) \tag{2.25}$$

$$Q_c = C_d w(s_{vmax} - s_v)\sqrt{\frac{2|p_v - p_{c2}|}{\rho}}\,\mathrm{sgn}(p_v - p_{c2}) \tag{2.26}$$

$$Q_d = C_d w s_v \sqrt{\frac{2|p_{c1} - p_T|}{\rho}} \mathrm{sgn}(p_{c2} - p_T) \tag{2.27}$$

where p_v is the proportional valve supply pressure, p_{c1} and p_{c2} are the pressure acting on the two sides of the piston of the cylinder, p_T is the tank pressure, w is the valve port width, s_v is the spool displacement, and s_{vmax} is the maximum spool displacement.

By applying the continuity equation to the hydraulic cylinder chamber, the pressures p_{c1} and p_{c2} are obtained as:

$$p_{c1} = \frac{B}{V_{c1}} \int (Q_b - Q_a - A_{cp}\dot{x}_{cp} - \frac{p_c}{R_L})dt \tag{2.28}$$

$$p_{c2} = \frac{B}{V_{c2}} \int (Q_c - Q_d + A_{cp}\dot{x}_{cp} + \frac{p_c}{R_L})dt \tag{2.29}$$

V_{c1} and V_{c2} can be calculated by the following equations:

$$V_{c1} = V_{ci} + A_{cp}x_{cp} \tag{2.30}$$

$$V_{c2} = V_{ci} - A_{cp}x_{cp} \tag{2.31}$$

where V_{ci} is half the cylinder total volume, A_{cp} is the cross sectional area of the control piston, x_{cp} is the piston displacement and R_L is the leakage resistance across the piston.

The pressure difference on the two sides of the control piston drives it to a new equilibrium position. The instantaneous angular speed and swash plate inclination angle are given by:

$$\dot{\alpha} = \frac{1}{I_e} \int [(p_{c1} - p_{c2})A_{cp}R_s + M_y - f_\alpha \dot{\alpha} - k_\alpha(\alpha + 0.09)]dt \tag{2.32}$$

$$\alpha = \int \dot{\alpha} dt \tag{2.33}$$

In evaluating the value of f_α, the viscous damping at the control piston and the swash plate supporting bearings, are considered. The value of k_α represents the spring action at the control piston. The moment of inertia of the swash plate and the parts attached to it as well as the moving mass of the control piston are considered in evaluating the value of I_e.

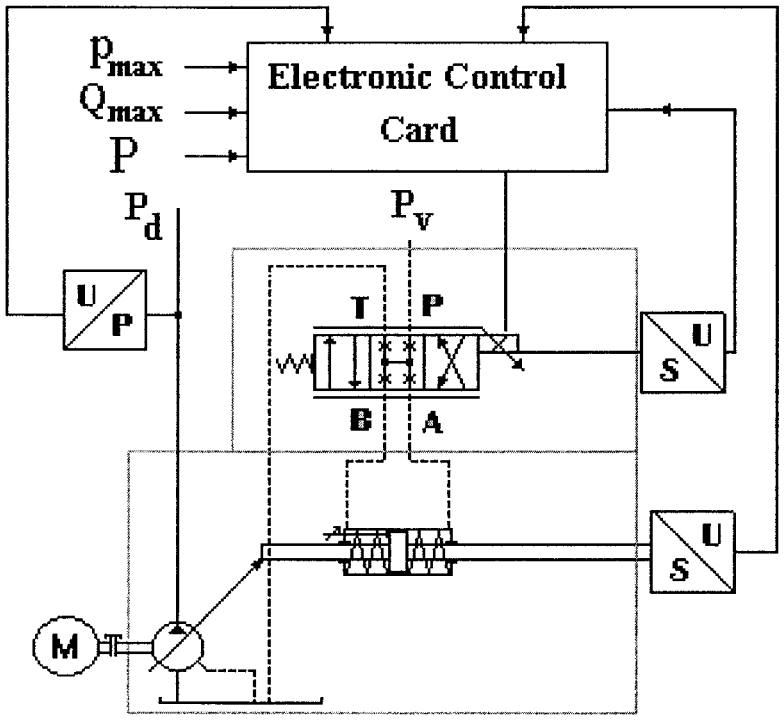

Figure 2.8 Symbolic representation of the constant power control unit [20]

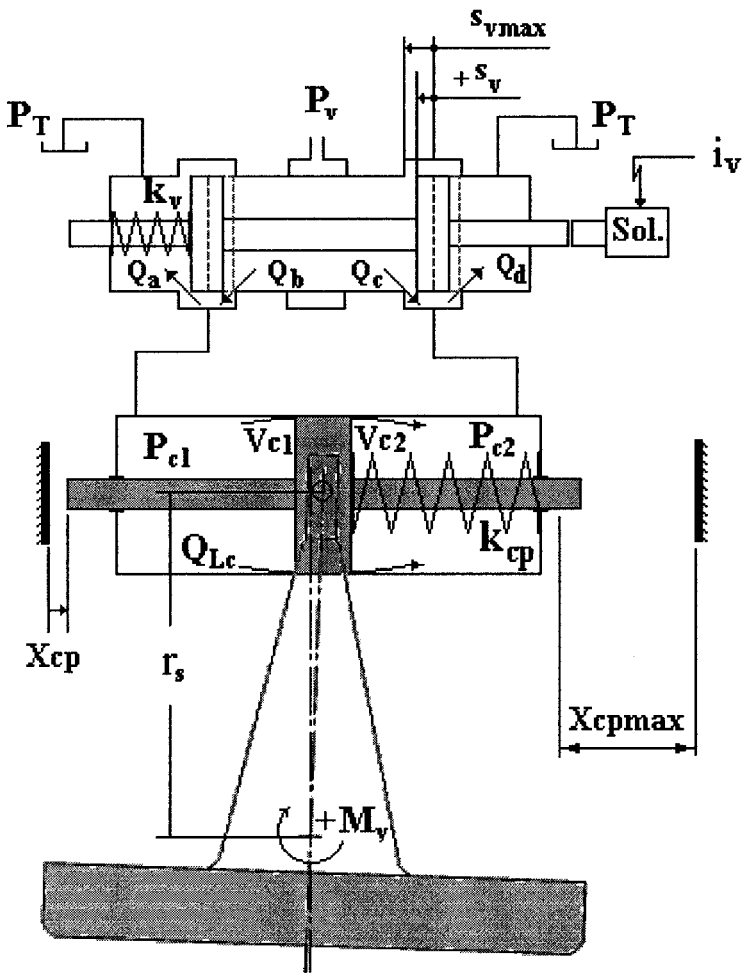

Figure 2.9 Schematic representation of the hydro-mechanical part of the control system shown in Figure 2.8 [20]

2.3 Modeling of the Electro-hydraulic Compensator

As shown in Figure 2.10, an electromagnetic proportional directional valve manufactured by Rexroth is employed as a pressure compensator. The Type of this valve is **4WRE10EA75-2X/G24K4/V.** It is symbolically represented as shown in Figure 2.11 and its main technical data is given in Table 2.1.

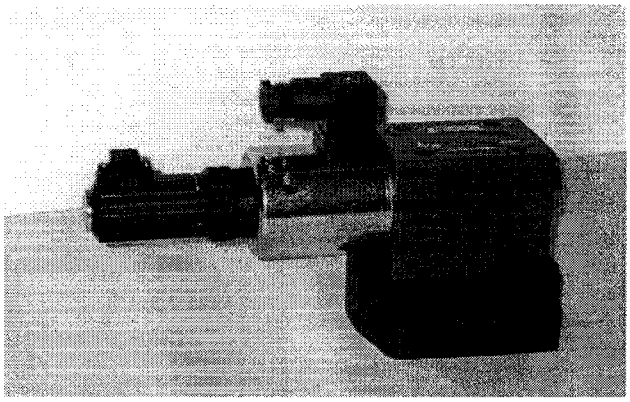

Figure 2.10 The outer shape of the proportional valve

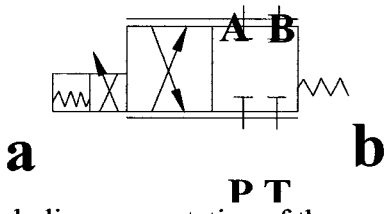

Figure 2.11 Symbolic representation of the proportional valve

Table 2.1 The main technical data of 4WRE10EA75-2X/G24K4/V

Item	Description		Value
1	Operating Pressure	Ports A, B, P	315 bar
		Port T	210 bar
2	Normal Flow Q_{vnom} at $\Delta p = 10$ bar		75 l/min
3	Command Value Signal Voltage Input "A1"		±10 V
4	Solenoid Coil Resistance		2 to 3 Ω
5	Max. Coil Temperature		Up to 150° C
6	Max. Permissible Flow		180 l/min
7	Viscosity Range		23 to 380 mm^2/s Preferably 30 to 46 mm^2/s

The pressure compensator can be simplified as shown in Figure 2.12 and Figure 2.13. Figure 2.12 shows the state in which the solenoid does not receive signal or receives a signal that is less than a certain value, such that the spool does not move. Consequently, the oil from the pump has to go to the tank via the relief valve. Therefore, $Q_{RV,}$ the flow rate of the relief valve, equals to the Q_S, the flow rate of the pump, and the supply pressure P_U will reach the maximum pressure.

As shown in Figure 2.13, when the solenoid receives a control signal $I_x(A)$ above zero, an electromagnetic force equals to $I_x k_i$ proportional to the input signal acts on the valve spool and causes it to move against its return spring. When the displacement of the spool is more than a certain value (1mm), the supply pressure Pu

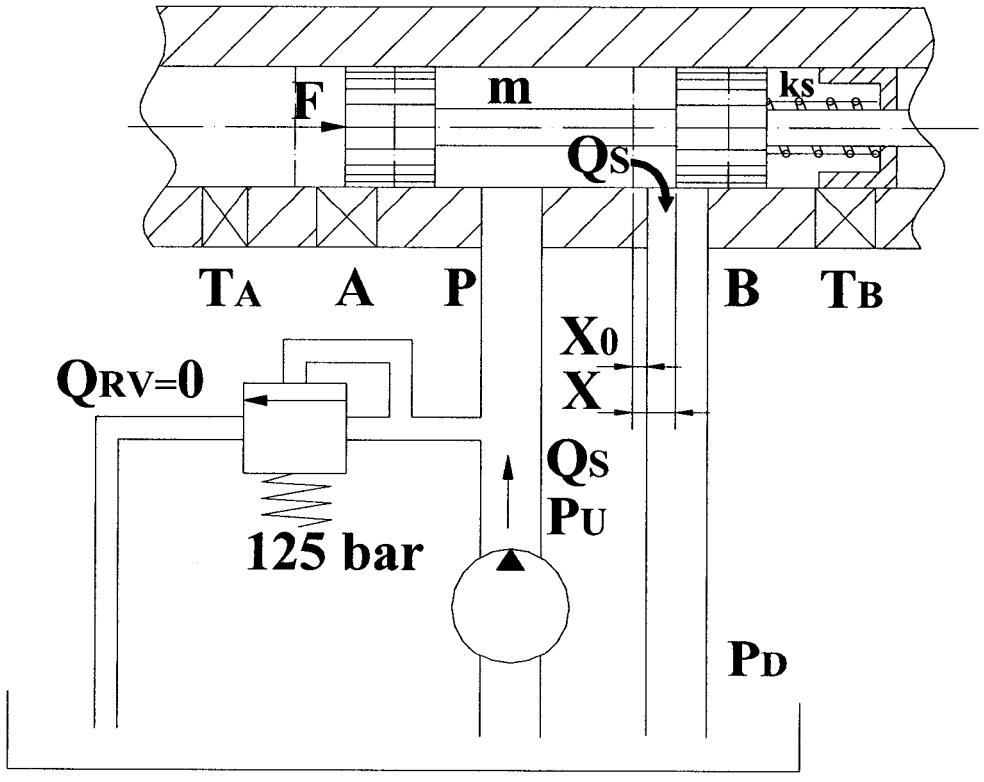

Figure 2.12 Schematic of the pressure compensator (initial state)

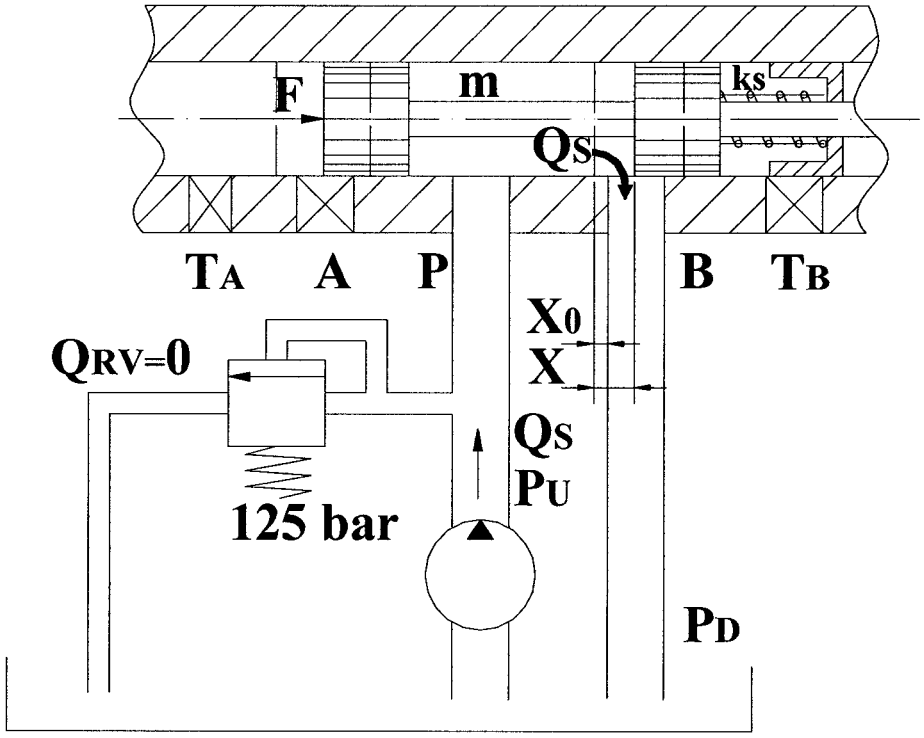

Figure 2.13 Schematic of the pressure compensator (working state)

will be less than the maximum pressure, and the relief valve is closed. In this case, the flow from the pump will go to the tank through the port B completely.

2.3.1 Analysis of Spool Motion

As shown in Figure 2.14, the spool of the compensator can be regarded as a body, and there are three forces acting on it. The first one is the electromagnetic force (F) of the solenoid, while the second one is the balance force (F_s) that is generated by the spring; the last one is the force due to the oil viscosity. Basically, the electromagnetic force F is proportional to the current, applied to the solenoid; the spring force F_s is proportional to the displacement of the spool, and the force due to the oil viscosity is proportional to the velocity of the spool.

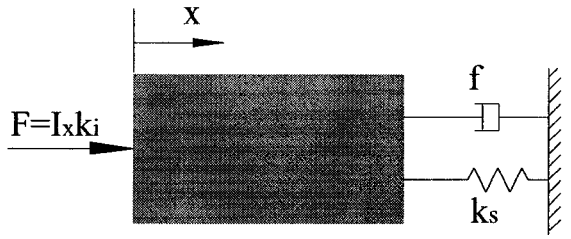

Figure 2.14 Analysis of the spool motion

Using Newton's second Law, we have the following equation:

$$I_x k_i - f\dot{X} - k_s X = m\ddot{X} \tag{2.34}$$

where: I_x - Current applying on the solenoid (AMP);

k_i - Current constant (N/AMP);

m - Mass of the spool (kg);

X - Displacement of the spool (m);

f - Viscous friction coefficient (Ns/m);

k_s - Spring stiffness (N/m);

The following equation can be readily obtained from the equation (2.34):

$$v = \frac{1}{m}\int (k_i I_x - fv - k_s X)dt \tag{2.35}$$

where: v - Velocity of the spool (m/s);

and: $$X = \int v dt \tag{2.36}$$

2.3.2 Transfer Function

Assuming zero initial condition, we take Laplace transform of the equation (2.34), and the following equation can be obtained:

$$(ms^2 + fs + k_s)X(s) = k_i I_x(s) \tag{2.37}$$

Consequently, the transfer function is obtained as below:

$$\frac{X(s)}{I_x(s)} = \frac{k_i}{ms^2 + fs + k_s} \tag{2.38}$$

Equation (2.38) can be rearranged to the following form:

$$\frac{X(s)}{I_x(s)} = \frac{k_i / m}{s^2 + \frac{f}{m}s + \frac{k_s}{m}} = \frac{k_i / m}{s^2 + 2\zeta\omega_n s + \omega_n{}^2} \tag{2.39}$$

where: ω_n - Natural frequency (rad/s);

ζ - Damping ratio;

and: $\omega_n{}^2 = \frac{k_s}{m}$ (2.40)

$$2\zeta\omega_n = \frac{f}{m} \tag{2.41}$$

From equation (2.40), $\omega_n = \sqrt{\frac{k_s}{m}} = \sqrt{\frac{4000}{0.1}} = 200 \text{ rad/s} = \frac{200}{6.28}\text{Hz} \approx 30\text{Hz}$

From equation (2.41), $\zeta = \frac{f}{2m}\sqrt{\frac{m}{k_s}}$ (2.42)

Let f be 48 Ns/m, then $\zeta = 1.2$, which means that the system is over damped.

Overall, the transfer function is shown as follows:

$$G(s) = \frac{X(s)}{I_x(s)} = \frac{50}{s^2 + 480s + 40000} \tag{2.43}$$

2.3.3 Modeling of Compensator

As shown in Figure 2.12 and 2.13, the proportional valve is employed as an electro-hydraulic pressure compensator in which the port A and port T are blocked. In

order to analyze the pressure and flow rate of the compensator conveniently, the compensator is simplified as shown in Figure 2.15.

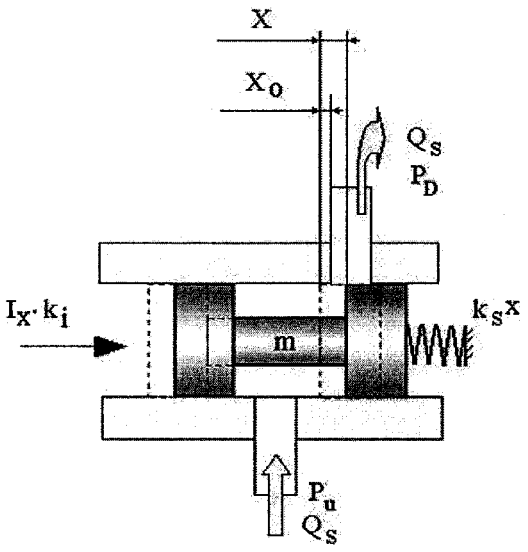

Figure 2.15 Schematic of the pressure compensator

When $X>X_0$, as shown in Figure 2.15 and assuming constant coefficient, zero pressure tank line, negligible internal leakage and compressibility effect, the flow rate Q_S can be calculated by the following equation:

$$Q_S = C_d A_f (X - X_0)\sqrt{\frac{2(P_U - P_D)}{\rho}} \tag{2.44}$$

where: C_d - Compensator discharge coefficient (0.611);

A_f - Compensator area coefficient (0.02);

X - Compensator displacement (m);

X_0 - Compensator displacement overlap (m);

ρ - Mass density of oil (900 kg/m^3);

P_U - Compensator upstream pressure (bar);

P_D - Compensator downstream pressure (bar).

From (2.44), the following equation can be obtained:

$$P_U = P_D + \frac{\rho}{2}\left[\frac{Q_S}{C_d A_f (X - X_0)}\right]^2 \tag{2.45}$$

2.4 Description and Modeling of the Electrical Control System

As shown in Figure 2.16, the overall electrical control system is composed of two interacting control schemes. First one is to control the pump flow rate Q_S and the other is to control the compensator upstream pressure P_U. Each control scheme consists of double negative feedback control loops.

The inner feedback control loop in the pump control scheme is used for the positioning of the proportional valve spool using displacement sensor and PID controller. In this loop a displacement sensor measures the actual spool position S of the proportional valve and feeds back the corresponding value in voltage. A signal conditioner reconverts this signal into a corresponding percentage of the spool position to be compared with a reference spool position S_r. PID controller receives the error in the spool position S_e and provides a corresponding control signal $I_s(V)$ in the form of voltage.

An amplifier is then used to provide a signal in current signal $I_x(A)$ powerful enough to drive the valve solenoid for positioning the valve spool in the required position. Similarly the outer loop works to control the swash plate inclination angle

and hence the pump flow rate. The only difference is that the controller is of PD type because the outer loop represents a system type 1 that has zero steady state error due to the presence of the symmetric hydraulic cylinder as a physical integrator. Under steady state conditions, both the error values are equal to zero and the valve spool is positioned at the center in order to hold the swash plate at the current position.

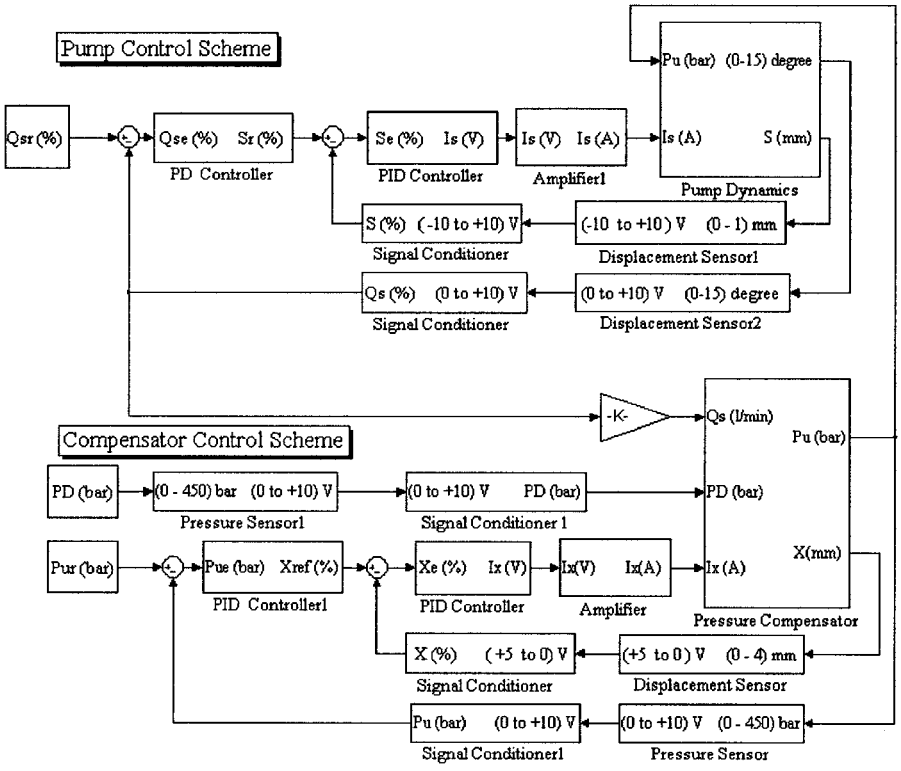

Figure 2.16 Block diagram of the control schemes and simulation subsystems

Construction of the compensator control scheme is similar to that used to control the pump flow rate. The inner feedback loop is used to control the compensator spool position, while the outer loop controls the compensator upstream pressure. PID controllers are used in both the loops.

If the downstream pressure increases, correspondingly the compensator opens more, and vise versa, in order to compensate the effect of the independent change in the downstream pressure and correspondingly the upstream pressure is kept constant. Controlling of the upstream pressure is takes place whenever the pressure difference across the compensator is more than nearly 4% of the upstream pressure. Alternatively, the upstream pressure will increase by increasing the downstream pressure.

The two control schemes are interactive where the pump flow rate affects the compensator operation and the compensator upstream pressure affects the pump dynamics. By controlling both the pump flow rate and the compensator upstream pressure, both rolling speed and rolling load are consequently controlled, respectively. It is evident that the rolling speed and rolling load are in open loop, but this is acceptable in the intermediate stages of the rolling process.

CHAPTER 3

SIMULATION AND PERFORMANCE INVESTIGATION OF THE CONTROL SCHEMES

As mentioned in chapter 2, the mathematical models were used to carry out analytical studies and simulations of the pump and pressure compensator performances. In addition, when the solenoid receives a signal $I_x(A)$ from the control card, the spool will move to the spring side and the relationship between the signal and the displacement can be obtained from the transfer function given in equation (2.43). Furthermore, the pressure across the compensator can be obtained from equation (2.45). In this chapter, simulation programs based on Matlab-Simulink are developed to simulate the motion of the spool and the pressure drop across electro-hydraulic compensator. Subsequently, simulation programs will be run to simulate the performance of the pump. Finally, simulations of the hydraulic control system will be carried out for different inputs to study its static and dynamic characteristics.

3.1 Simulation of the Compensator Performance

3.1.1 Simulation of the Spool Motion

(i) Open Loop for the Spool Motion Figure 3.1 and 3.2 show the block and the simulation modeling of the open loop, respectively. The simulation parameters are chosen as shown in Figure 3.3 and the data is provided by the following M-file:

$m = 0.1;$	Mass of the spool (kg)
$k_i = 5.3;$	Current constant (N/Amp)
$k_s = 4000;$	Spring stiffness (N/m)
$f = 48;$	Viscous constant

Figure 3.1 The open-loop block of the spool motion

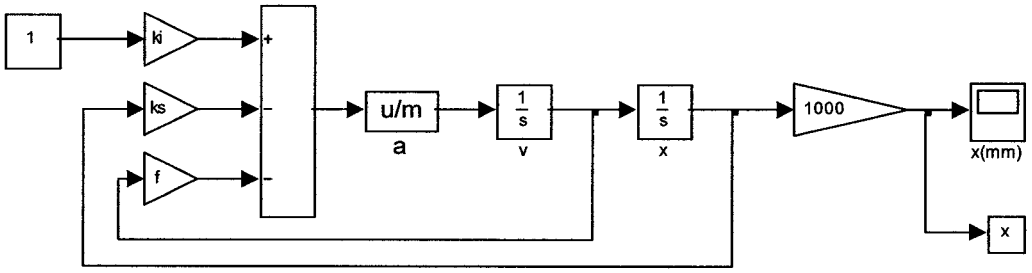

Figure 3.2 The open-loop modeling of the spool motion

The result of the simulation is shown in Figure 3.4. From this result, we know that the steady-state value is 1.25 mm and the settling time is 0.0398 seconds within ±2% error of the steady-state value.

(ii) Closed Loop for the Spool Motion In order to improve the performance of the system, a closed-loop is built, as shown in Figure 3.5. The corresponding modeling is shown in Figure 3.6.

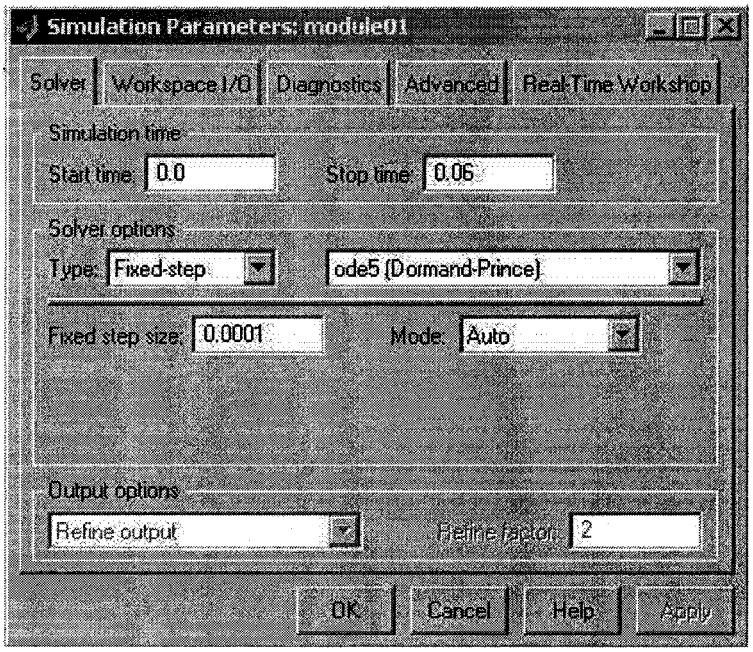

Figure 3.3 The simulation parameters of the spool motion for open loop

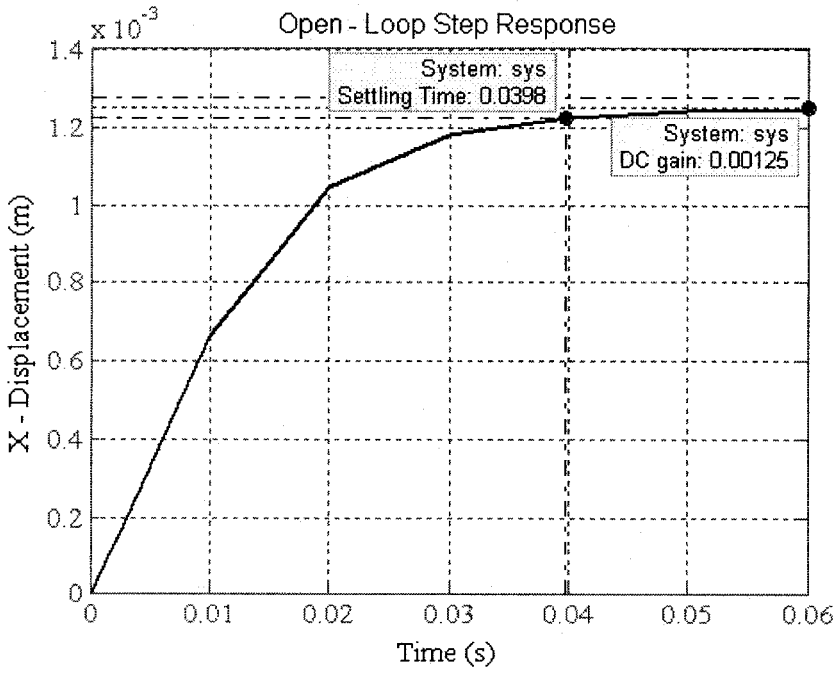

Figure 3.4 Open-loop step response of the spool motion

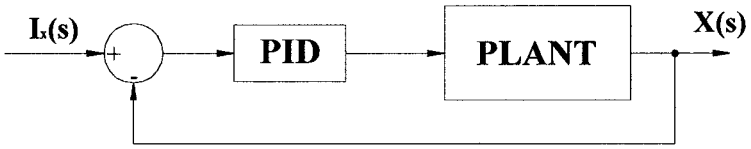

Figure 3.5 The closed-loop block of the spool motion

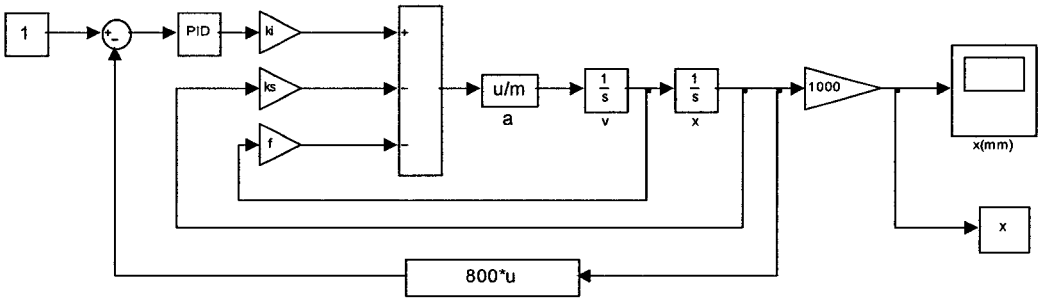

Figure 3.6 The closed-loop modeling of the spool motion

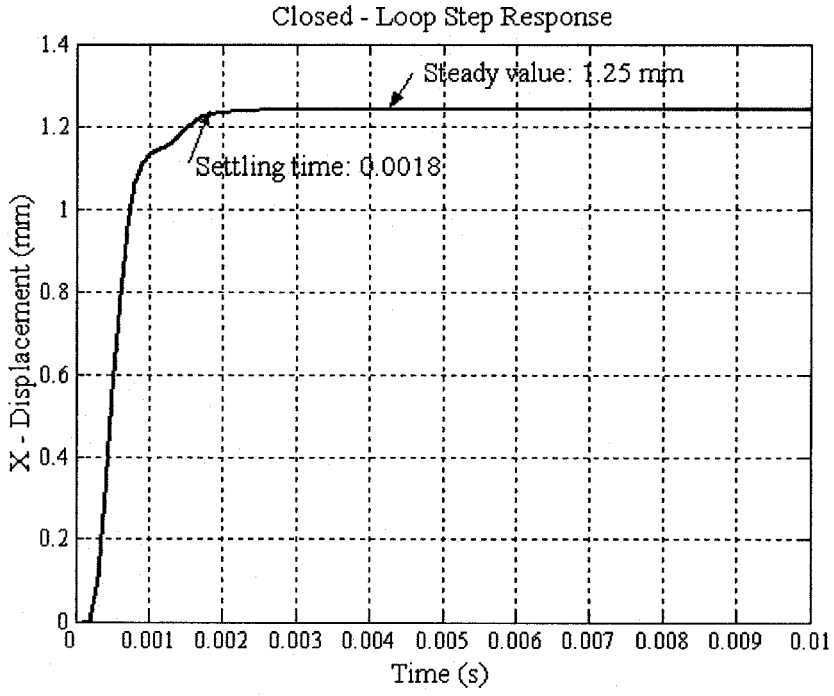

Figure 3.7 Closed-loop step response of the spool motion

In this closed-loop, a PID controller is employed. The parameters of PID controller are: K_p = 200, K_i = 0 and K_d = 0.1. The other data and the simulation parameters are same as in the open loop. The simulation result is shown in Figure 3.7. As can be seen, the steady state value is 1.25 mm and the settling time is 0.0018 seconds within ±2% error of the steady-state value.

3.1.2 Simulation of the Compensator Performance

In order to study the compensator performance for different reference commands, the simulation modeling is built as shown in Figure 3.8. The data is provided in the command window as follows:

m = 0.1;	Mass of the spool (kg)
X_0 = 0.001;	Width of overlap (m)
P_T = 100000;	Pressure (Pa)
V = 0.0004;	Volume of the control oil (m^3)
B = 1.3e9;	Bulk modulus (Pa)
Q_S = 0.001;	Flow rate (m^3/s)
A_f = 0.02;	Area constant
C_d = 0.611;	Discharge coefficient
k_i = 5.3;	Current constant (N/A)
k_s = 4000;	Spring stiffness (N/m)
f = 48;	Viscous constant

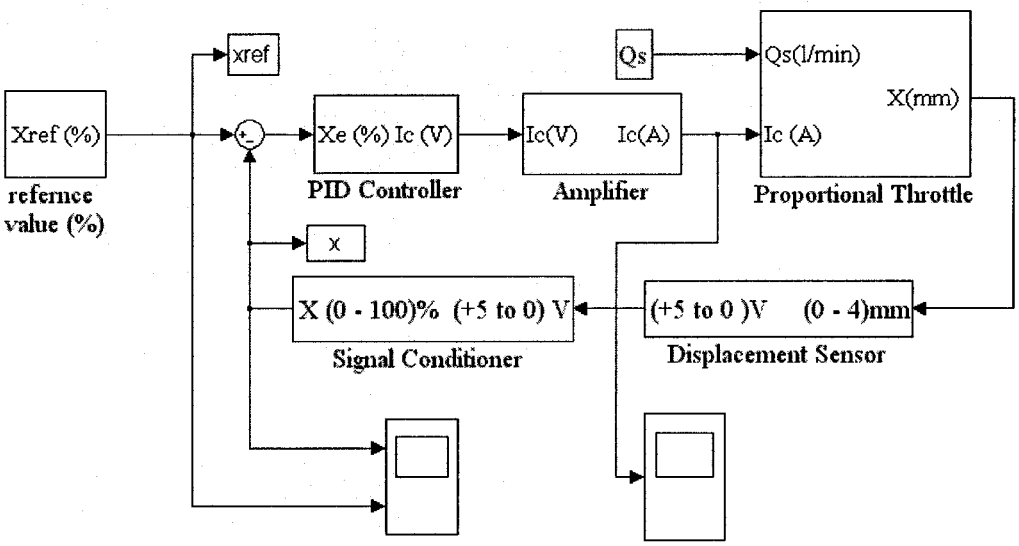

Figure 3.8 The simulation modeling of the compensator

(i) Static Performance of the Compensator The Matlab-Simulink program is used to simulate the static performance of the compensator, with reference command and simulation parameters as shown in Figure 3.9 and 3.10, respectively.

After running the program, the reference command and the static response can be obtained by running the M-file "plot (x_{ref})" and "plot (x)" in the command window, as shown in Figures 3.11 and 3.12, respectively. The static performance of the spool displacement, shown in Figure 3.12, is found to be perfectly linear as expected.

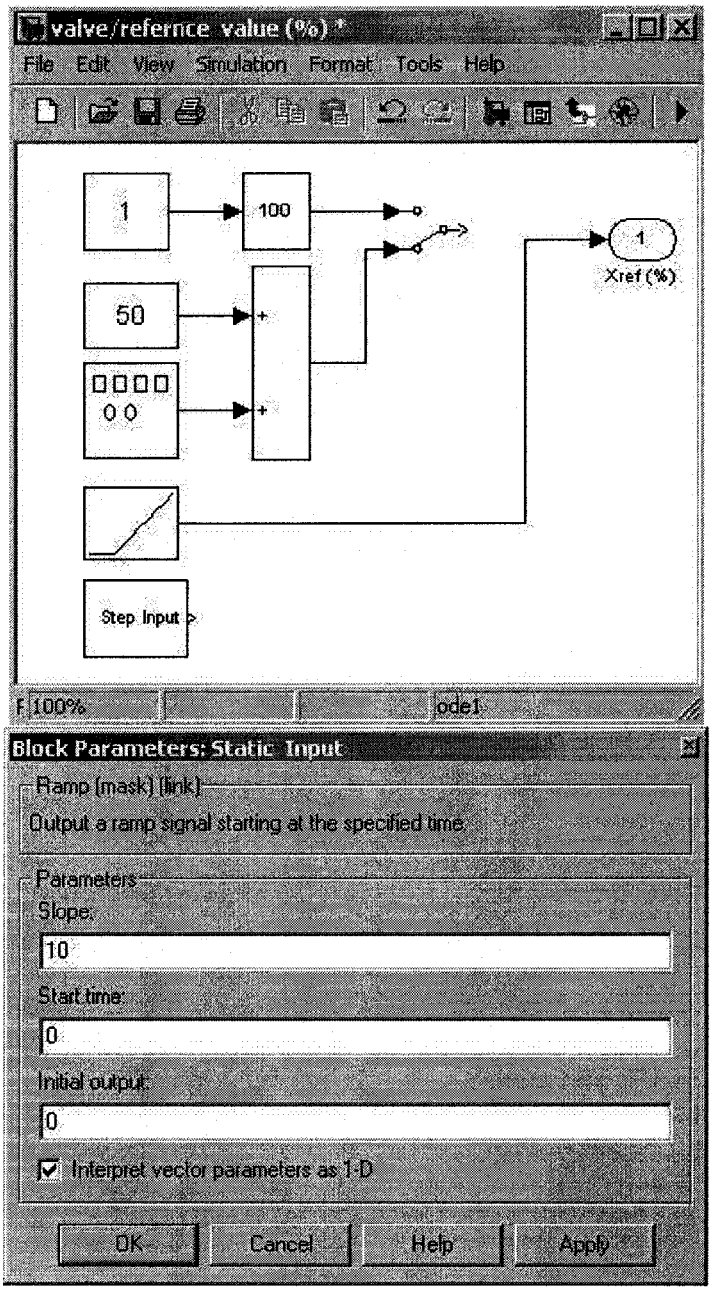

Figure 3.9 Reference command setting and parameters for static performance simulation of compensator

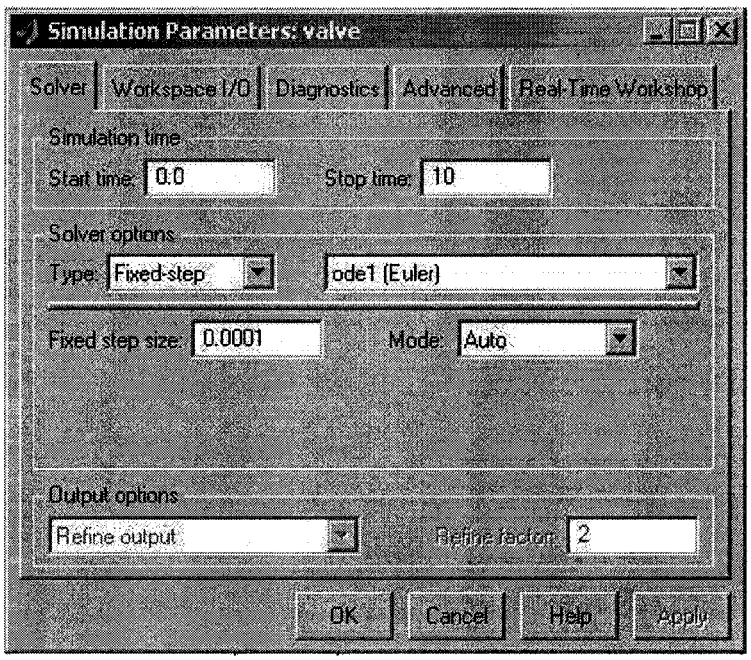

Figure 3.10 Simulation parameters for static performance of compensator

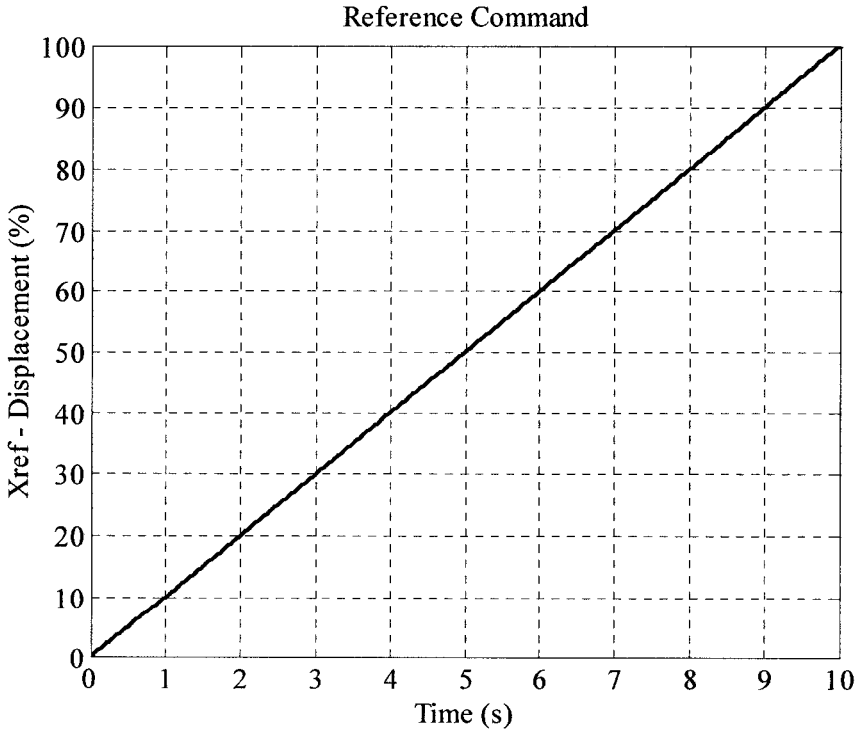

Figure 3.11 Reference command for static performance simulation of compensator

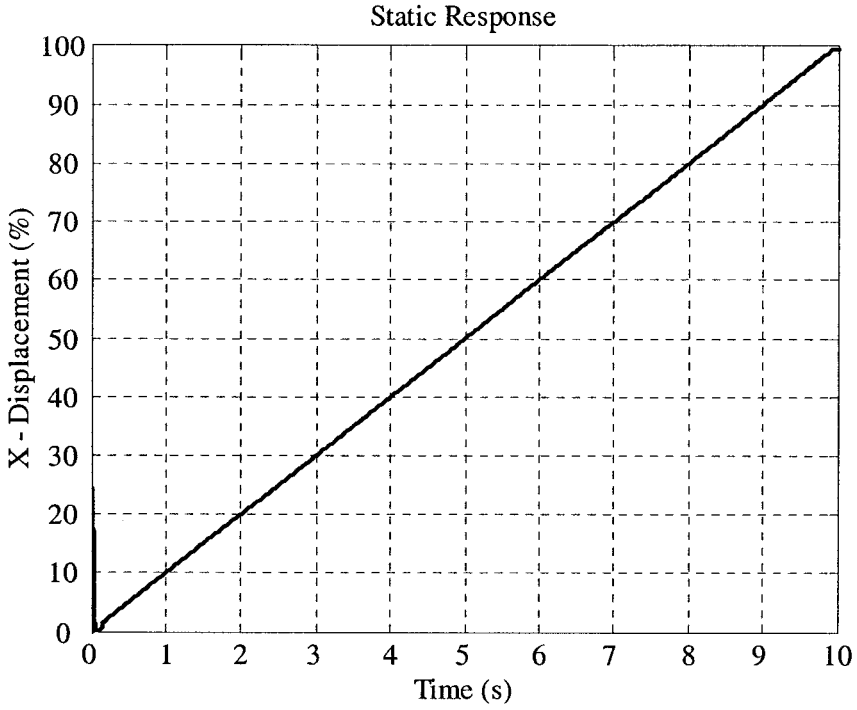

Figure 3.12 The static response of compensator

(ii) Step Response of the Compensator Using successive step input command signals at 25%, 50%, 75% and 100% of the maximum displacement of the spool, simulations are carried out to investigate the step response. Step input parameters and reference command X_{ref} are designated as shown in Table 3.1 and Figure 3.13, respectively. The simulation parameters are same as those used to study the static performance.

Table 3.1 Parameters for step inputs

step input number	1	2	3	4	5	6	7	8
step time (s)	1	2	3	4	5	6	7	8
initial value (%)	0	0	0	0	0	0	0	0
final value (%)	25	-25	50	-50	75	-75	100	-100
sample time (s)	0.001	0.001	0.001	0.001	0.001	0.001	0.001	0.001

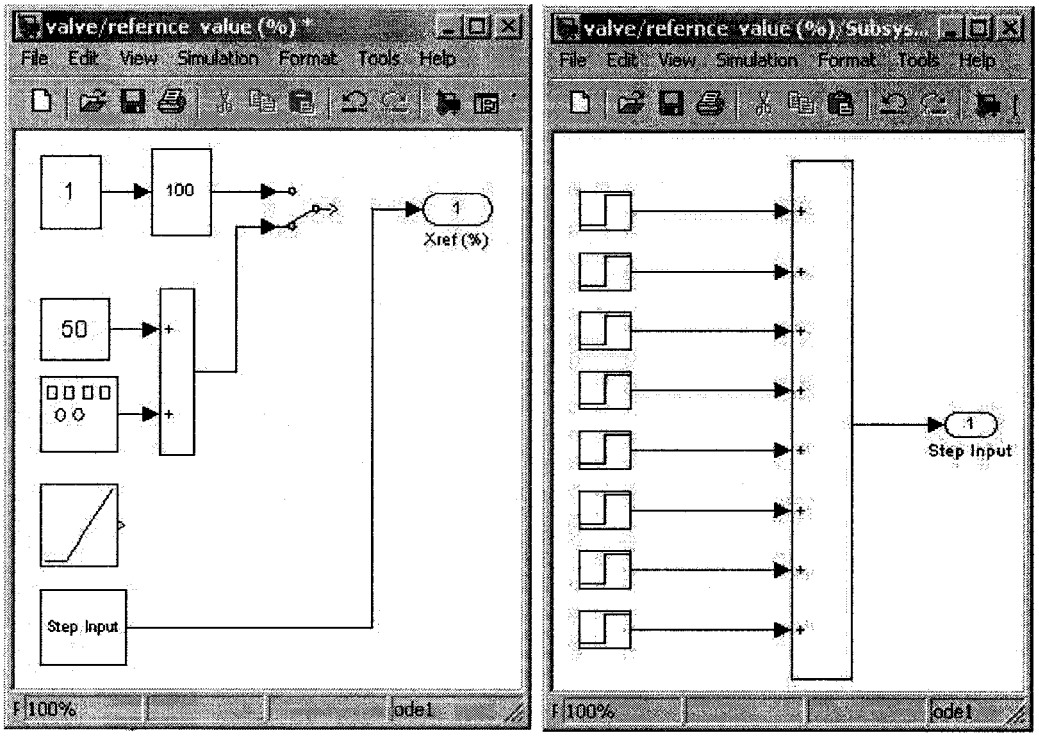

Figure 3.13 Reference command setting for simulation of step response of compensator

After running the program, the reference command and the step response can be obtained by running the M-file "plot (x_{ref})" and "plot (x)" in the command window, as shown in Figure 3.14 and 3.15, respectively.

Figures 3.16 and 3.17 show a zoomed view of the compensator step response when the spool moves from the zero position to a certain percentage of its full stroke and vise versa.

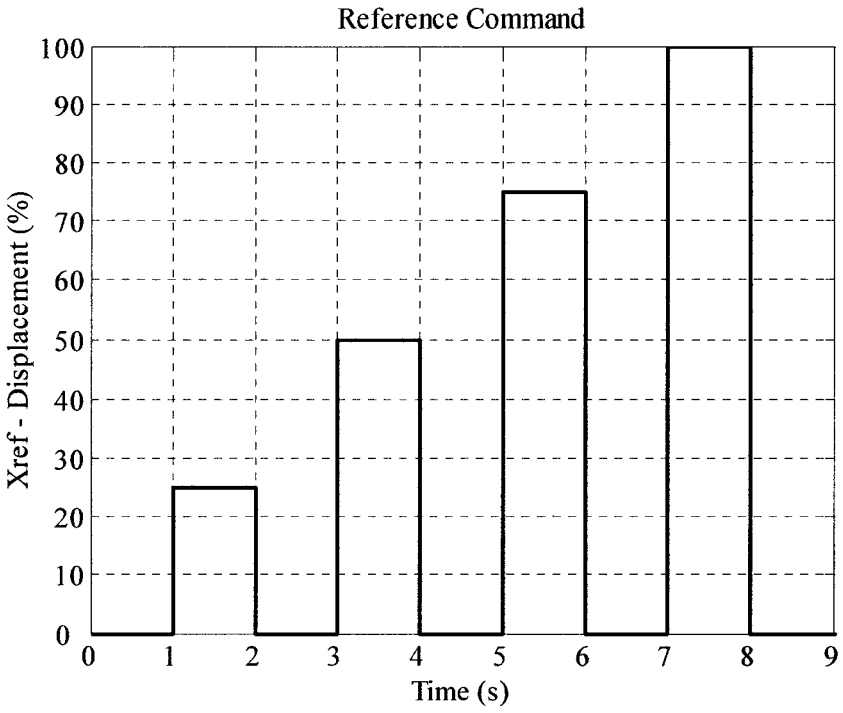

Figure 3.14 Reference command for step response simulation of compensator

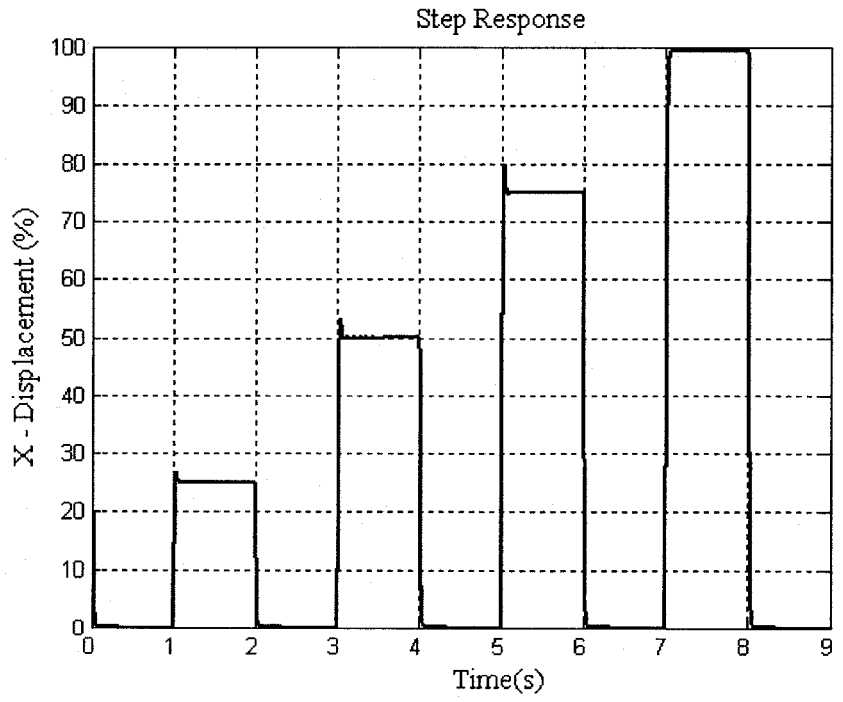

Figure 3.15 The step response of compensator

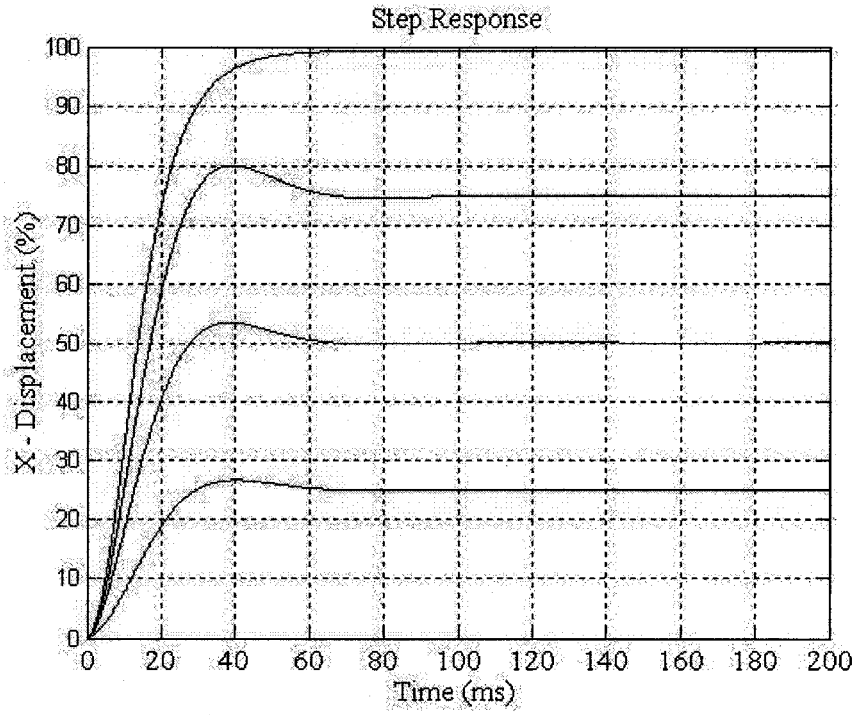

Figure 3.16 Step response of compensator when the spool moves from zero position to different percentages of its full stroke

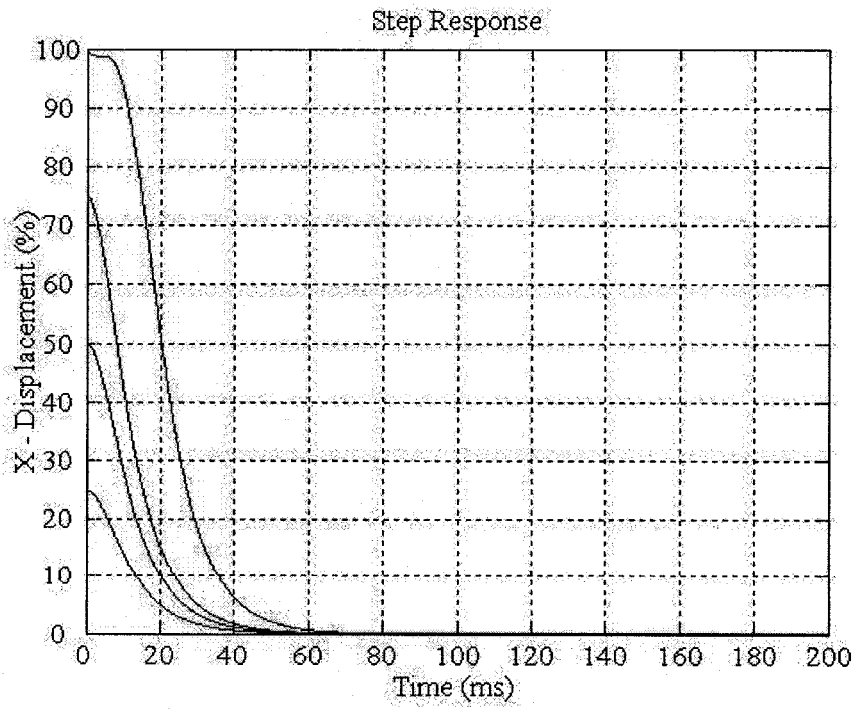

Figure 3.17 Step response of compensator when the spool moves from different percentages of its full stroke to zero position

(iii) Harmonic Response of the Compensator The harmonic signals are used as reference commands, as shown in Figure 3.18, in order to investigate the frequency response of the compensator. Frequencies are set at 1 Hz, 10 Hz, 20 Hz, and 30 Hz, which covers the pump speed of 1450 rpm. Running the program, we get the reference commands and the outputs at 1 Hz, 10 Hz, 20 Hz, and 30 Hz, as shown in Figure 3.19.

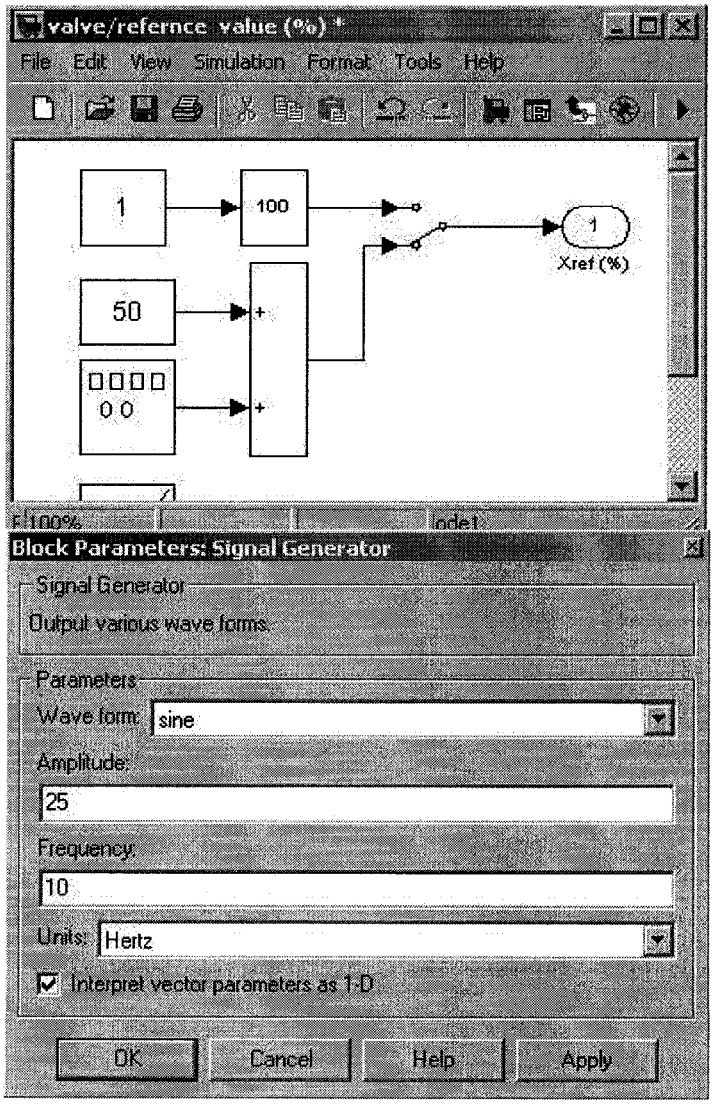

Figure3.18 Reference command setting for the simulation of harmonic response of compensator

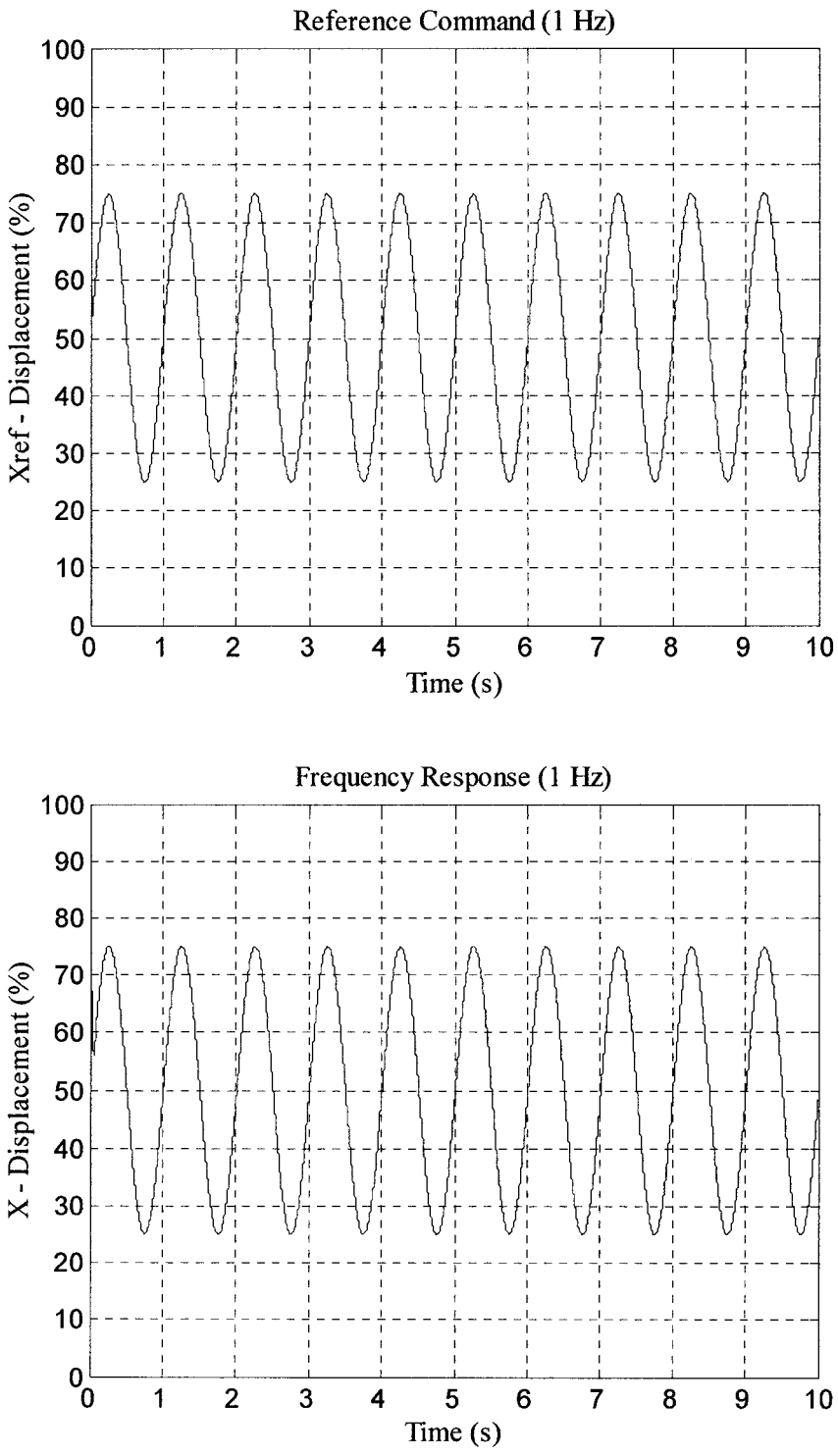

Figure 3.19(a) The reference commands and the frequency response of compensator

(Case 1 Frequency = 1 Hz, Amplitude = 25%)

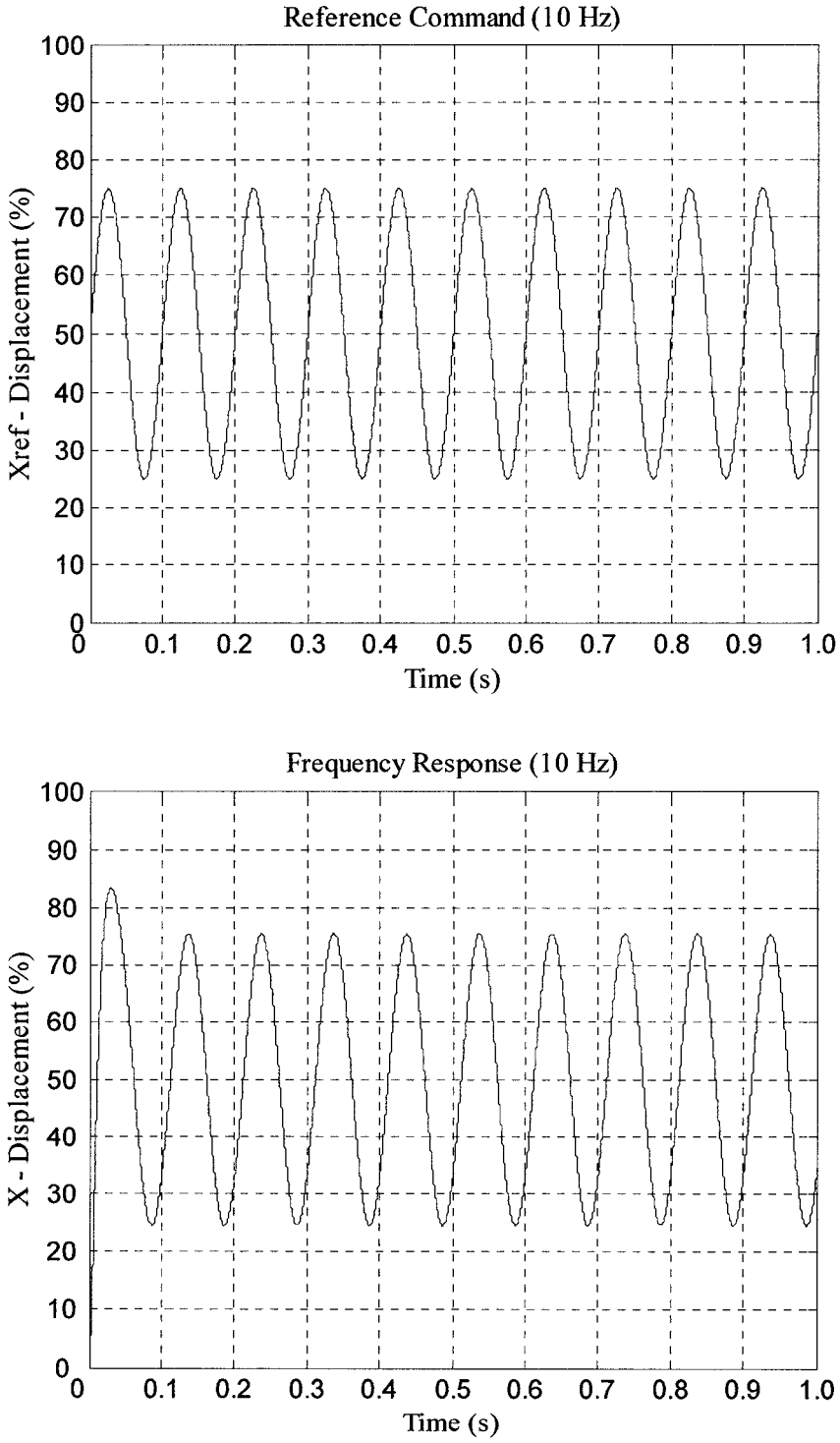

Figure 3.19(b) The reference commands and the frequency response of compensator

(Case 2 Frequency = 10 Hz, Amplitude = 25%)

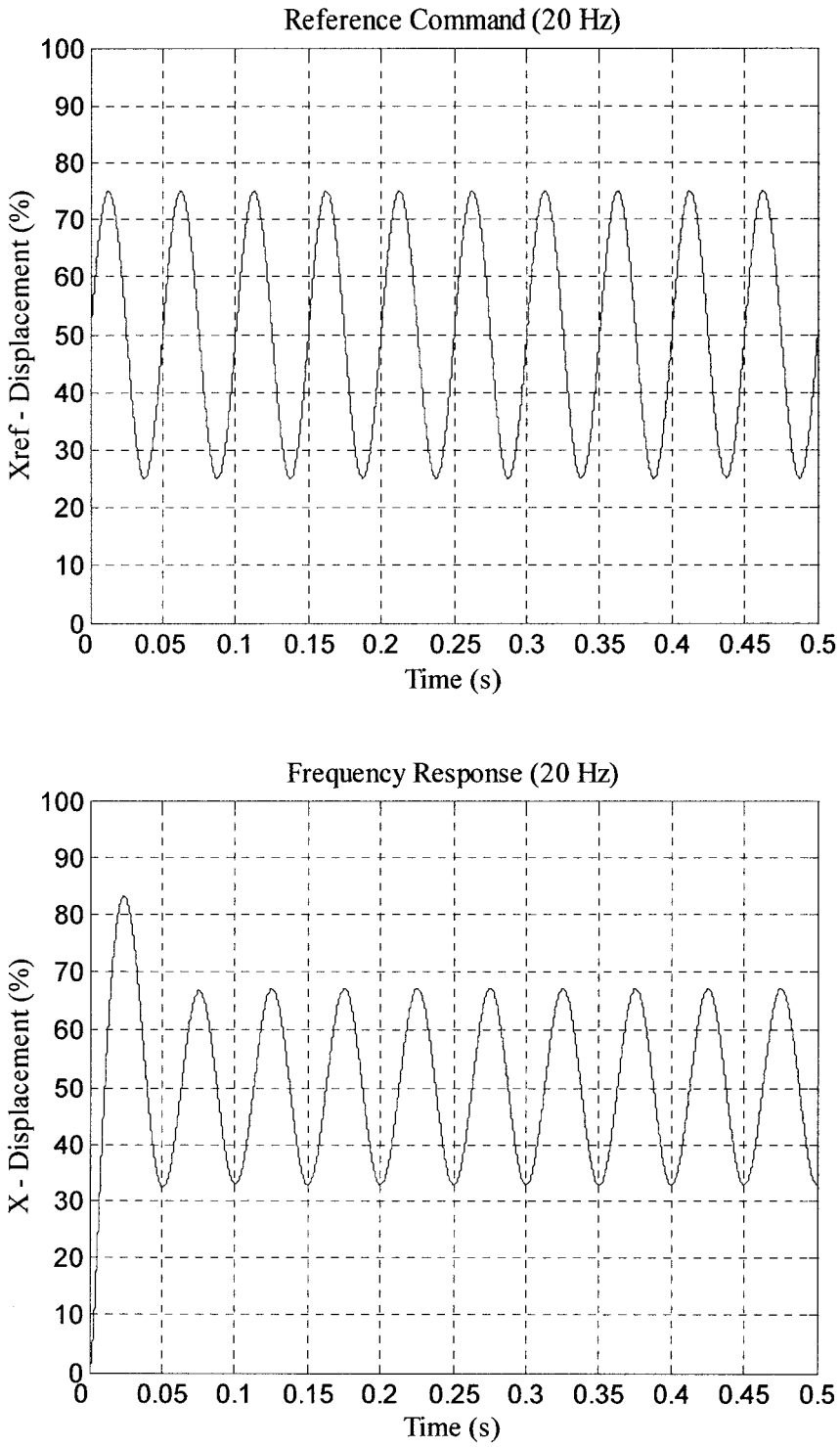

Figure 3.19(c) The reference commands and the frequency response of compensator

(Case 3 Frequency = 20 Hz, Amplitude = 25%)

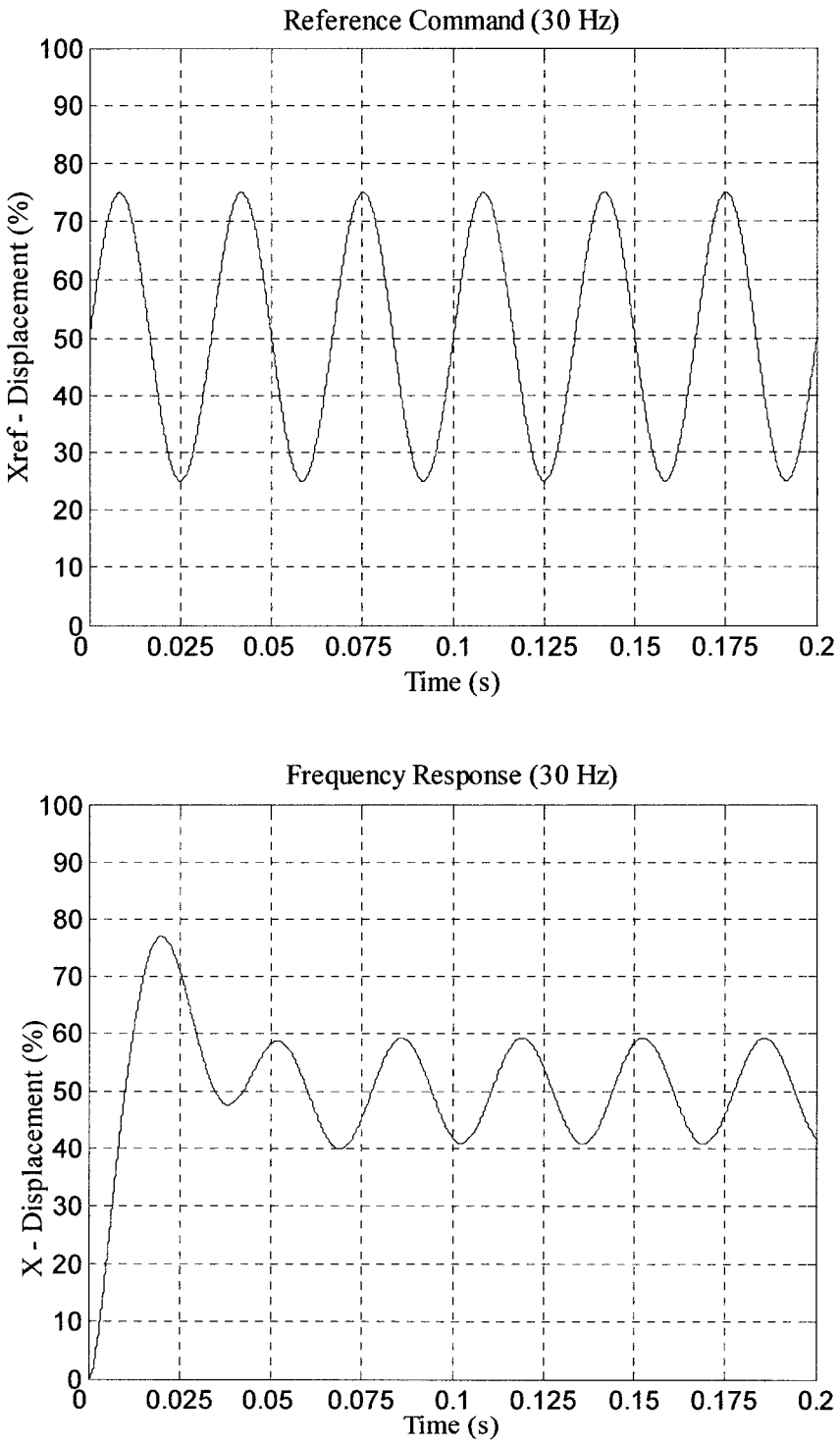

Figure 3.19(d) The reference commands and the frequency response of compensator

(Case 4 Frequency = 30 Hz, Amplitude = 25%)

3.2 Simulation of the Variable Displacement Pump

3.2.1 Proposed Control Schemes

The pump performance will first be simulated using double negative feedback control loops as shown in Figure 3.20. The figure illustrates an inner closed loop that represents system type 0 and is used to control the position of the proportional valve spool using a PID controller. The outer closed loop represents system type 1 and is employed to control the swash plate swiveling angle using a PD controller [20].

A single negative feedback control loop is proposed [23] as the second control scheme and is shown in Figure 3.21. In this scheme, only the outer control loop is considered based on the acceptable open loop characteristics of the proportional valve. The reason behind this is to make the system less responsive and consequently to get rid of the steady state vibration of the swash plate. At the same time, the control scheme and its electronic hardware is simplified and there is a reduction in the cost of the pump system.

The dynamic performance of the proportional valve has been investigated already in both open and closed loop conditions [20].

The Matlab-Simulink simulation program was further developed to simulate the pump and its valve dynamics with the different control schemes proposed.

3.2.2 Simulation of the Pump Step Response at Constant Load

The Matlab-Simulink simulation program is now used to simulate the pump static and dynamic characteristics with the two proposed control schemes as shown in Figure 3.20 and 3.21. Simulations were carried out to study the static and dynamic performance of the 9-piston pump with a 40 cc/rev geometric volume that has the design parameters presented in Appendix A.

These two control schemes were: (i) with a double feedback control loop, and (ii) with a single feedback control loop, studied by Dr. Medhat Khalil [20].

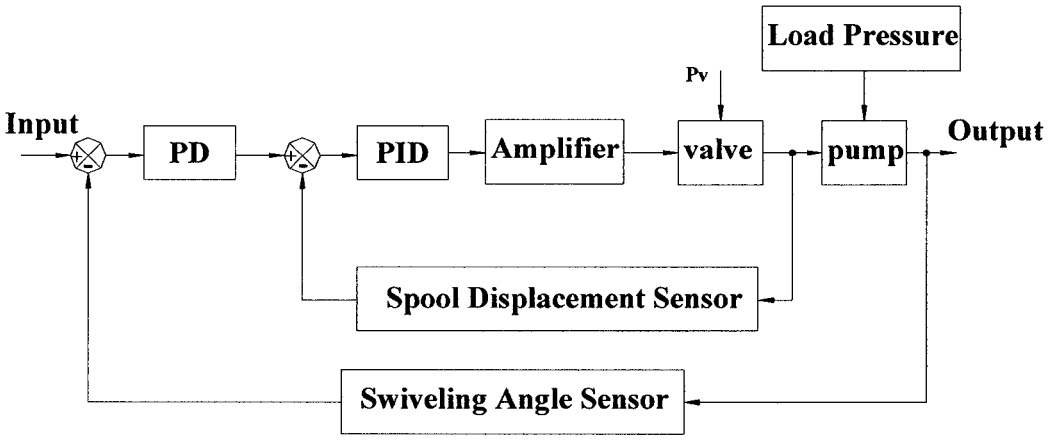

Figure 3.20 Pump controlling using double feedback loops and PID controller [20]

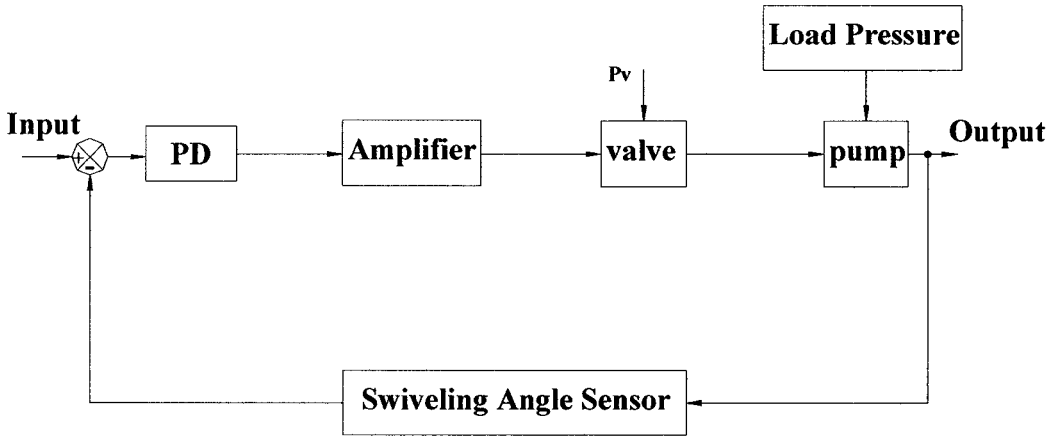

Figure 3.21 Pump controlling using single feedback loop and PD controller [20]

Using successive step input command signals equal to 25%, 50%, 75% and 100% of the maximum swash plate swiveling angle, simulations were carried out at constant load pressure equal to 10MPa. When the pump step response to the previous signals reach the steady state, the command signals are also reduced to zero in a stepwise manner. The simulations are run twice; once for each proposed control scheme.

(i) Double Feedback Control Loops The first control scheme considered in the simulation is a double feedback control loops as shown in Figure 3.20, in which the outer closed loop employed a PD pump controller whereas the inner closed loop used a PID valve controller. An ultimate sensitivity method is used to begin to parameterize the PD pump controller, which ended up having a relatively large settling time. Considering the future constant power operation of the pump, a short

settling time is recommended in order to protect the prime mover against power shocks during the transient periods in which the loading pressure increases. Therefore, the PD parameters were then tuned a little more, and were found to be $K_p = 1$, $T_i = \infty$ and $T_d = 0.02$. The parameters of the PID proportional valve controller were found to be $K_p = 1$, $T_i = 0.01$ and $T_d = 0.001$.

With these PID parameters and the control scheme, the simulation modeling was built. Figure 3.22 illustrates the response of the pump to successive step inputs at a constant load pressure during a 9 second time span. Figures 3.23 and 3.24 show a zoomed view of the transient periods of pump response when the swiveling angle increases from the zero position to different percentages of its maximum value and vise versa [20]. Considering this control scheme and the selected PID parameters, the transient periods have a nearly 80 ms settling time when the swiveling angle is increasing, and 60 ms when the swiveling angle is decreasing, as shown in Figure 3.23 and 3.24, respectively. Both cases experience a 10ms delay time. The figures demonstrate that the settling time is reduced on account of having a steady state swiveling angle vibration. The magnitude of the steady state vibration is reduced to 1% instead of the 3% that was recorded in Figure 4.11a in [20].

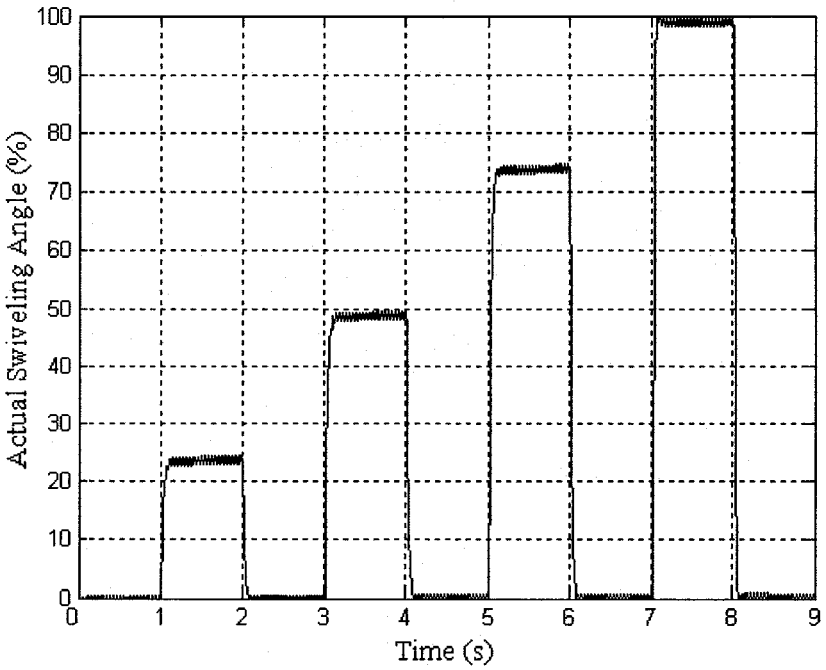

Figure 3.22 Pump step response at constant load pressure using double feedback control loops with PID controller [20]

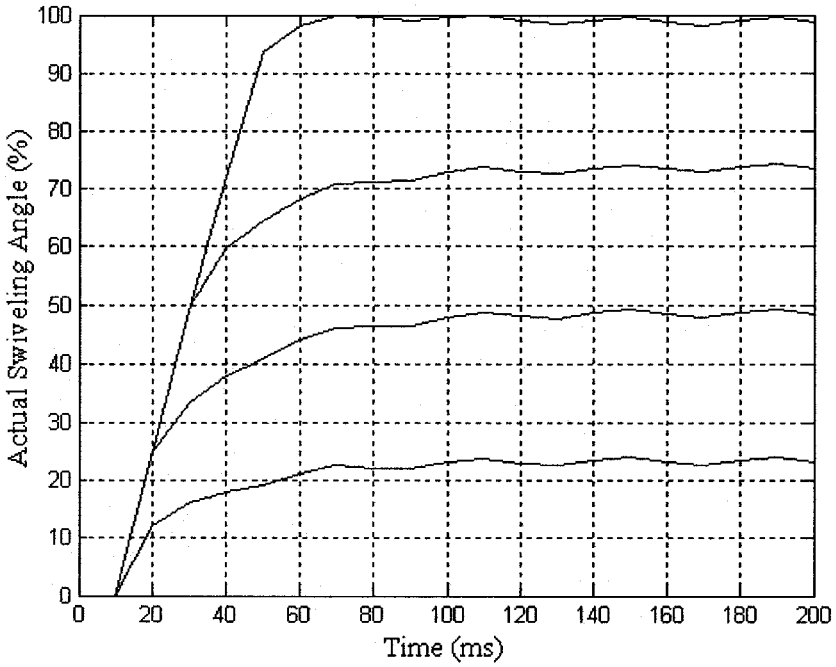

Figure 3.23 Variation of swiveling angle with time using double feedback control loops with PID controller [20]

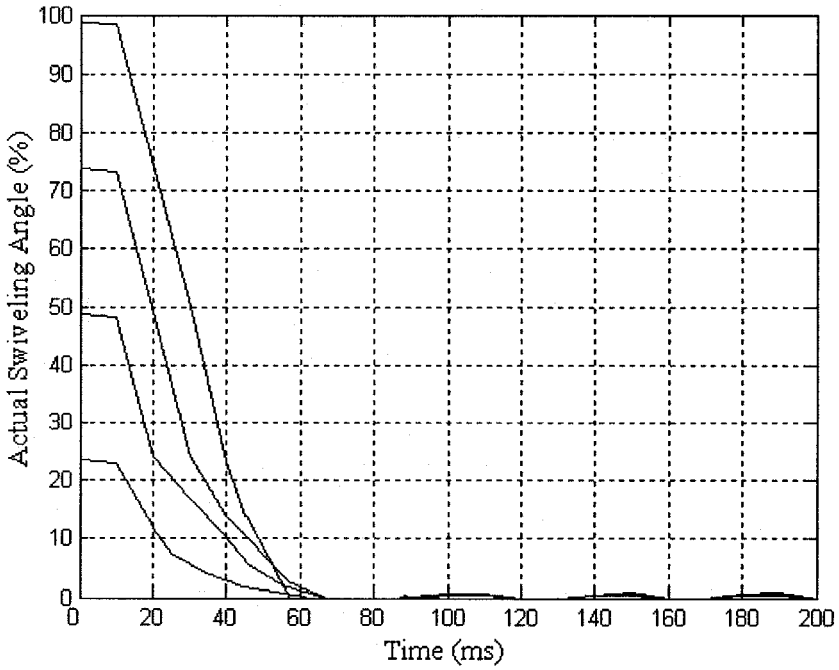

Figure 3.24 Variation of swiveling angle with time using double feedback control loops with PID controller [20]

(ii) Single Feedback Control Loop The second control scheme with a single feedback control loop with PD pump controller is then considered for simulation. There are two motives for considering such a control system. First is to make the system less responsive in order to suppress the swash plate steady state vibration so that the pump flow rate will be smoothened as much as possible. Second is for the reductions in cost of manufacturing the pump by removing the electronic circuit of the proportional valve as well the spool displacement sensor. The trial for decreasing the settling time with the single feedback loop in order to keep the convenience of the constant power operation of the pump leads to an unstable system. The PD controller is then retuned to satisfy the requirements of the system stability. The new parameters were found to be $K_p = 1$, $T_i = \infty$ and $T_d = 0.01$ [20].

With these PD parameters and the control scheme, the simulation modeling was built. As shown in Figure 3.25, the result was a less responsive system that avoided the steady state vibration of the swash plate. Figures 3.26 and 3.27 show a more gradual change of the swiveling angle in the transient periods and the settling time increases to 200 ms, which is inconvenient for the constant power operation of the pump. On the other hand, this can be considered an advantage when the control piston reaches the end of its stroke with a nearly zero velocity, which reduces the end impact.

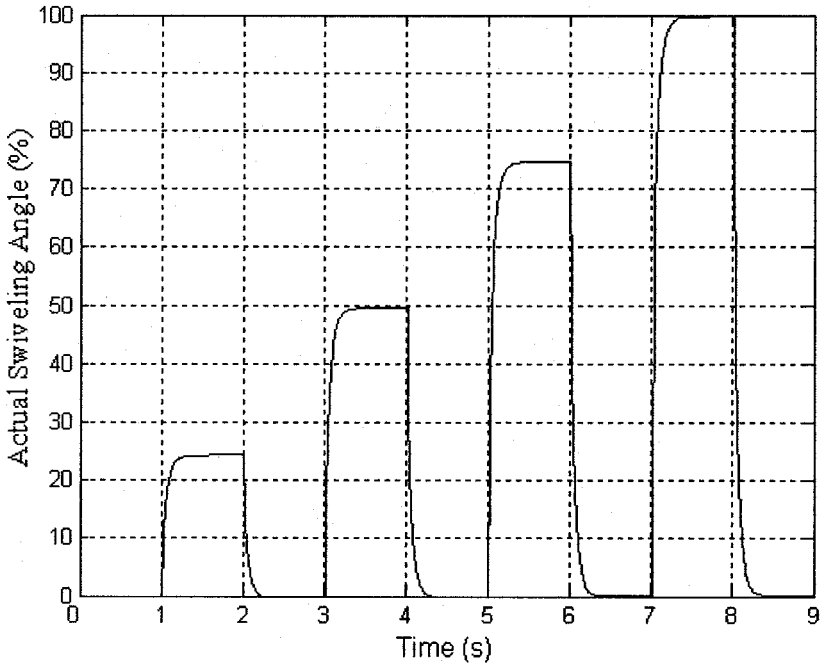

Figure 3.25 Pump step response at constant load pressure using single feedback control loop with PD controller [20]

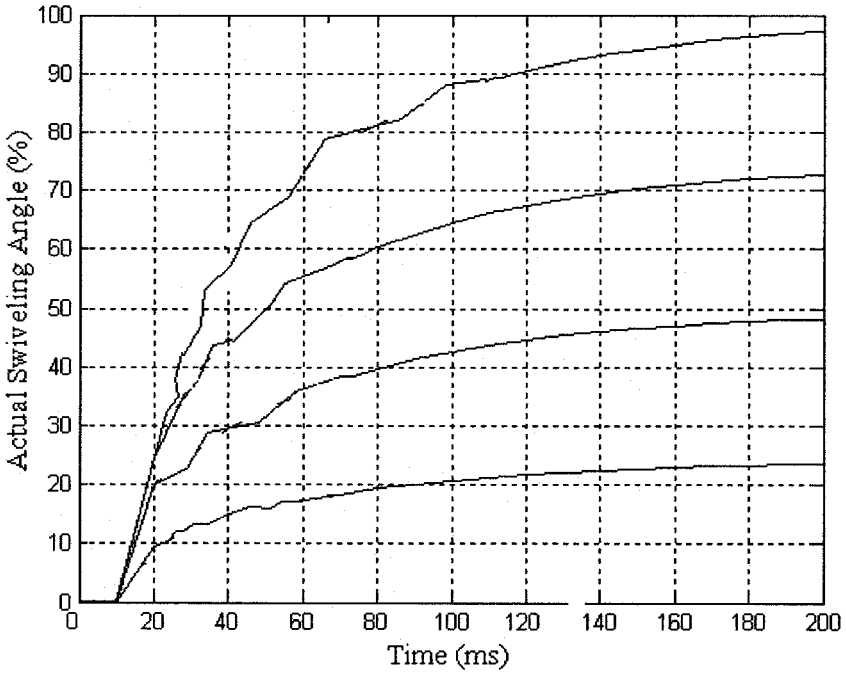

Figure 3.26 Variation of swiveling angle with time using single feedback control loop with PD controller [20]

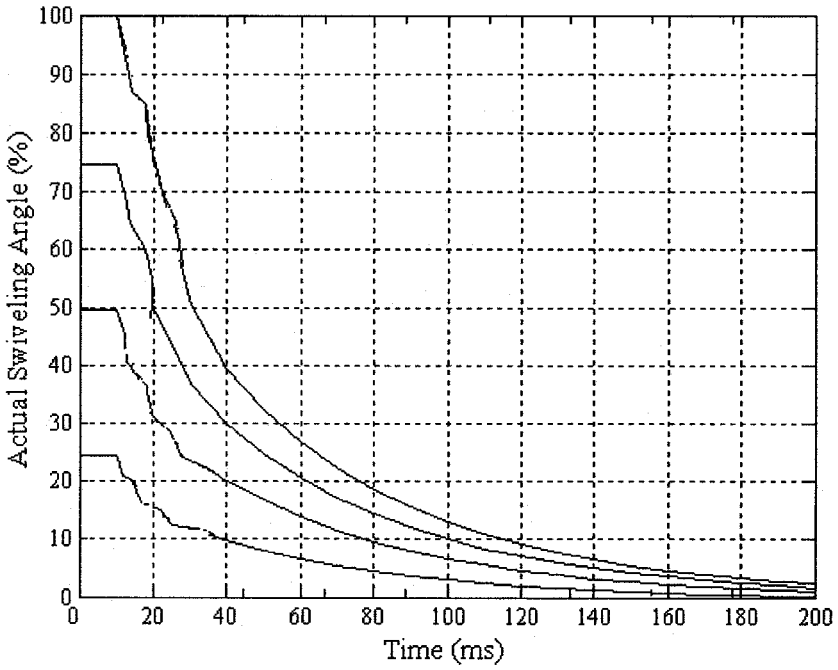

Figure 3.27 Variation of swiveling angle with time using single feedback control loop with PD controller [20]

3.2.3 Simulation of the Pump Static Characteristics at Constant Load

Having established the control schemes and discussed the pump step response in the previous section, the pump static characteristics may now be investigated. The command signals are assumed to change slowly and gradually from zero to 100%, while the corresponding normalized changes in the swash plate swiveling angle are recorded. The static characteristics of the simulated pump confirm the presence of the steady state vibration when the double negative feedback control loop is considered with a PID controller, as shown in Figure 3.28. Using the single feedback loop eliminates the swiveling angle steady state vibration as shown in Figure 3.29. In both the proposed control schemes, the simulation results show linear characteristics of the pump through out the full range of the command signal.

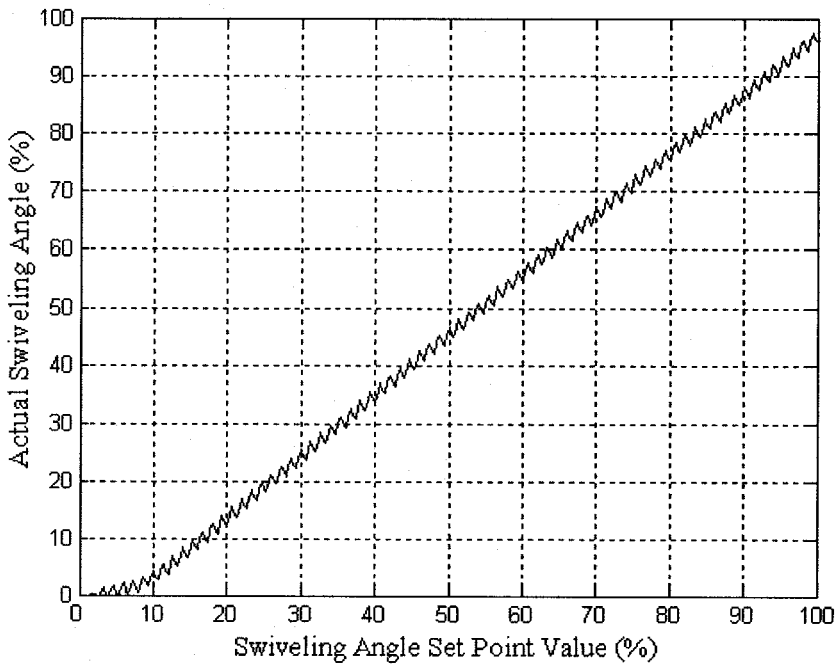

Figure 3.28 Pump static characteristics at constant load pressure using double feedback control loops with PID controller [20]

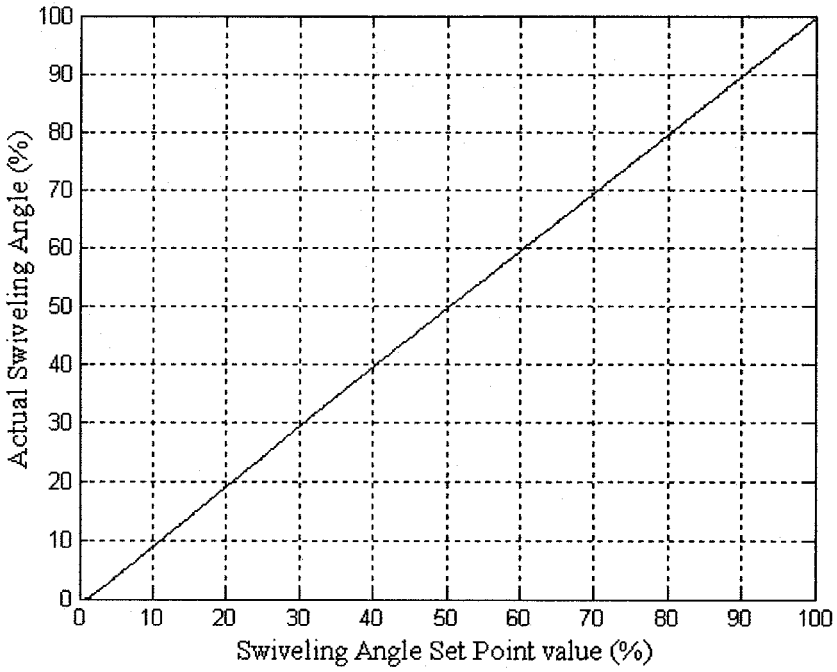

Figure 3.29 Pump static characteristics at constant load pressure using single feedback control loop with PD controller [20]

3.2.4 Simulation of the Pump Frequency Response in Constant Power Operation

A harmonic variation is the first approximation for any type of variations in the load pressure is quite common in practical applications. Therefore, it is important to study the pump response to harmonic input. As shown in [24], the swash plate was assumed to have an initial position equal to 50% of its maximum inclination angle. The pump is then subjected to a sinusoidal change in load pressure. The change in load pressure is sensed by the pressure sensor and fed back to the arithmetic unit. The latter generates the sinusoidal swash plate inclination angle set point α_{sp} value in accordance with the load pressure change to achieve constant power operation. The

value of α_{sp} is fed to the main process controller in one of the two proposed control schemes. The actual swash plate inclination angle α is then monitored.

Successive simulation runs were carried out with the input frequency increased in steps of 5 Hz to cover a range up to 30 Hz. Simulations were carried out only for the first control scheme (the double feedback control loops). The simulation result presented in Figure 3.30 shows that, the swash plate responds with a sinusoidal fluctuation that has nearly the same input amplitude up to a 15 Hz input frequency.

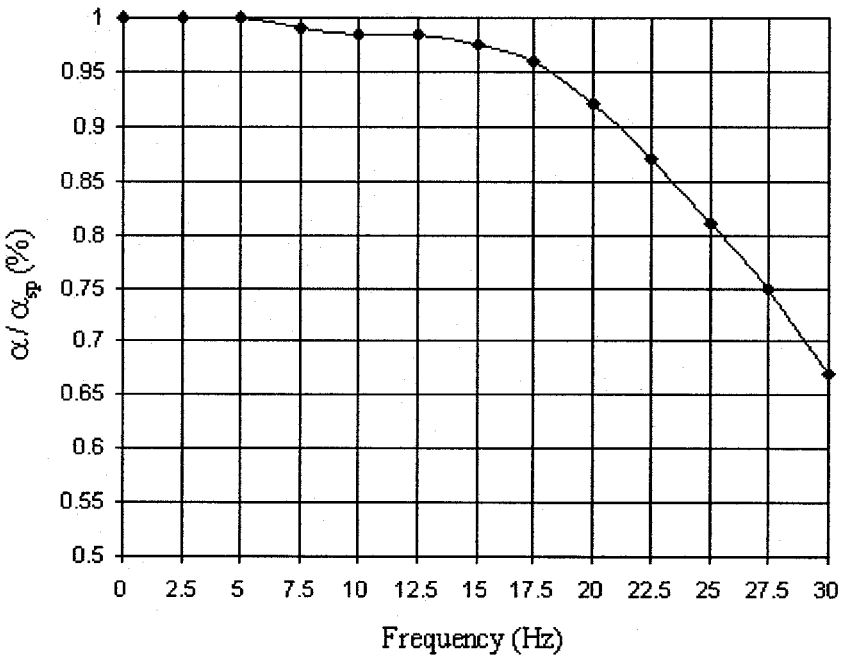

Figure 3.30 Pump constant power operation using double feedback control loops with PID controller [20]

3.3 Simulation of the Hydraulic Control System

Software based on Matlab-Simulink is developed in order to simulate the performance of the hydraulic control system. The simulation modeling is built, as shown in Figure 3.31, to simulate the entire electro-hydraulic control system. The design parameters of the pump are taken from [25]. The design parameters of the compensator are estimated based on its dynamics that are reported by the manufacturer, and then tuned afterwards in the experimental work to be closer to reality.

The control signal that is coming out of the controller equals $K_p[1+1/(T_i s)+(T_d s)]$, where K_p = 0.6 of the ultimate gain, T_i = 0.5 of the ultimate period and T_d = 0.125 of the ultimate period. As reported in [25], the parameters of the PID proportional valve controller are found to be K_p = 1, T_i = 0.01 and T_d = 0.001. The parameters of the PD pump controller are K_p = 1, T_i = ∞ and T_d = 0.02.

Same method is applied in order to parameterize the PID controllers of the compensator control scheme. Parameters of the compensator spool position are K_p = 1, T_i = 0.007 and T_d = 0.005. Parameters of the compensator upstream pressure are K_p = 20, T_i = 0.2 and T_d = $5x10^{-5}$.

Computer runs are carried out to simulate the static and dynamic performance of the system. Rolling mill operating conditions are assumed at very arbitrary steady state values. Rolling speed and rolling load reference values were assumed to be at 40% and 60%, respectively.

The simulation parameters are chosen as shown in Figure 3.32 and the data will be supplied by the M-file in Appendix B.

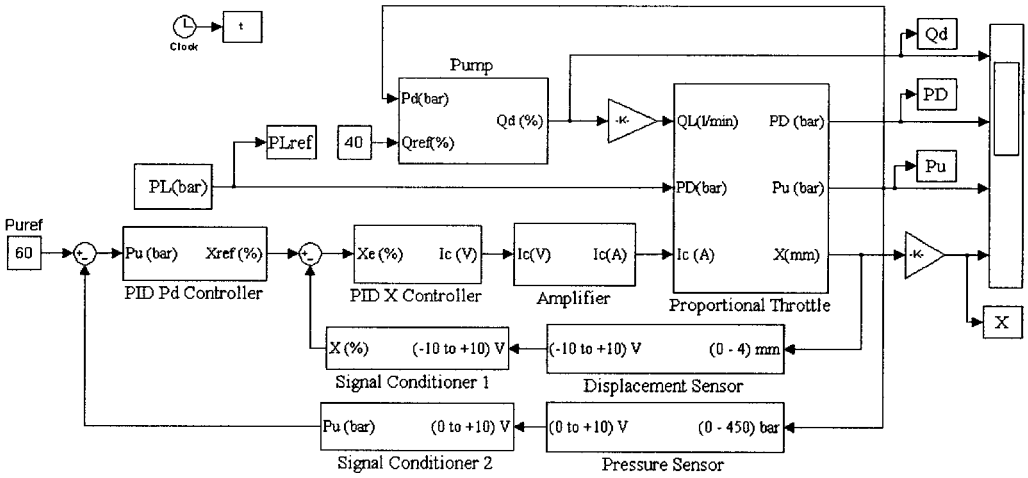

Figure 3.31 The modeling of entire electro-hydraulic control system

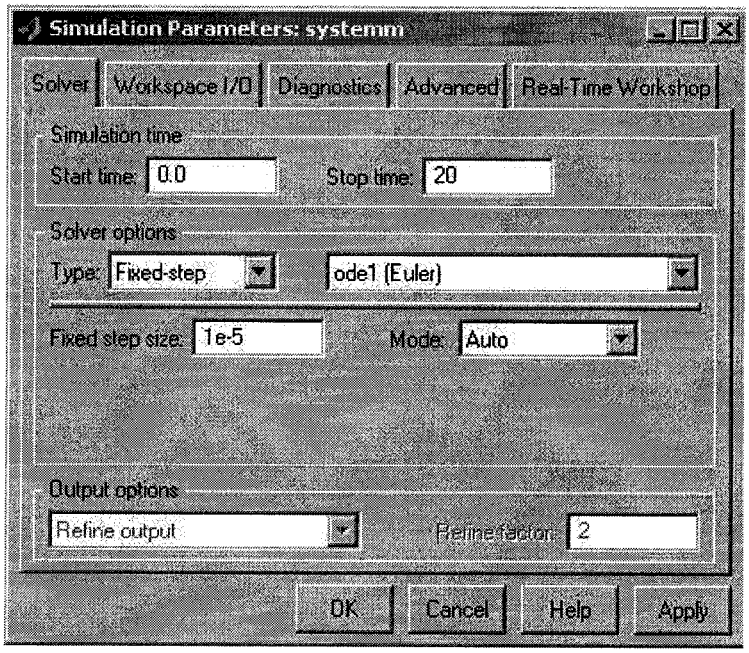

Figure 3.32 Simulation parameters for the hydraulic control system

3.3.1 Simulation of the Hydraulic Control System to the Step Change in the Rolling Torque

To start with, step response of the hydraulic control system is investigated. The downstream pressure P_D is assumed to increase and decrease in a stepwise manner while the other conditions are monitored. As a consequence, the rolling torque changes in a stepwise manner. The reference command is designated as shown in Figure 3.33 and the parameters for step inputs is listed in Table 3.2.

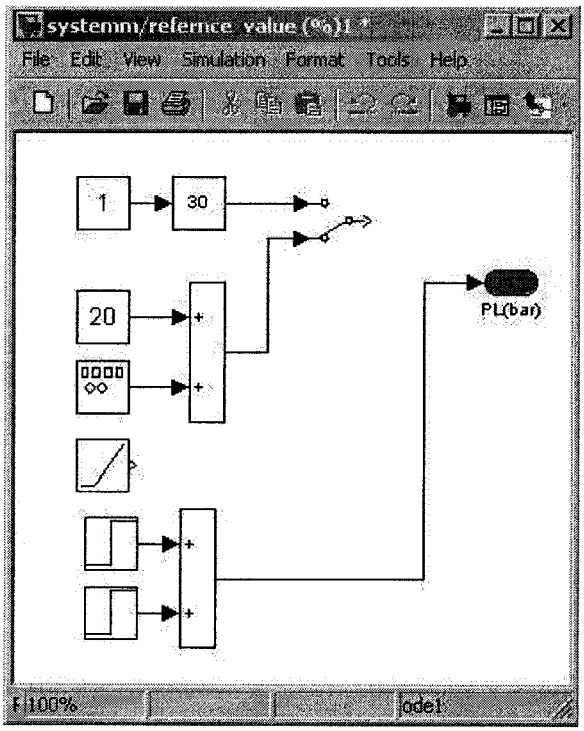

Figure 3.33 Reference command setting for simulation of the hydraulic control system to the step change in the rolling torque

Table 3.2 Parameters for step inputs

step input number	1	2
step time (s)	5	15
initial value (%)	0	0
final value (%)	20	-20
sample time (s)	0.001	0.001

After running the program, the step response of the hydraulic control system can be obtained by executing the commands "plot (t, PD, t, Pu, t, Qd, t, X)" in the command window and the reference command will follow the same way. Figure 3.34 to 3.35 show the reference command and the step response of hydraulic control system, respectively. Figure 3.35 reveals that the rolling speed will not be affected by

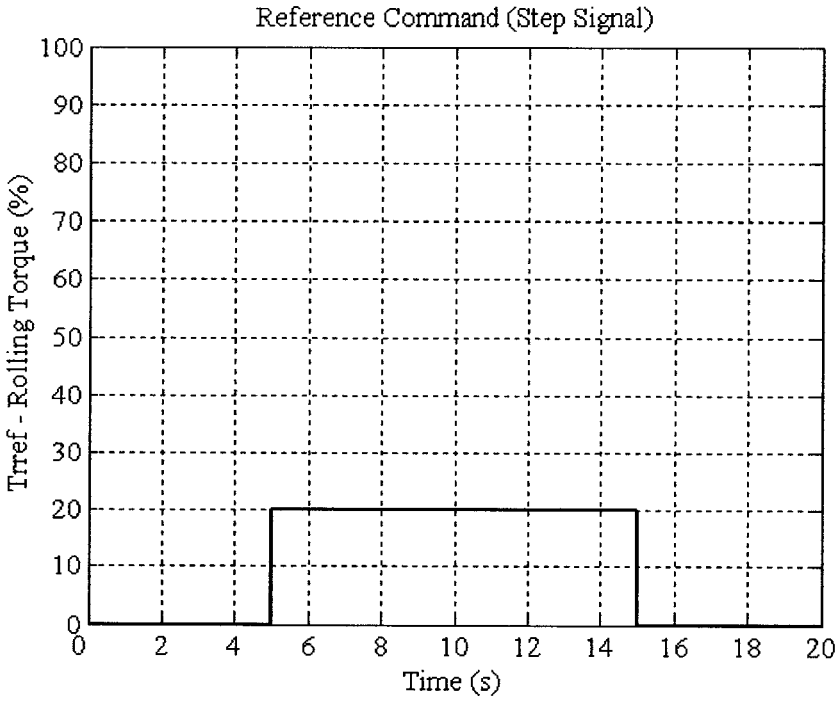

Figure 3.34 The reference command – rolling torque (step signal)

the change in the rolling torque and rolling load experiences shocks at the transient periods of the stepwise change in the rolling torque. In addition, the rolling speed is kept constant.

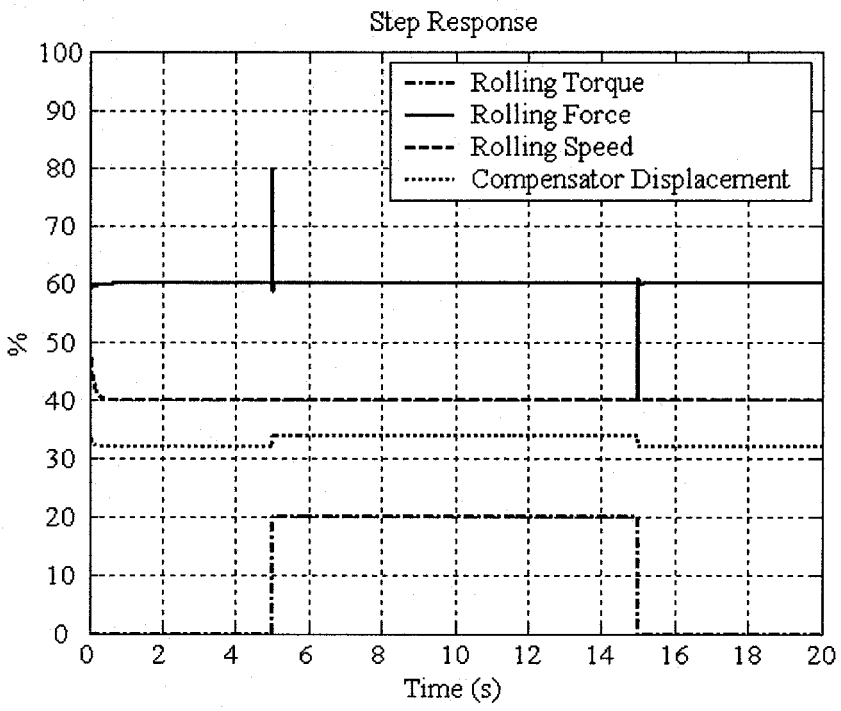

Figure 3.35 The step response of the hydraulic control system

3.3.2 Simulation of the Hydraulic Control System Static Characteristics

Static characteristic of the hydraulic control system is then investigated. Rolling torque is assumed to change gradually from zero to 100%. Reference command is set as shown in Figure 3.36.

The reference command and the static response of hydraulic control system can be obtained in the same way as mentioned in 3.3.1, as shown in Figure 3.37 and Figure 3.38, respectively.

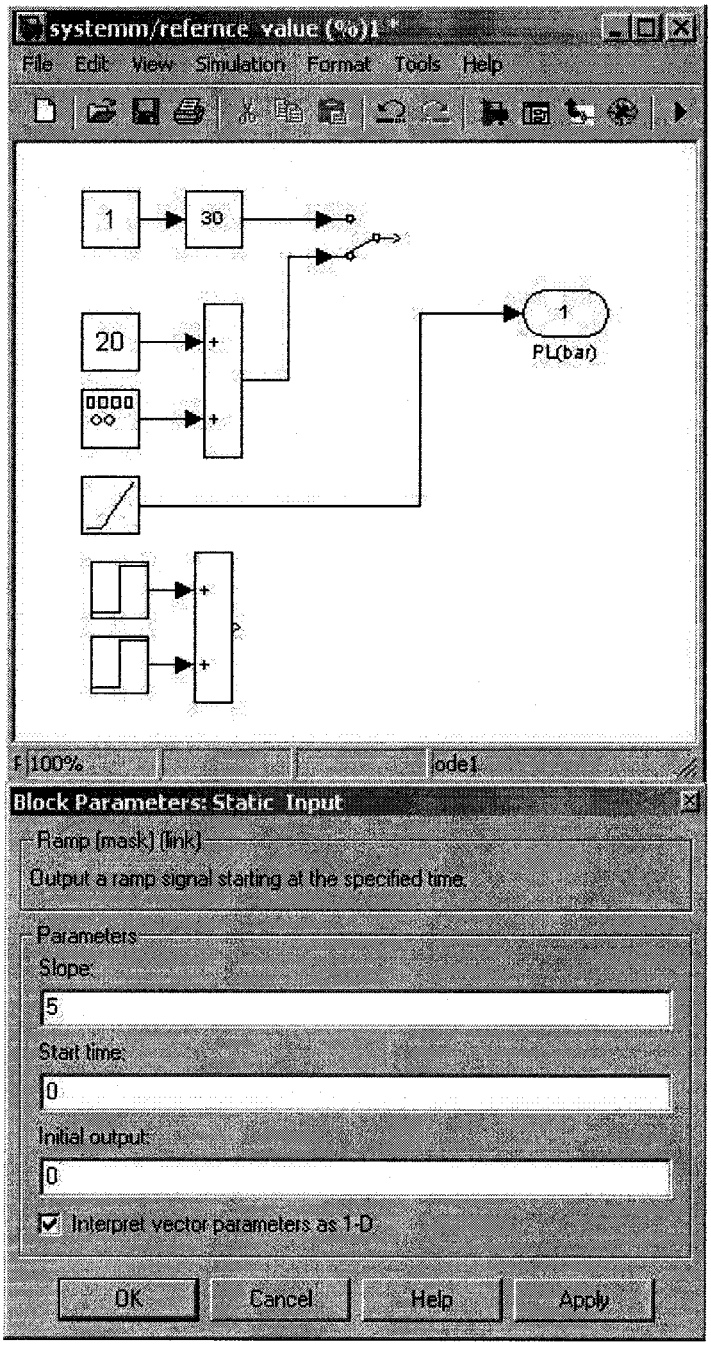

Figure 3.36 Reference command setting and parameters for static performance simulation of the hydraulic control system to the gradual change in the rolling torque

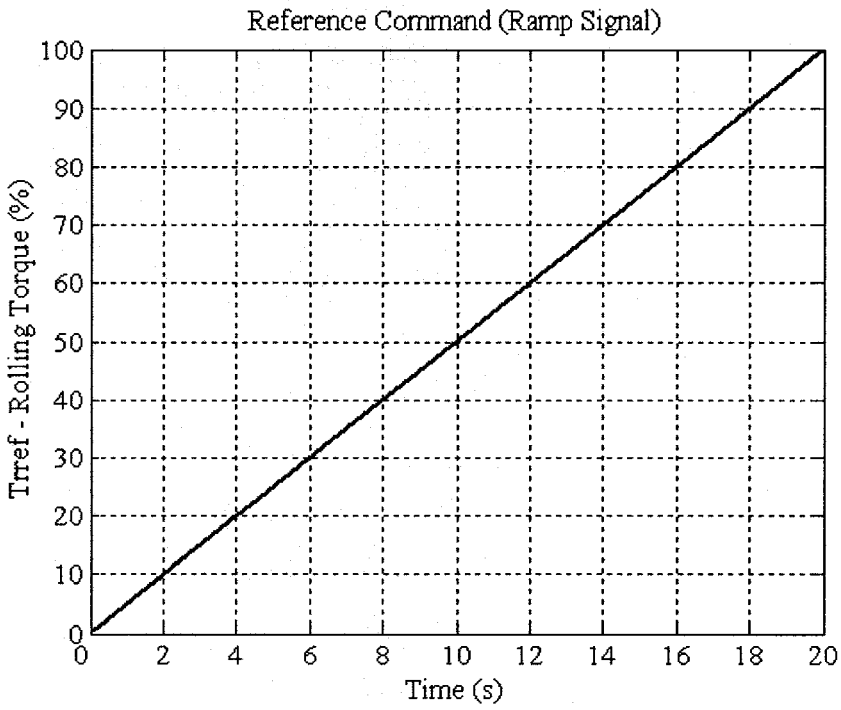

Figure 3.37 The reference command – rolling torque (ramp signal)

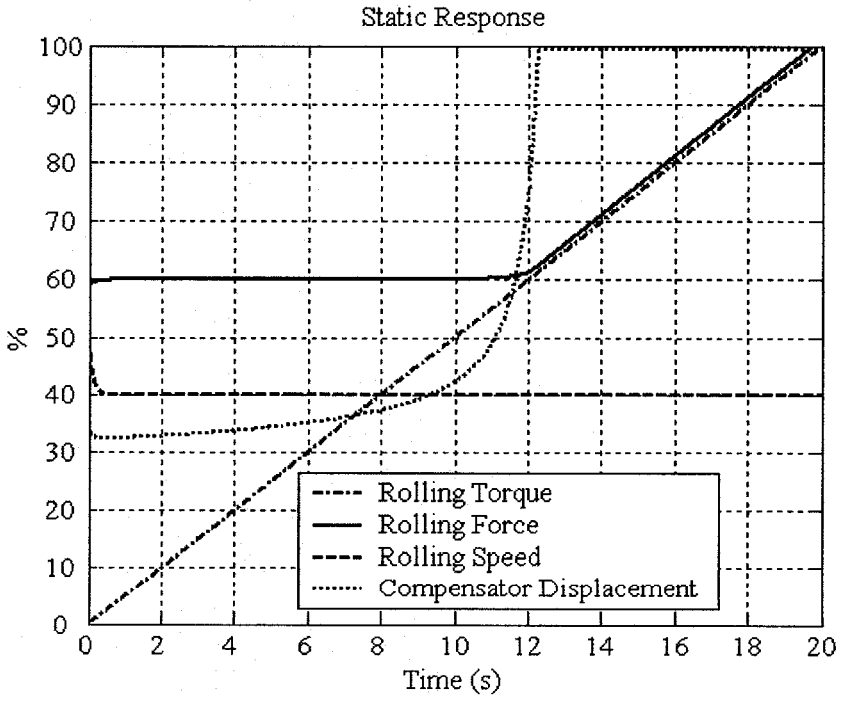

Figure 3.38 The static response of the hydraulic control system

3.3.3 Frequency Response of the Hydraulic Control System

Frequency response of the hydraulic control system is finally investigated. The downstream pressure P_D is assumed to change in a harmonic manner. As a consequence, the rolling torque also changes in a harmonic manner. A sinusoidal signal, of 10% amplitude and 0.1 Hz frequency, represents harmonic change of the rolling torque. The reference command is designated as shown in Figure 3.39.

After running the program, the frequency response of the hydraulic control system can be obtained by executing the commands "plot (t, PD, t, Pu, t, Qd, t, X)" in the command window and the reference command follows in the same way. Figure 3.40 and 3.41 show the reference command and the frequency response of hydraulic control system, respectively. Results show that the rolling speed is not affected and the spool of the compensator responds sinusoidally in order to keep the rolling load constant.

Next we will investigate the frequency responses of the system due to a wide range of frequencies. The frequencies of the input signals are 0.5 Hz, 1 Hz, 2 Hz and 3 Hz, respectively. Figures 3.42 to 3.49 show the reference commands and the simulation results, respectively. From these results it is verified again that the rolling speed is not affected and the spool of the compensator responds sinusoidally in order to keep the rolling load constant. However, it is found that the amplitude of the displacement of the compensator decreases with the increase in the frequency of the input signal.

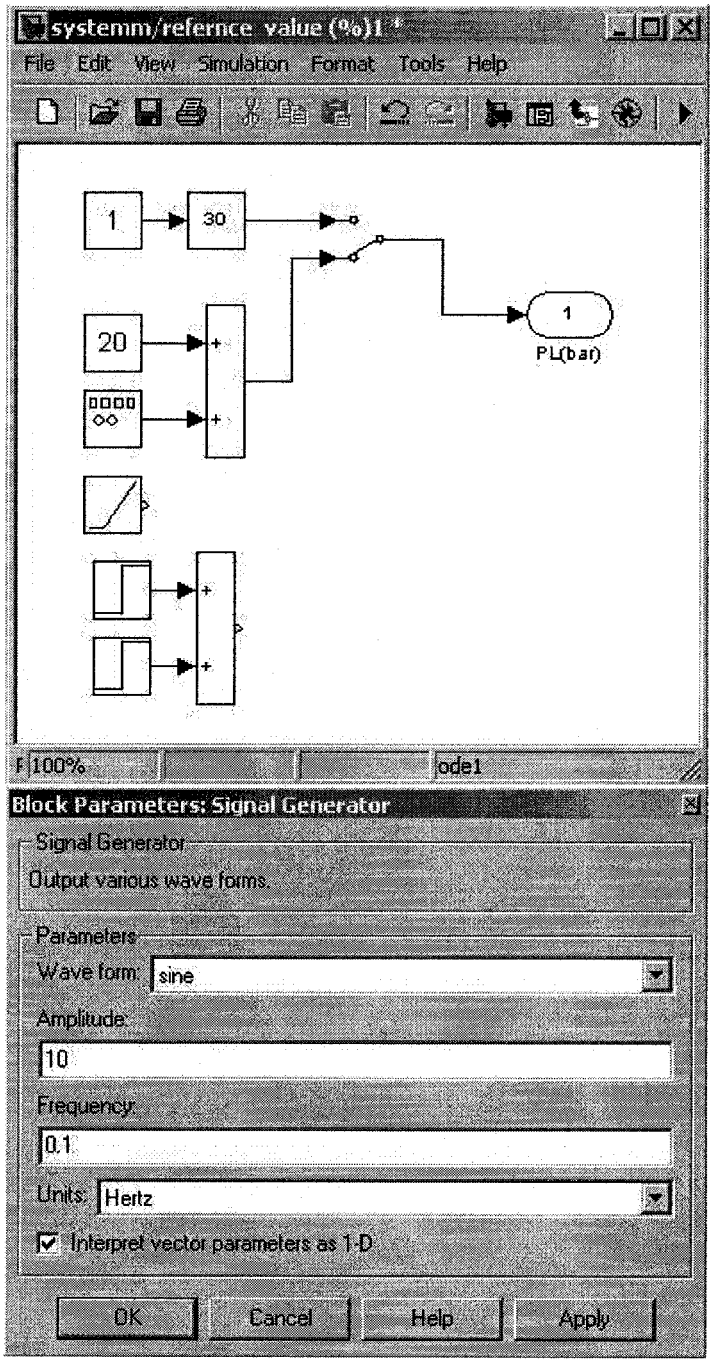

Figure 3.39 Reference command setting and parameters for frequency response of the hydraulic control system

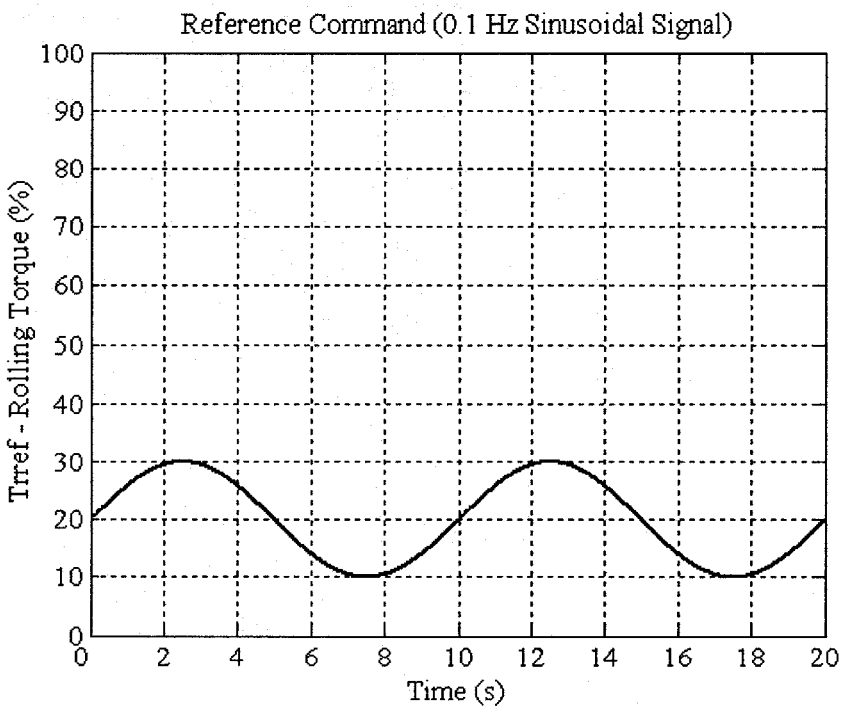

Figure 3.40 The reference command – 0.1 Hz sinusoidal rolling torque

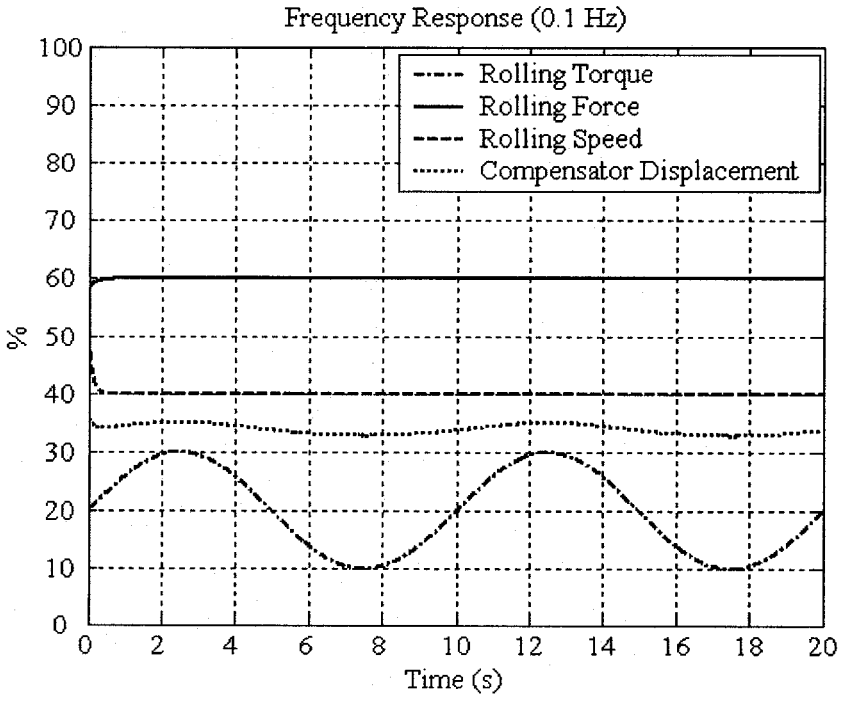

Figure 3.41 The frequency response of the hydraulic control system (0.1 Hz)

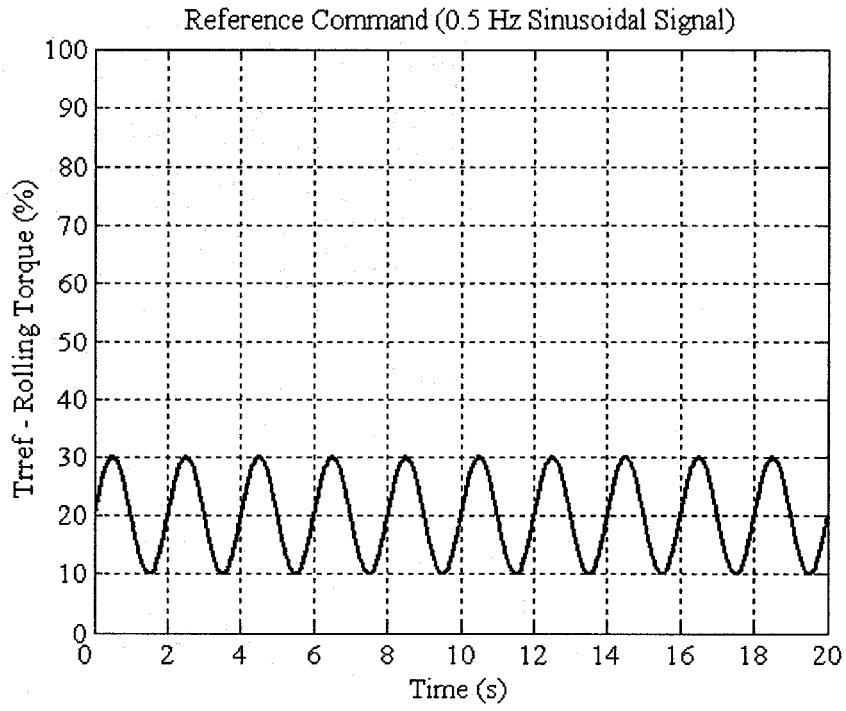

Figure 3.42 The reference command – 0.5 Hz sinusoidal rolling torque

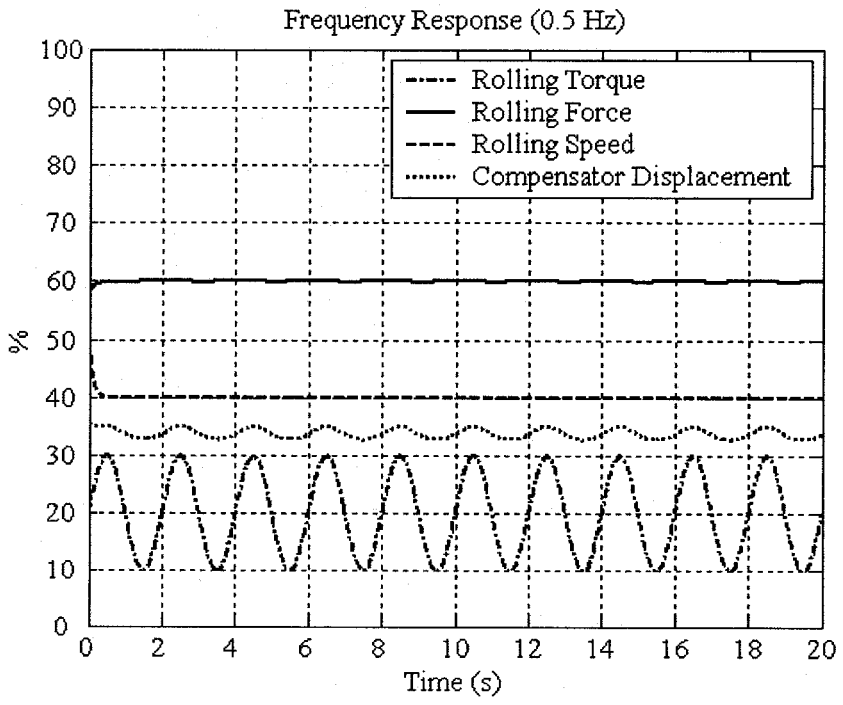

Figure 3.43 The frequency response of the hydraulic control system (0.5 Hz)

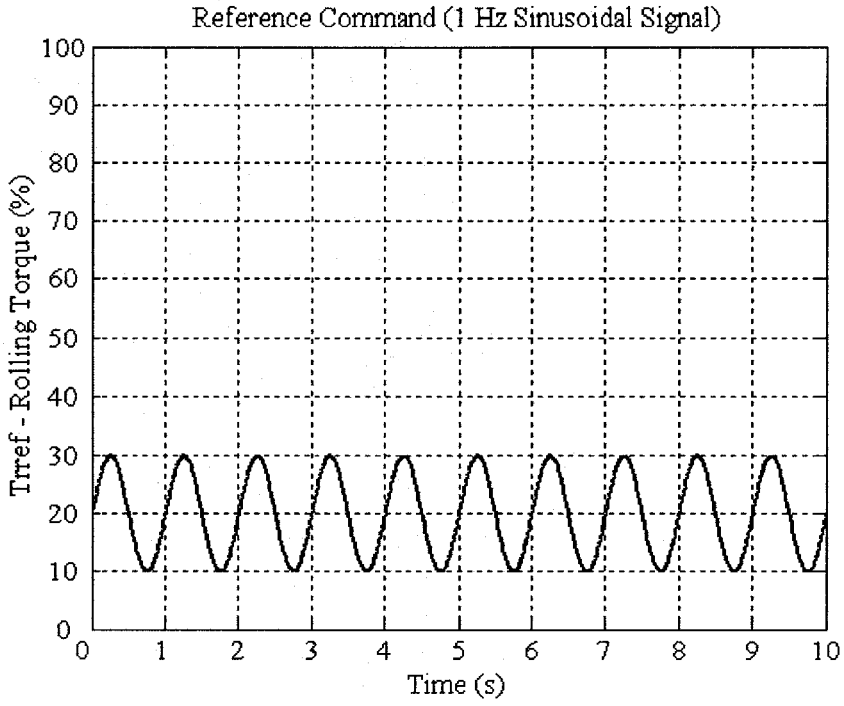

Figure 3.44 The reference command – 1 Hz sinusoidal rolling torque

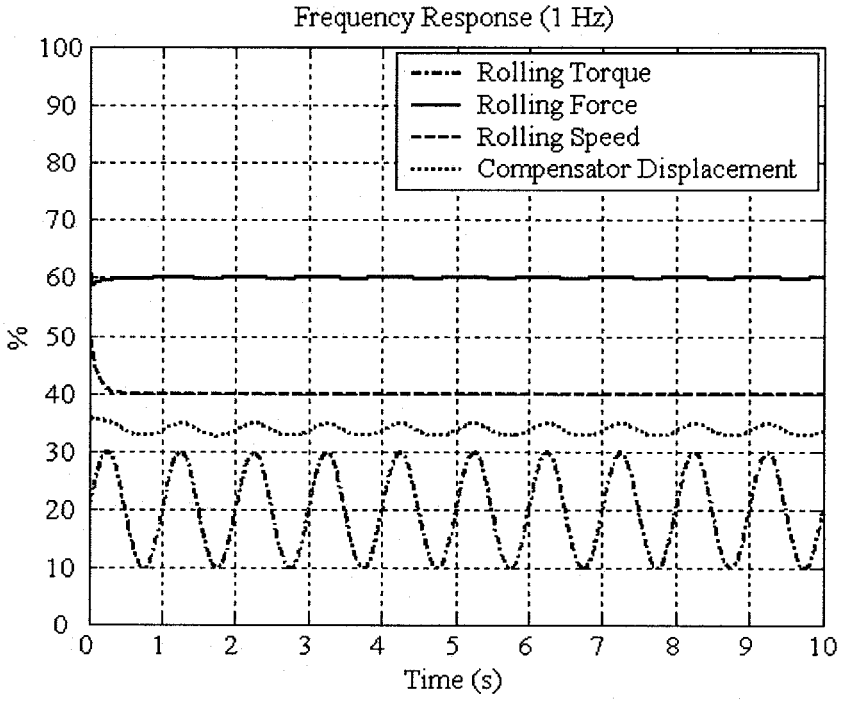

Figure 3.45 The frequency response of the hydraulic control system (1 Hz)

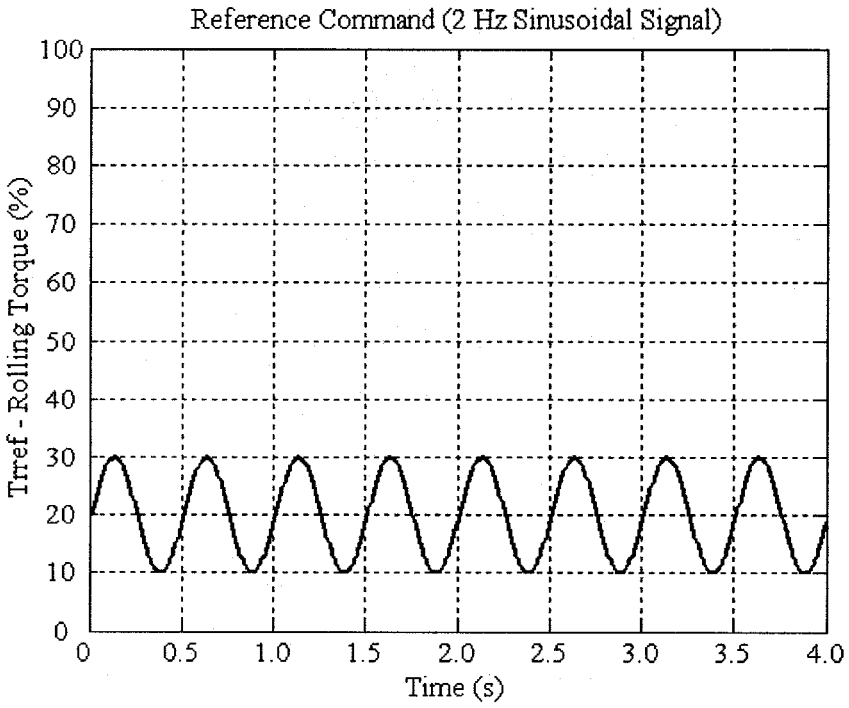

Figure 3.46 The reference command – 2 Hz sinusoidal rolling torque

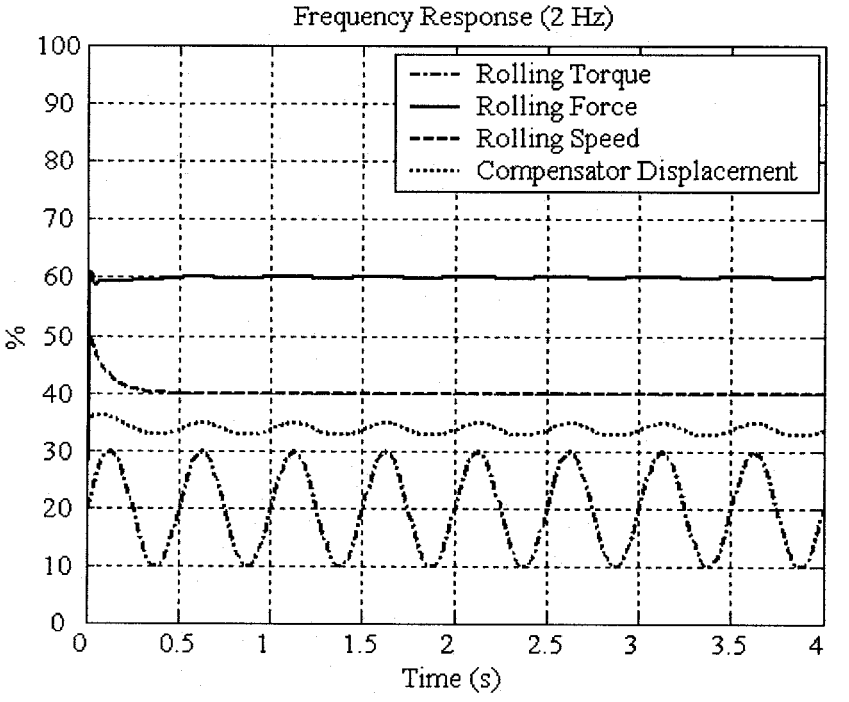

Figure 3.47 The frequency response of the hydraulic control system (2 Hz)

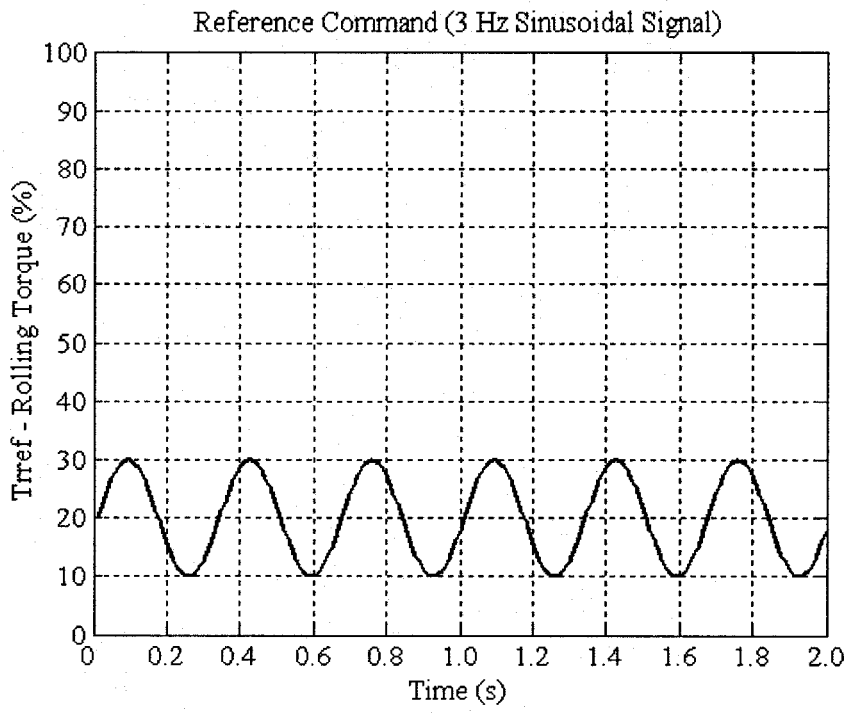

Figure 3.48 The reference command – 3 Hz sinusoidal rolling torque

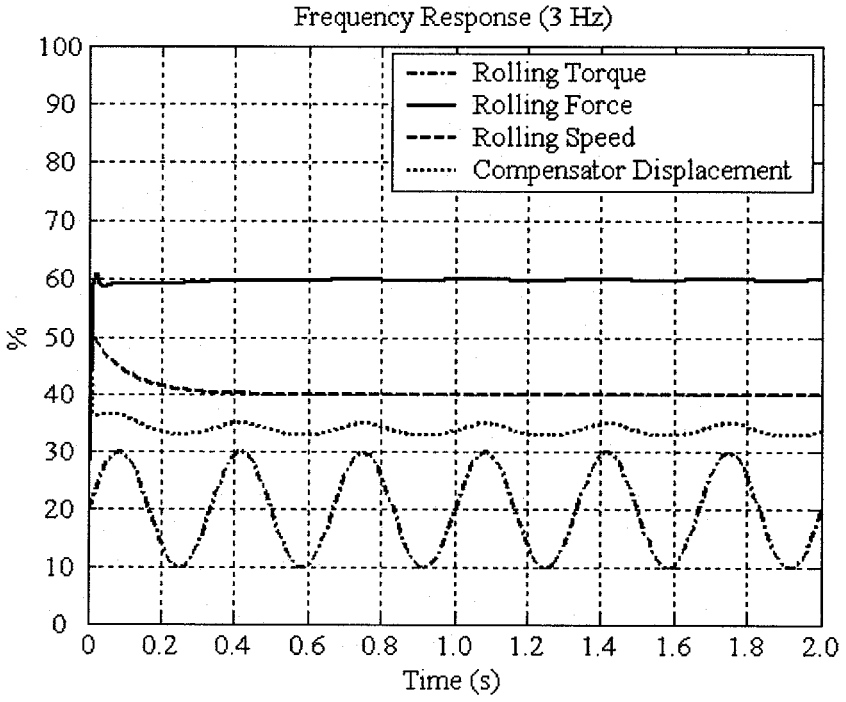

Figure 3.49 The frequency response of hydraulic control system (3 Hz)

CHAPTER 4

MATHEMATICAL MODEL VALIDATION AND EXPERIMENTAL VERIFICATIONS

In the previous chapter, simulations of the pump performance with different control schemes and simulations of the hydraulic control system were presented. In this chapter, hydraulic control system model is validated by experimental measurement of the static and dynamic performance of the system. Experimental setup consists of a hydraulic test bed interfaced with real time control software. Data acquisition system has been built for measuring the hydraulic control system performance. The experimental setup is initially used to measure the step response of the hydraulic control system, which consists of 2 double negative feedback control loops. The analytical results are compared with the experimental results in order to validate the hydraulic control system model. The experimental results for the static and dynamic characteristics are then obtained in the same sequence.

4.1 Description of the Hydraulic Test Bed

As shown in Figure 4.1, the hydraulic test bed consists of four main units; the hydraulic test pump unit, the control pressure supply unit, the load disturbance unit and the oil-conditioning unit.

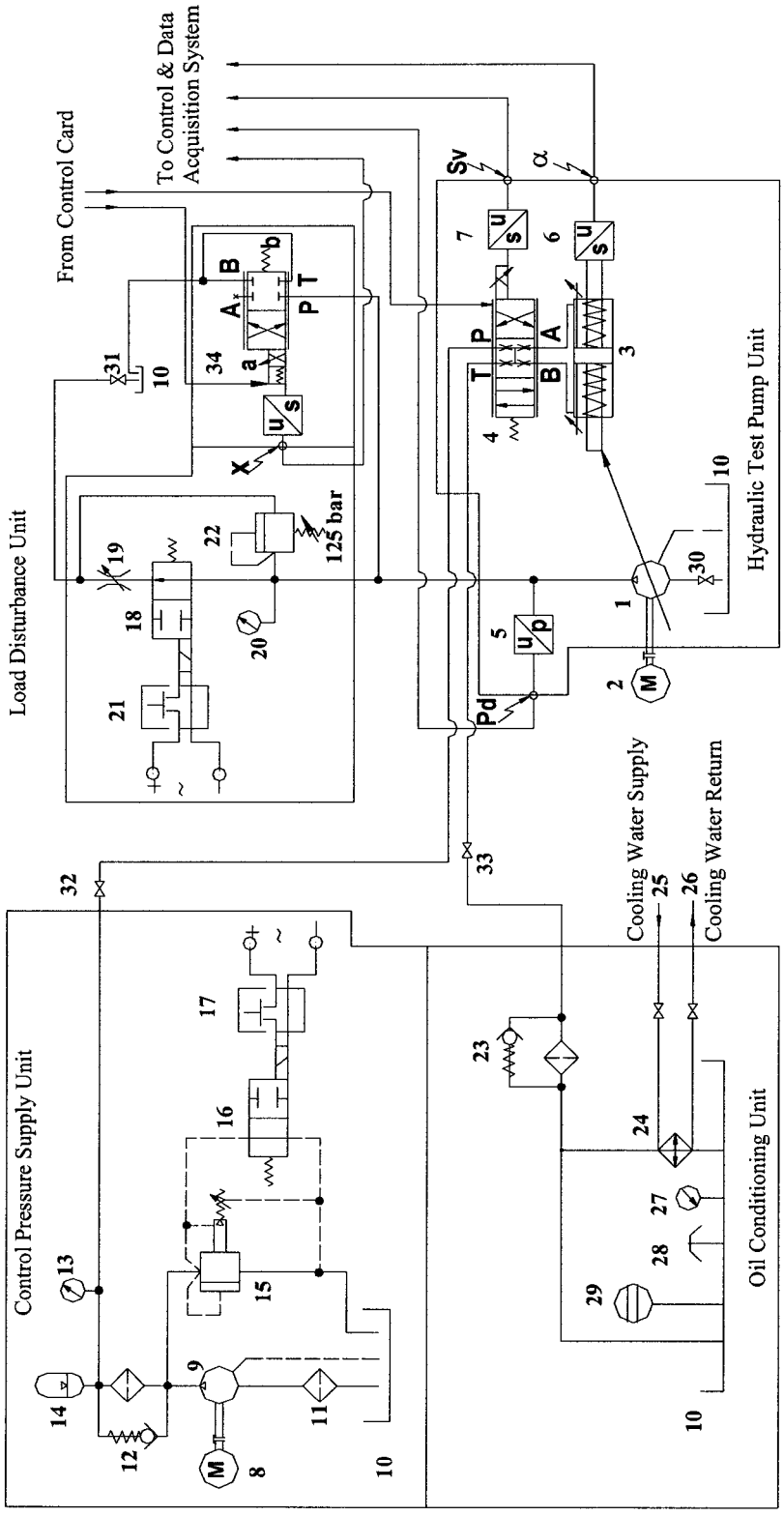

Figure 4.1 Hydraulic test bed

4.1.1 Hydraulic Test Pump Unit

As shown in Figure 4.1, the unit of the hydraulic test pump consists mainly of the test pump (1), which is a 9 piston pump of a 40cc/rev geometrical size that has a conical cylinder block. The construction and design parameters of the pump are presented in Appendix A. The test pump is shown in Figure 4.2.

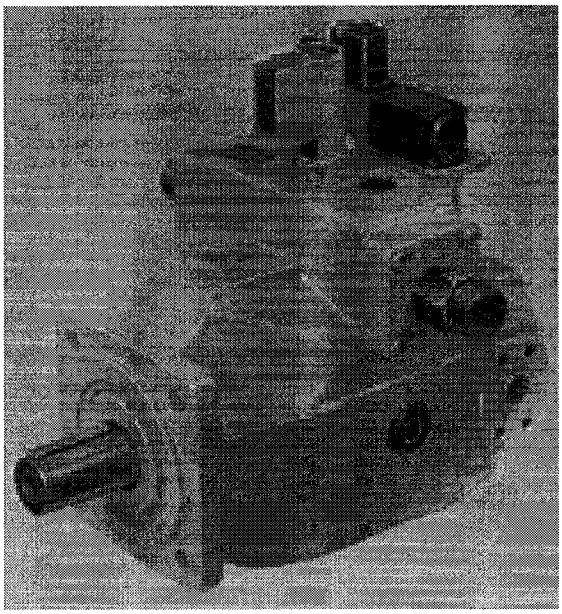

Figure 4.2 Outer shape of the test pump [26]

The test pump is coupled with an electric motor (2) that has 7.5 kW of output power and uses a flexible coupling to absorb any axial and/or lateral vibration between the connected shafts. The swash plate is rigidly connected to a built in symmetrical hydraulic cylinder (3), which drives the swash plate to change its inclination angle. The position of the symmetrical hydraulic cylinder piston (3) is controlled by means of a hydraulic proportional valve (4) integrated with the pump.

The hydraulic proportional valve is supplied with control pressure p_v from the control pressure supply unit. The hydraulic proportional valve also receives the actuating electrical signal i_v from the control and data acquisition system. The tested pump is equipped with three sensors; a pressure sensor (5) that senses the pump delivery pressure, and LVDT position sensors (6) and (7) that sense the swash plate position and the proportional valve spool displacement. These sensors produce voltage signals proportional to the measured variables. The output signals are fed back into the control and data acquisition system.

4.1.2 Control Pressure Supply Unit

The control pressure unit supplies the control pressure to the hydraulic proportional valve. In earlier designs, the control pressure was taken as a branch from the pump delivery pressure. However, a separate constant control pressure supply would help to avoid the effects of frequent changes in the pump delivery pressure on the control process, particularly when using reduced system loads. The external control pressure supply unit consists of an electric motor (8) of suitable output power coupled with the control pressure pump (9) that allows for a pressure of up to 15 MPa. The control pressure pump draws fluid from the main reservoir (10) via a 100 μm mesh size strainer (11). In view of the high sensitivity of the test pump to contamination of the hydraulic fluid, the control pressure pump is equipped with a pressure line filter (12) of a proper flow capacity and a 5 μm size mesh. Control pressure is measured using the dial pressure gauge (13). The control pressure supply line is connected parallel to an accumulator (14) in order to absorb the possible variation of pressure and to keep it constant. The control pressure pump is protected

against overload by a pilot operated pressure relief valve (15), which should be connected parallel to the main supply line as close to the pump exit as possible. The pressure relief valve is integrated with an unloading valve (16) in order to remotely apply or release control pressure. The unloading valve initially connects the pilot line to the tank so that the control pressure pump is initially unloaded. When the push button (17) is down, the spool of the unloading valve moves against the side spring to close the pilot line and apply the control pressure. When the push button is released, the spring returns the unloading valve to its initially open position and consequently the control pressure pump is once again unloaded.

4.1.3 Load Disturbance Unit

The load disturbance unit is built to simulate different modes of change in external load pressure and it is composed of two subunits. The first subunit consists of a 2/2 hydraulic directional loading valve (18) that initially connects the test pump supply line to the tank via a throttle valve (19), which is controlled by hand. The throttle valve is used to adjust the test pump loading pressure p_d to a certain value that can be measured by the dial gauge (20).

When the push button (21) is down, the spool of the loading valve moves against the side spring, thereby closing the current connection of the pump with the tank line. Consequently, the tested pump is suddenly subjected to maximum pressure adjusted by the pressure relief valve (22), while the swash plate is driven from its current position to the position of the minimum inclination angle. When the push button is released, the spring returns the loading valve to its initial position. As a

result, the loading pressure is reduced to the value that was adjusted to before by the throttle valve. The swash plate inclination angle is then suddenly returned to its previous values. Such a mode of the load disturbance simulates the stepwise change in the load pressure.

Measuring a pump performance while it is in constant power operation requires a gradual change of load pressure. For this purpose, the hydraulic directional loading valve (18) is left in its initial position connecting the test pump with the tank via the throttle valve (19). The throttle valve in this case could be used manually to change the load pressure gradually.

The second subunit consists of a 2/2 electromagnetic proportional directional valve (34) and it is parallel to the first one. This valve initially is set in the maximum open position so that the pressure will not be very high at the beginning. At the same time the valve (18) is closed, so that the oil flow has to go to the tank via the valve (34). The valve (34) can be controlled by applying various current signals to the solenoid. Consequently, the pressure can be controlled by computer. The maximum pressure is also set by the relief valve (22).

4.1.4 Oil Conditioning Unit

The oil-conditioning unit maintains the hydraulic fluid conditions as recommended by the pump specifications. The important oil conditions, monitored in most hydraulic control systems, are the class of oil cleanliness and the oil temperature. The oil is kept clean by using an online return filter (23) in the direction

of the control pressure return line. A water oil cooler (24) is connected parallel to the main return line after the return filter in order to partially cool the return oil and keep its temperature within a 55° to 60°C range as recommended. The oil cooler is positioned in the direction of the return oil after the filter, primarily for the following two reasons: (i) filtration and capturing the contaminants from hot oil is easier than capturing from cold oil (ii) clean oil inside the filter ensures an efficient cooling process. The cooler is connected to the cooling water supply and returned via the shutoff valves (25) and (26).

The oil tank (10) has a significant role in performing oil conditioning. In order to have better heat radiation, some design aspects for the oil tank internal space should be considered and the outside dimensions should be properly calculated. The oil tank is equipped with some necessary accessories. A thermometer (27) is used for measuring oil temperature, an air breather (28) works to guarantee clean breathing, and an oil level indicator (29) is used to measure the quantity of oil in the tank. The test pump suction and return lines are connected to the oil tank via shutoff valves (30) and (31), respectively. Also, the control pressure supply and return lines are connected to the oil tank via shutoff valves (32) and (33), respectively. These valves are considered in the hydraulic circuit design in order to facilitate disconnection of the different units from the tank without the need to empty the tank.

4.2 Description of the Control and Data Acquisition System

The pump is currently supplied with an electronic control card denoted in the text by card (A). Figure 4.3 shows how the pump is connected to card (A). Figure 4.3

also shows the basic contents of the amplifier card (A). It contains the arithmetic logic unit, the swash plate controller of the PD type, and the proportional valve spool displacement controller of the PID type; all being physically built onto the card. The contents of card (A) form the double negative feedback loops for the hybrid control of the pump perfonnance. The card is used physically with an analogue and/or digital setting unit for parameterization of the pump static characteristic limits, which are the maximum pressure, the maximum flow rate and the maximum power. Measuring sockets are found in the front panel of card (A) and they are used for measuring pump pressure and flow rate. The power for Card (A) is supplied by a 24 DC voltage.

For testing purposes, control and data acquisition systems are constructed and are composed of software and hardware parts. During the test, the basic contents of the original amplifier card (A) are not used, and card (A) is used only to transfer the output from the sensors to the I/O card.

4.2.1 Real Time Control and Data Acquisition Software

Real time control software is built based on the Matlab-RT workshop to replace the physical contents built on card (A). Using such real time control software facilitates parameterization of the pump controllers, the pressure controller, and constructing the newly proposed control schemes. Figure 4.4 illustrates the double feedback control loops scheme with PD and PID controllers for the test pump and the double feedback control loops scheme for the pressure compensator. The figure also shows that the real time control software includes a unit for monitoring and for data acquisition. It also contains a unit for setting the pump static characteristic limits that

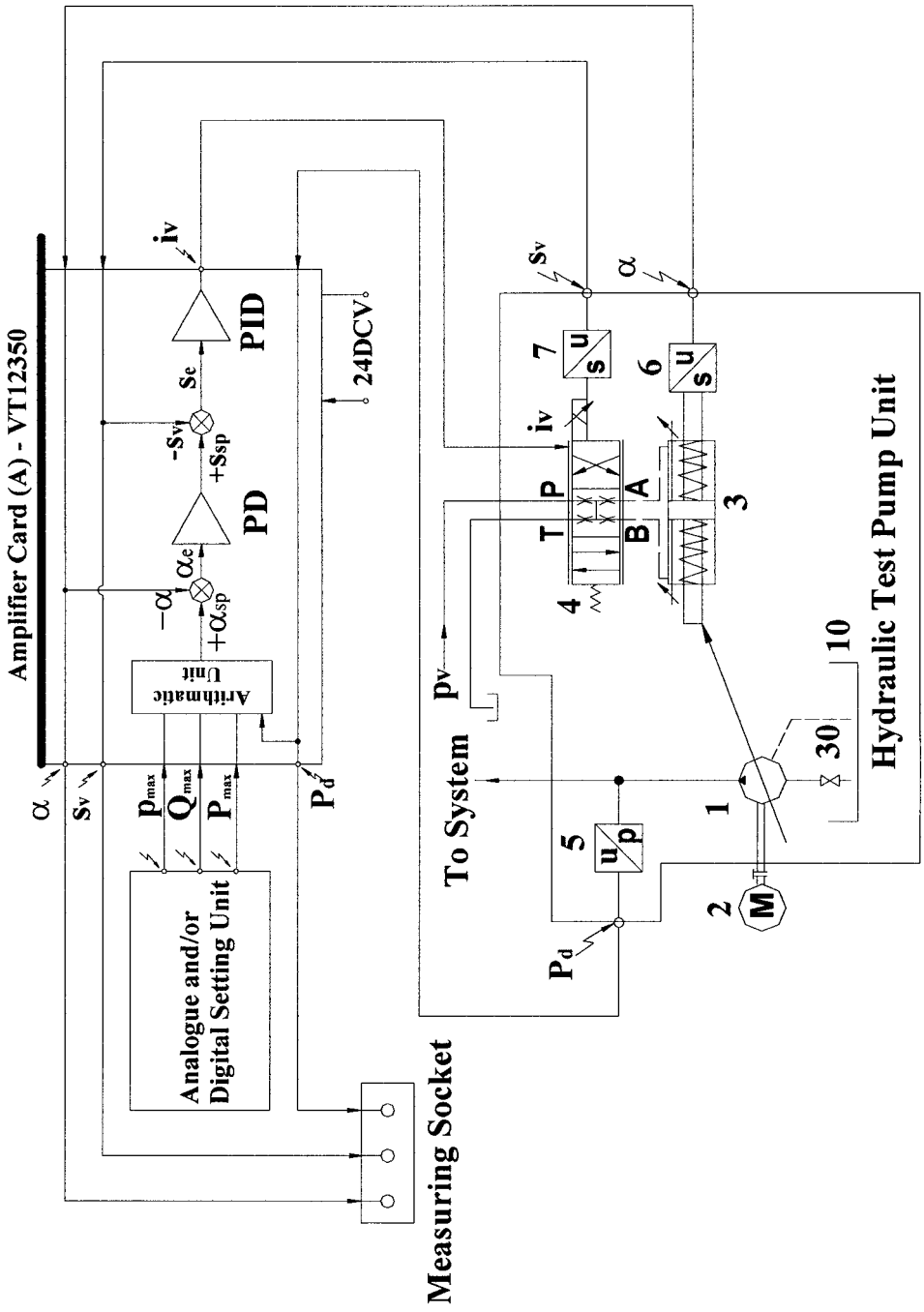

Figure 4.3 The test pump connection configuration with the original amplifier card (A) [20]

should be respected by the control scheme. The first limit is the power P_{max}, which should not be exceeded by the pump. The second limit is the maximum pressure p_{max} after which the pump controller should drive the pump to the minimum discharge position. The third limit is the maximum pump flow rate Q_{max}. Based on the value of actual pump pressure fed back to the arithmetic logic unit, the latter calculates the corresponding pump flow rate in order to achieve constant power operation with the static characteristic limits respected. The calculated pump flow rate is then represented by the set point value of the swash plate inclination angle α_{sp}. The swash plate inclination angle set point value is compared to the actual inclination angle. The error value α_e is fed to the swash plate PD controller. Consequently, the swash plate controller produces another set point value s_{sp} for the position of the hydraulic proportional valve spool. The spool position set point value is compared to the actual value of s_v. The resulting error value s_e is fed to the spool position PID controller that eventually produces the control current signal i_v that is sent to the proportional solenoid. The control scheme is designed to respect the preset limits when they are reached, regardless of power.

4.2.2 Hardware Part of the Control and Data Acquisition System

Figure 4.4 also shows that the hardware is composed of an I/O card and locally developed amplifier cards denoted in the text as amplifier card (B), card (B1) and card (C). The I/O card is used to interface the real time control software with the amplifier cards. Only standard I/O interface cards that are adaptable to Matlab-RT can be used. It should have at least four input analogue channels and two analogue output channels.

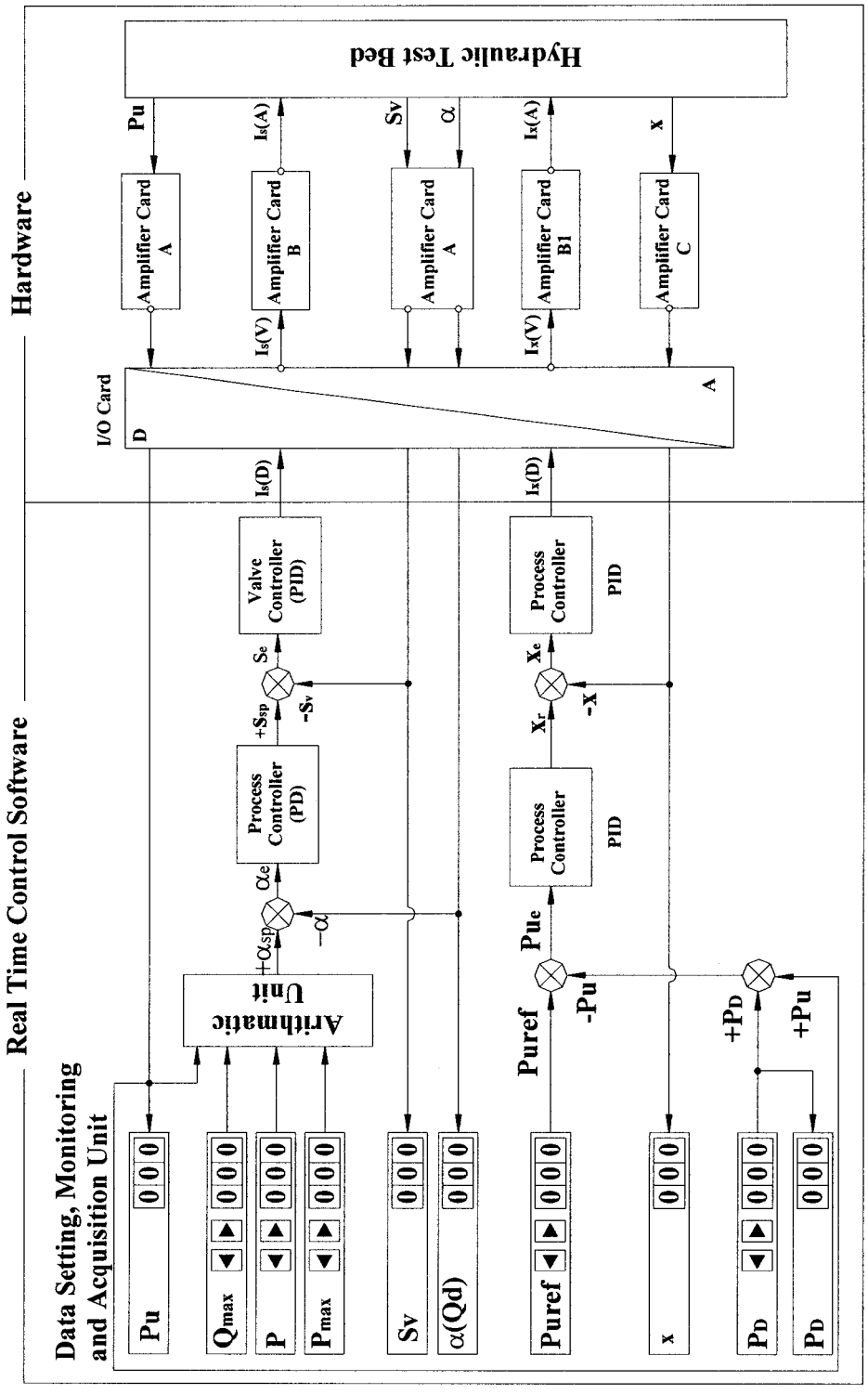

Figure 4.4 Block diagram of control and data acquisition system

Information from the hydraulic test bed is transmitted to the real time control software through the analogue input channels on the I/O card via the card (A) and card (C). Consequently, it is converted into digital form and received by the real time control software that yields the corresponding control signals in the digital form $I_s(D)$ and $I_x(D)$. The signals in the digital form are converted into analogue form and transmitted out of the computer in analogue voltage form $I_s(V)$and $I_x(V)$ through the output channels in the I/O card. The amplifier card (B) and card (B1) are employed to convert the control signals from analogue voltage form into analogue current form $I_s(A)$ and $I_x(A)$ with enough power to drive the proportional hydraulic valve solenoid of the test pump and the proportional solenoid of the pressure compensator.

4.3 Test Preparations and Calibrations

In the following, the installation instructions for the setup and the steps that should be taken to integrate its different components are described. Figure 4.5 shows the symbolic presentation of the experimental setup as completely integrated and with the different units connected to each other. The figure also illustrates the two double feedback control loops.

The schematic layout and photographic view of the experimental setup are shown in Figures 4.6 and 4.7, respectively. It must be noted that the component numbering system used in Figures 4.5 and 4.6 are the same. It is important now to check the proper functionality of each part of the setup to facilitate the diagnosis of any malfunctions in the setup. Therefore, in the following sections, a step-by-step explanation for the setup integration, pretests and calibrations are presented.

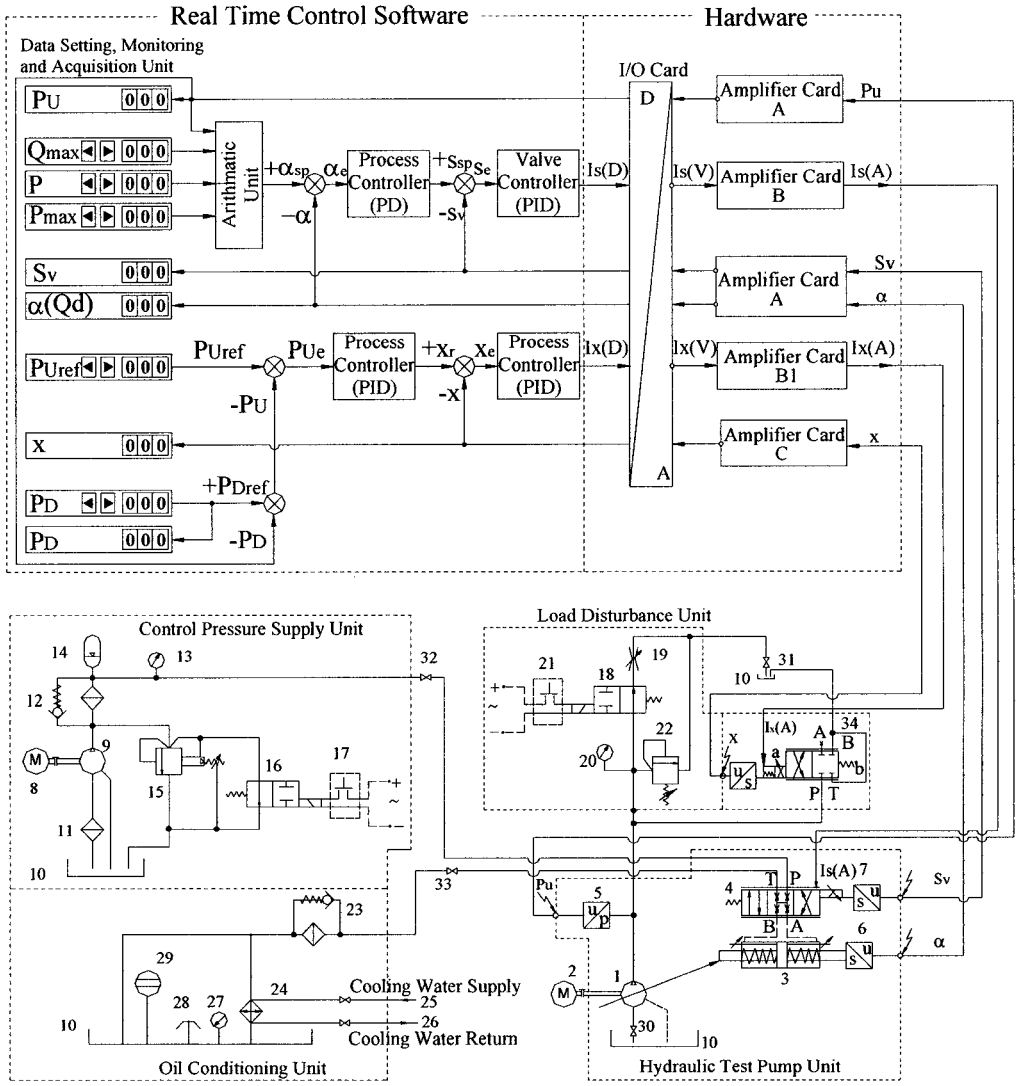

Figure 4.5 Block diagram of the integrated experimental setup

4.3.1 Integration of the Hydraulic Test Bed

A well-organized preparation for the test ensures accurate and dependable results. In the following steps, instructions for the integration of the test setup are given.

(i) Preparing the Hydraulic Fluid Used in the Test: The hydraulic oil cleanliness class must be at an appropriate level. In the case of axial piston pumps, class 6 is fairly acceptable. This class specifies, according to standard code NAS 1638, the upper limit of contamination of the oil used with such pumps and control components. In this regard, samples of the used oil are tested using the electronic particle counter. The oil tank is cleaned and thoroughly flushed, and then filled with the specified oil up to the maximum oil level mark. All types of hydraulic fluid of a petroleum base are suitable for providing the recommended oil viscosity.

(ii) Integrating the Pump with the Drive Motor: As shown in Figure 4.5, the pump is coupled with the drive motor and mounted on the lower level of a table. The motor is bolted over two pairs of dampers to absorb the vibration coming out of the pump and the motor. A coupling between the drive motor and pump is correctly assembled and aligned.

(iii) Fixing the Disturbance Unit: Elements of the disturbance unit are initially cleaned by compressed air and then integrated in one manifold block which is fixed on the upper level of the table, as shown schematically in Figure 4.6.

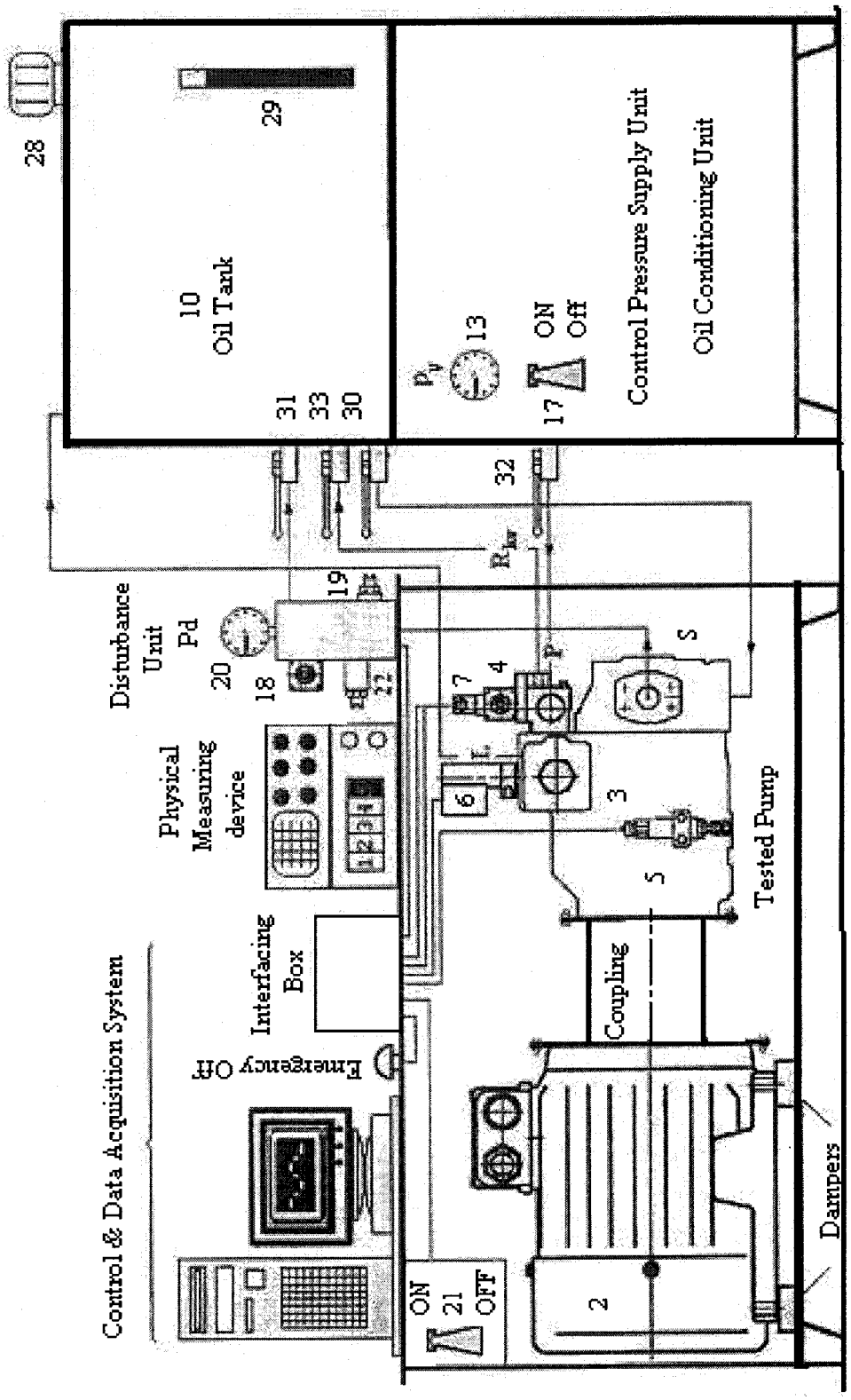

Figure 4.6 Schematic layout of the integrated experimental setup [20]

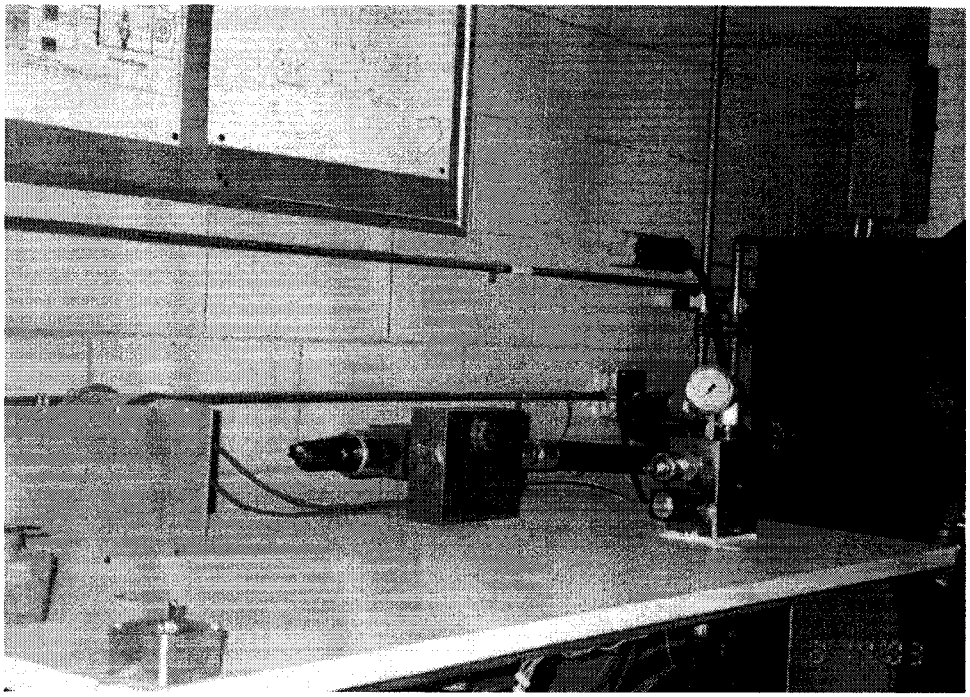

a-A view of the pump loading unit and real time controller interface

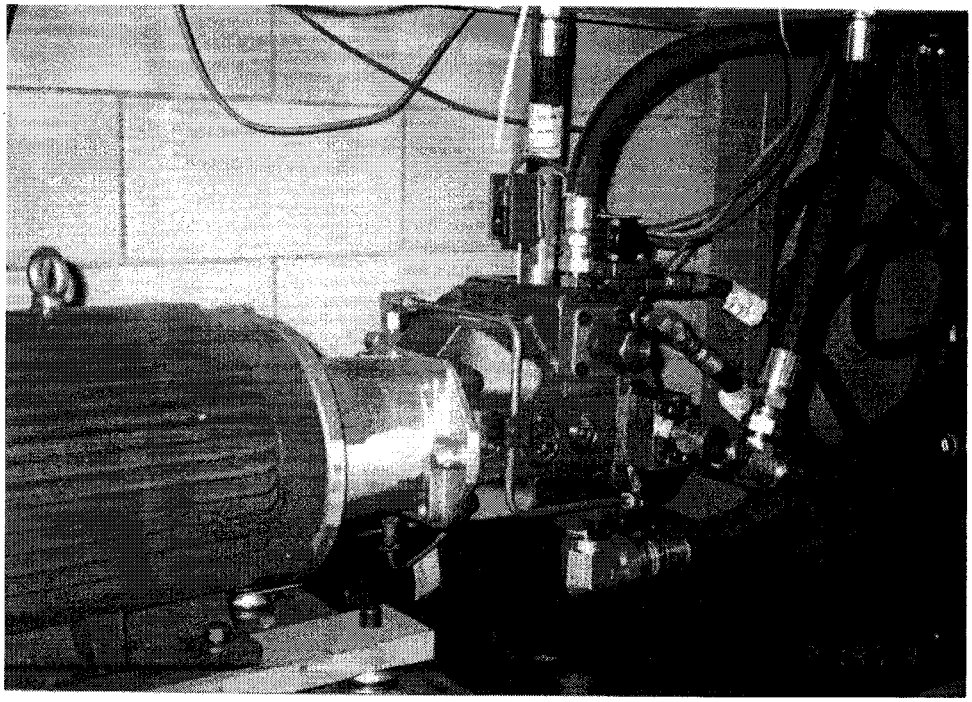

b-A view of the pump with the integrated control unit and set of sensors

Figure 4.7 Photographic view of the experimental setup

(iv) Pipelines Work: The pipes are cleaned with compressed air. Also, the pipes are color coded in order to avoid confusion. The diameters of the pipelines are chosen so as not to be less than the corresponding port dimension at the pump. As presented in [26] and shown in Figure 4.6, the pump ports are defined as follows: "S" for suction port, "B" for pressure port, "L" for case drain port, "P" for the control pressure supply port, and "R_{kv}" for the control pressure return port. The pipelines are then connected and correctly arranged to be free of tension and excessive bending. In open hydraulic circuits, this type of pump can be used with a suction pressure ranging from a -0.8 bar gauge pressure up to a 30 bar posting pressure. As shown in Figures 4.6 and 4.7, the pump is mounted where suction port "S" is lower than the free surface of the oil in the tank by approximately half a meter head, which is considered in the pump mathematical model by 0.5 bar posted suction pressure. Pressure port "B" is connected to the disturbance unit inlet. There are different drain ports "L" in the pump and the port in the highest position is selected and the others are plugged. The drain line is connected directly to the oil tank below the oil level to avoid generating oil turbulence. Both the control pressure and return line are connected to the pump ports "P" and "R_{kv}", respectively, with the general recommendations observed.

(v) System Air Bleeding: In order to avoid air pockets during the first run of the system, the air in the system is bled. The pump housing is filled with oil. For a pump positioned horizontally as shown schematically in Figure 4.6, the pump case is filled from the upper port (drain port "L"). Filters, heat exchangers and suction lines are to be filled with oil also.

(vi) Control Pressure Supply Unit and Oil Conditioning Unit: These units are prepared to function properly. Accumulator charging pressure is reviewed and control pressure is adjusted. The cooling water supply and return lines are connected as shown in Figure 4.5.

(vii) Electrical Power Connections: The electrical power supply is provided to the drive motor, "Emergency Off" button, directional valve in the disturbance unit and the control pressure supply unit. Before carrying out functional testing, the "Emergency Off" button is tested to ensure its proper functioning.

(viii) Testing the Correct Direction of Rotation of the Drive Motor: This is an important step in order to avoid pump cavitation and occasional failure if the motor is improperly rotated. The letter "R" in the ordering code of such pumps designates that the pump direction of rotation is to the right. This conventionally means that when one looks at the pump from the side of the drive shaft, i.e. from the drive motor fan side, the fan should rotate clockwise. Before testing, valves 19, 22, 30 and 31 are kept fully open. Switching the pump ON without a load for a very short time verifies the direction of rotation.

4.3.2 Interfacing with the Control and Data Acquisition System

In this step, both the real time control software and I/O card must be tested for proper functioning. In this regard, as shown in Appendix 2[20], module 1, three physical function generators and one oscilloscope are used. The function generators are connected to the analogue input channels on the I/O card to simulate the

information coming from the sensors. The oscilloscope is connected to the analogue output channels on the I/O card. The function generators are adjusted to generate three different signals. Real time control software is built to read from the function generators through the I/O card, which then outputs one of the incoming signals outside to be read again by the oscilloscope. The proper functionality of the I/O card and the real time control software is tested for an error free connection with the outside world, and proper phase shifting based on the coincidence between the output of the physical devices and the readings of the real time control software.

4.3.3 Calibrations and Pretests

Configuration and calibration of amplifier card(B), calibration and conditioning of the hydraulic proportional valve, establishing the closed control loop for the proportional valve etc, have been presented in detail in [20]. Calibration of amplifier card (B1) for the pressure compensator is same as that of the card(B). Next let us focus on conditioning of the pressure compensator.

(i) Calibration and Conditioning of the Compensator: In this step, the compensator spool displacement is to be calibrated in an open loop. A real time control software, as shown in Figure 4.8, is designated to produce a reference signal from zero to 10 voltages, and to read the corresponding amount of the spool displacement. As shown in Figure 4.9, the output signal of the amplifier card(B1) is connected to the compensator solenoid, while the sensor of the compensator spool displacement is connected to the amplifier card(C), and then connected to the I/O card. A normalized Input-Output relation representing the compensator static

characteristics is presented in Figure 4.10. Non-linearity was found with a maximum value of 17%.

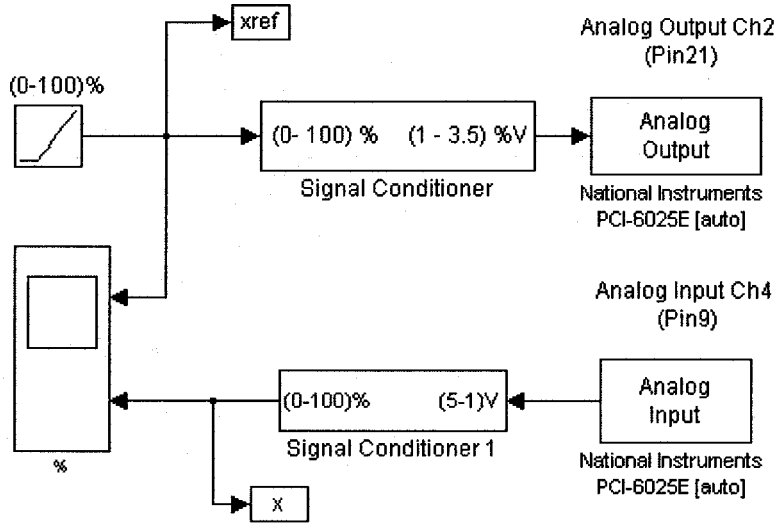

Figure 4.8 Conditioning of the pressure compensator spool displacement in an open loop

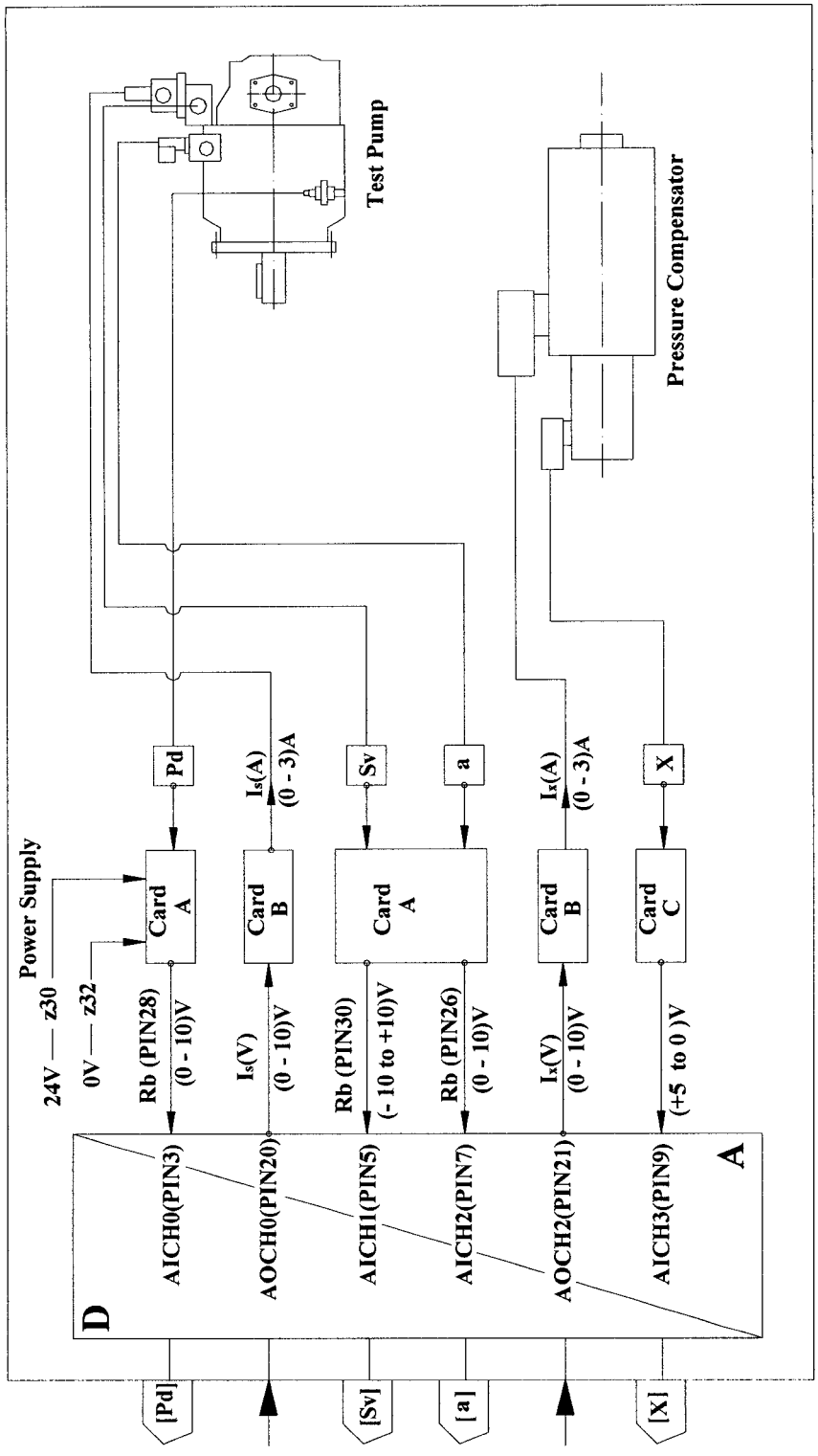

Figure 4.9 Connection scheme of real time control

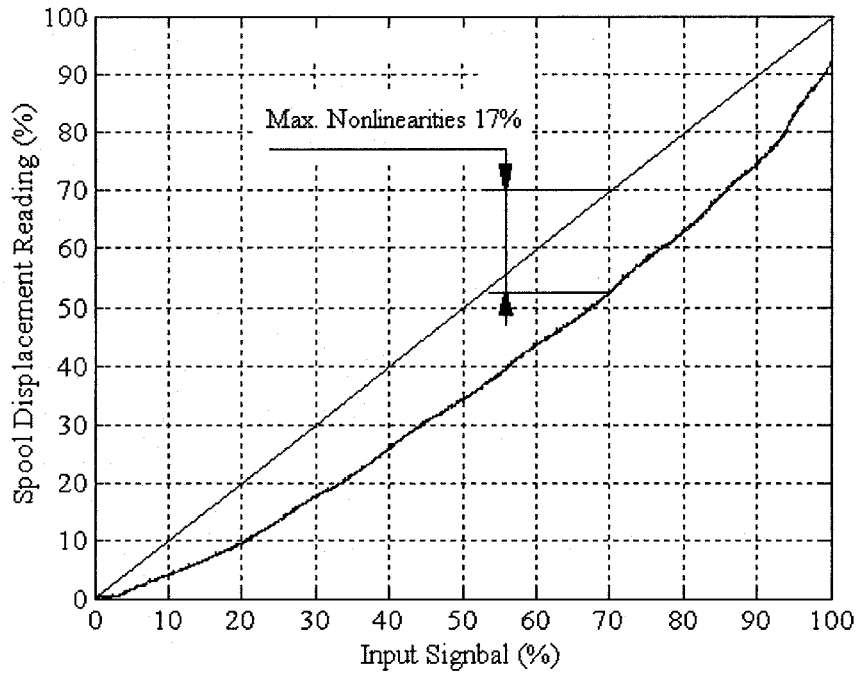

Figure 4.10 Measurement of open loop static characteristics of the compensator

(ii) Establishing the Closed Control loop for the Compensator: In this step, the real time control software, as shown in Figure 4.11, is further developed to implement a closed loop to control the position of the compensator spool. The software is designed to produce a normalized reference input signal that changes slowly and gradually from zero to 100%. The corresponding normalized spool displacement is recorded and compared with the simulated results shown earlier in Figure 3.12. Figure 4.12 shows acceptable agreement between the simulation result and the measurement showing perfect linearity along the whole range of the input signal.

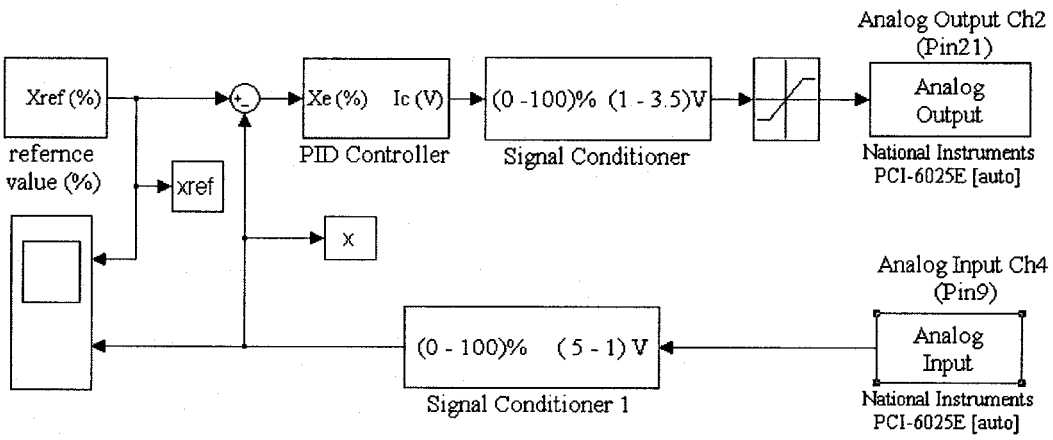

Figure 4.11 Conditioning of the pressure compensator spool displacement in a closed loop

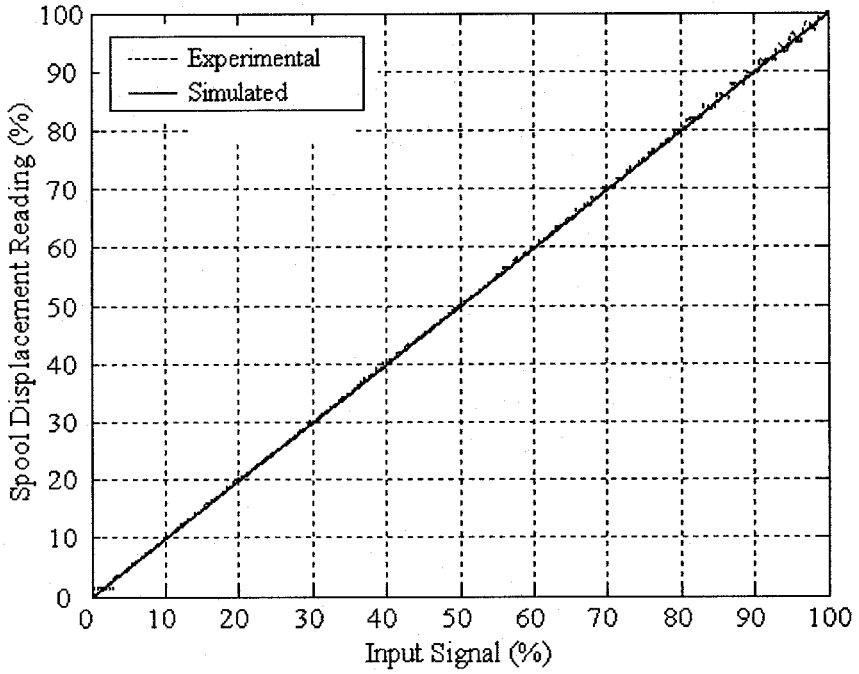

Figure 4.12 Measurement of closed loop static characteristics of the compensator

The same module is used for measuring the step response of the pressure compensator. The software is designed to produce a step input signal following the same procedure used in chapter 3, section 3.1. The compensator step response is then measured and recorded. Figure 4.13 shows global agreement between the simulated and measured step response of the compensator during a 9 second time span. Figures 4.14 and 4.15 show an enlarged view of the measured compensator step responses as compared with the simulation results when the spool moves from the zero position to a certain percentage of its full stroke and vise versa. A comparison of the results shows relative agreement with those obtained from the simplified modeling of the compensator. However, the most important feature of the compensator dynamic, the settling time, is nearly equal in both analytical and experimental results.

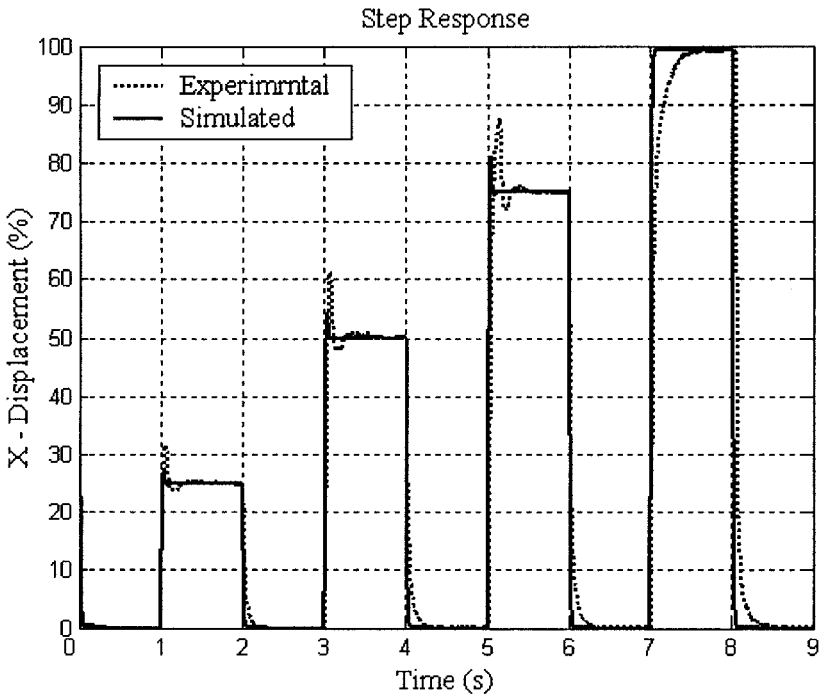

Figure 4.13 Measurement of the step response of the compensator

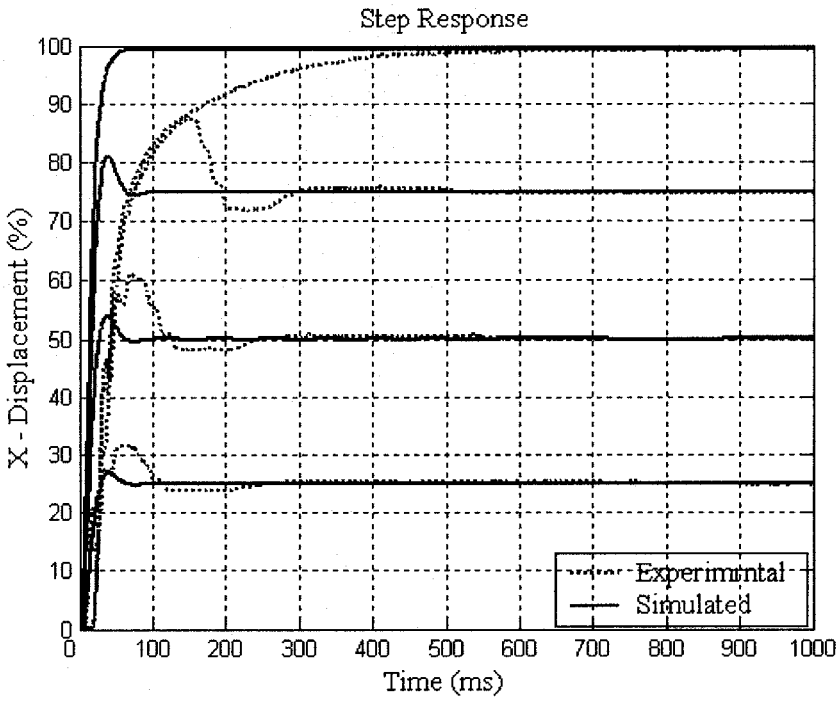

Figure 4.14 Measurement of the step response of the compensator moving from zero position to a different percentage of its full stroke

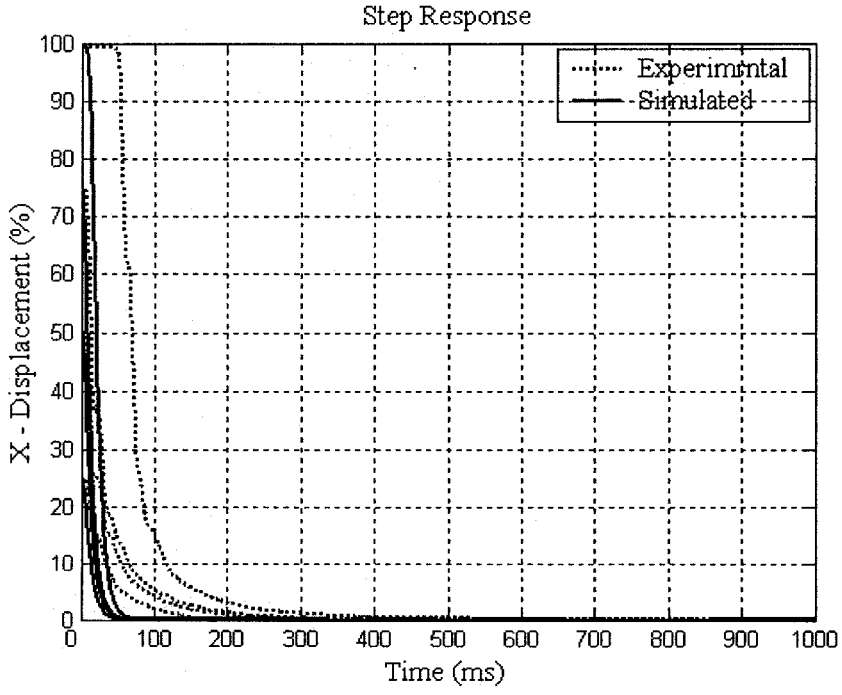

Figure 4.15 Measurement of the step response of the compensator moving from different percentage of its full stroke to zero position

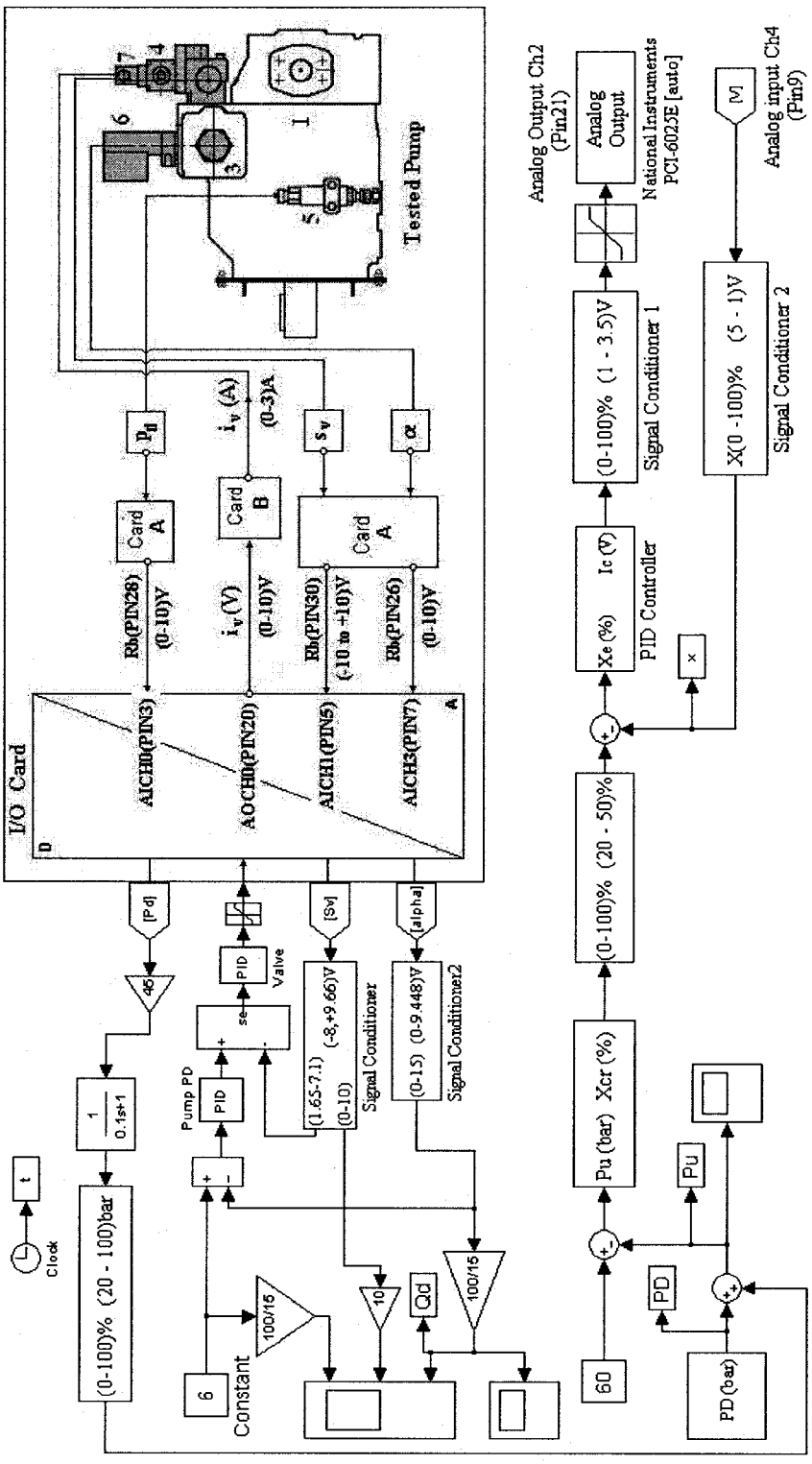

Figure 4.16 A real time control software module for testing the characteristics of the hydraulic control system

4.4 Testing of the Control System Performance

The experimental setup is now finished and ready to measure the control system static and dynamic characteristics. In this section, the model of the control system will be experimentally verified and the control system characteristics, found in Chapter 3, will be validated. In order to achieve the above objective, a real time control software module, shown in Figure 4.16, is designated. The pump mathematical model has been experimentally verified and the characteristics of the pump have been validated in [20]. Hence, the measurement of the pump performance will not be carried out again. We only concentrate on the measurements of the control system.

4.4.1 Measurement of the Step Response of the Hydraulic Control System due to the Step Change in the Rolling Torque

Step response of the hydraulic control system was simulated earlier in Chapter 3. The simulation program was fed with a signal that was assumed to increase and decrease in a stepwise manner. The same input signal is used for measuring the actual step response of the hydraulic control system. After running the real time control system, the actual step response can be measured and recorded. Figures 4.17 to 4.20 show the comparisons of rolling torque, rolling force, rolling speed and displacement of spool between the measured and simulated step responses of the control system, respectively. The comparison shows a close agreement between the measured results in steady state and simulated results. The high frequency oscillations with very small amplitudes in Figure 4.18, 4.19 and 4.20 are due to the noise in the measured signals.

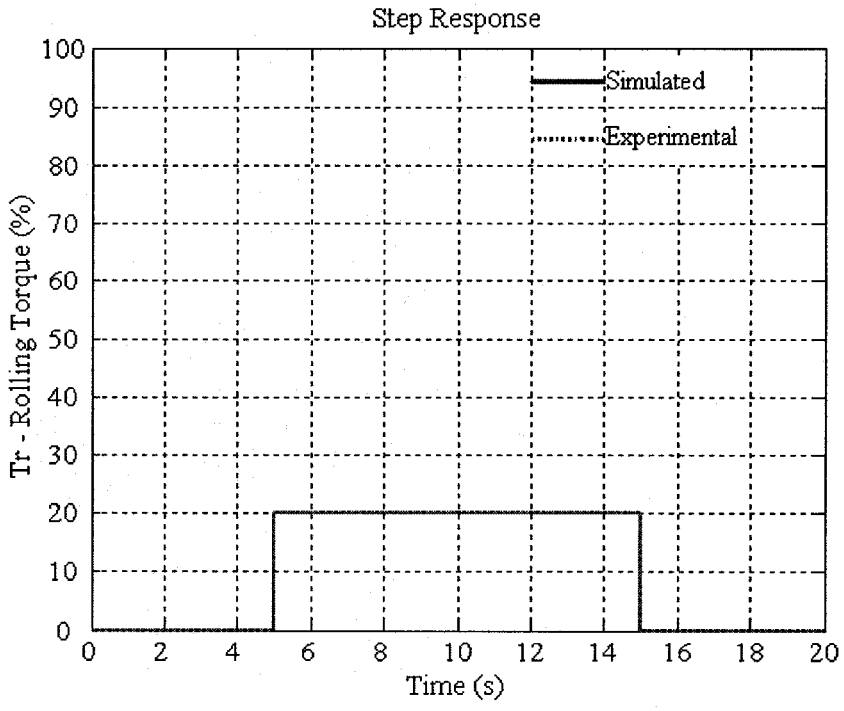

Figure 4.17 Measured rolling torque step response as compared with the simulation result

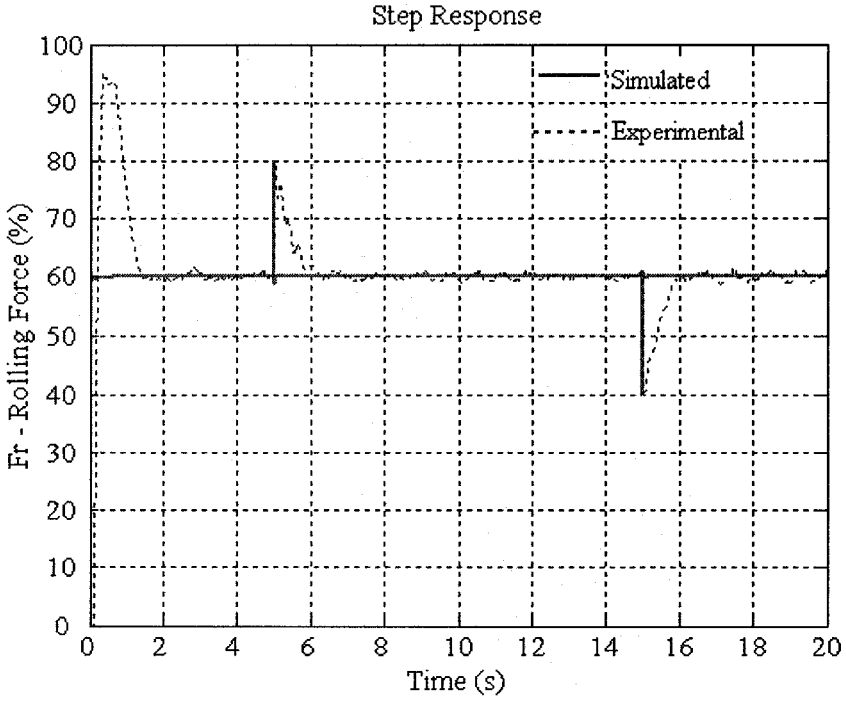

Figure 4.18 Measured rolling force step response as compared with the simulation result

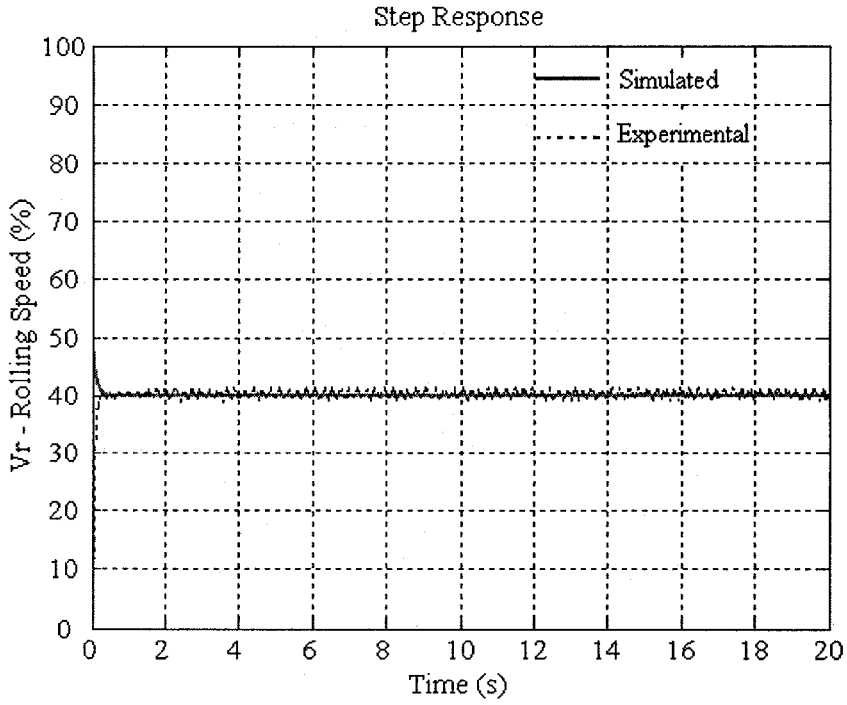

Figure 4.19 Measured rolling speed step response as compared with the simulation result

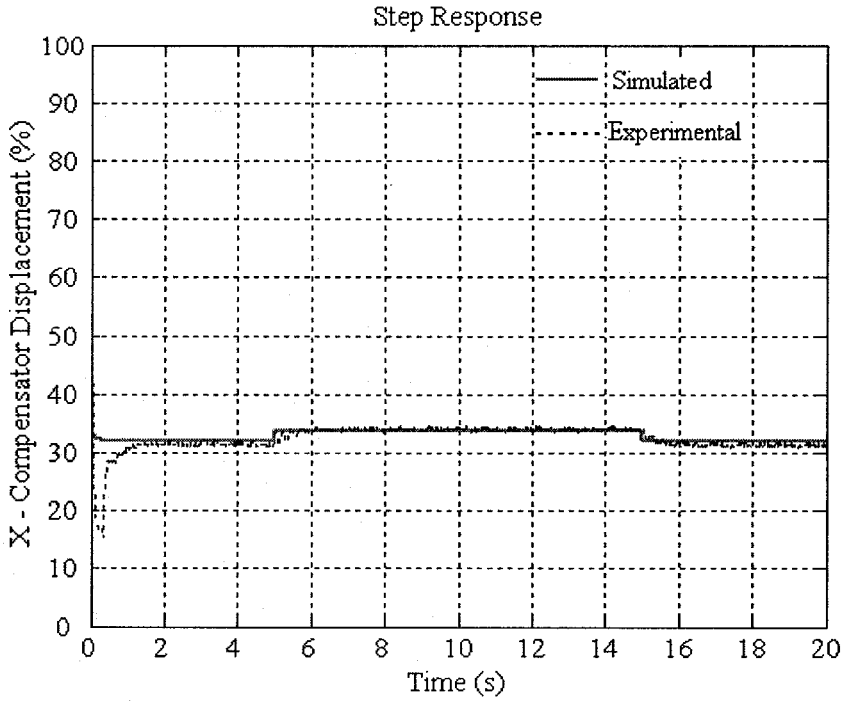

Figure 4.20 Measured displacement of spool step response as compared with the simulation result

4.4.2 Measurement of the Static Response of the Hydraulic Control System due to the Ramp Change in the Rolling Torque

The same real time control module is used to measure the static characteristics of the hydraulic control system. The command signal - the rolling torque, is assumed to change gradually from zero to 100%. After running the real time control system, the actual static response can be measured and recorded. Figures 4.21 to 4.24 show the comparisons of rolling torque, rolling force, rolling speed and displacement of spool between the measured and simulated static responses of the control system, respectively. We can see that the measured results in steady state agree with the simulated results very well.

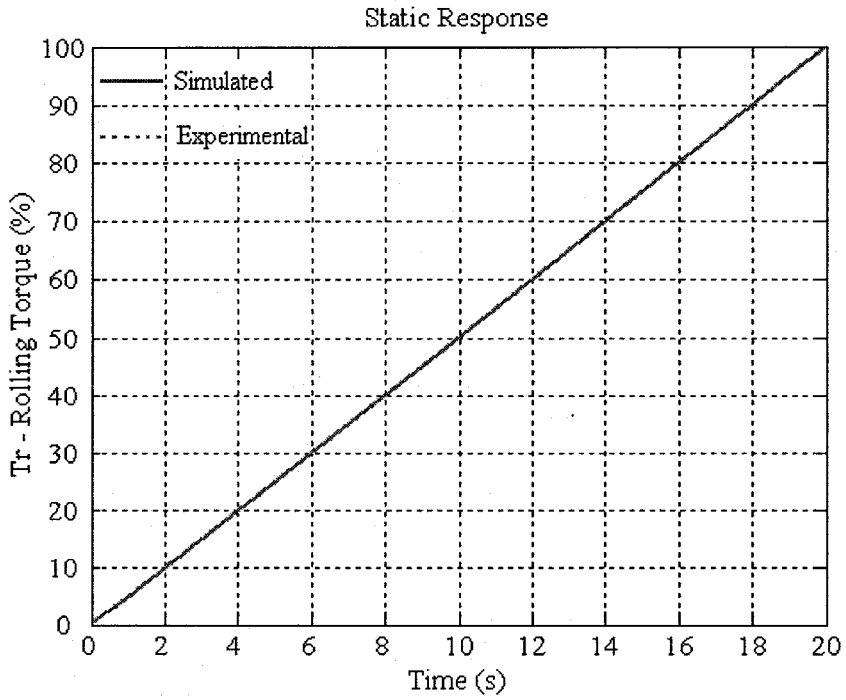

Figure 4.21 Measured rolling torque static response as compared with the simulation result

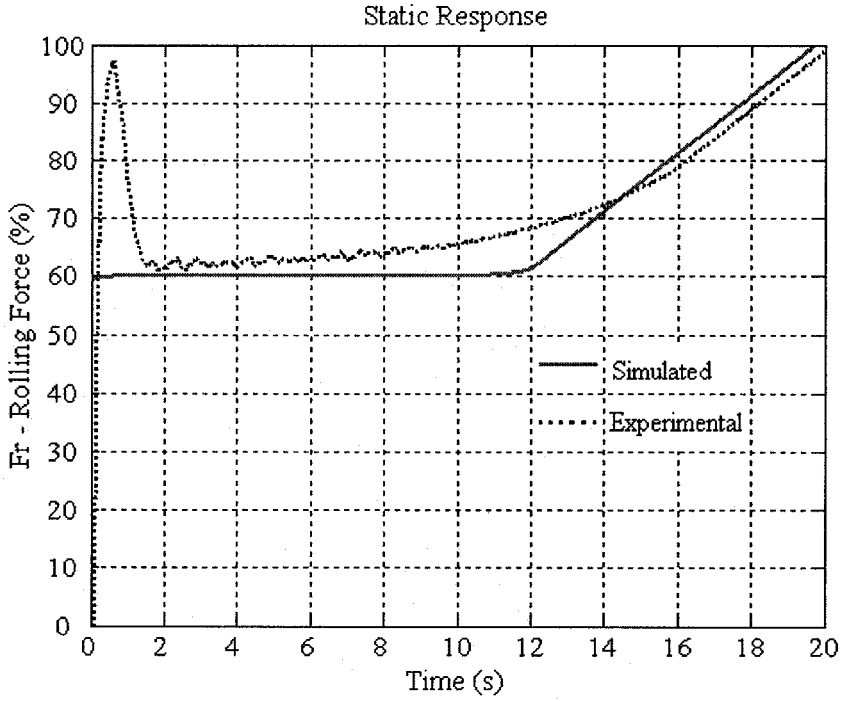

Figure 4.22 Measured rolling force static response as compared with the simulation result

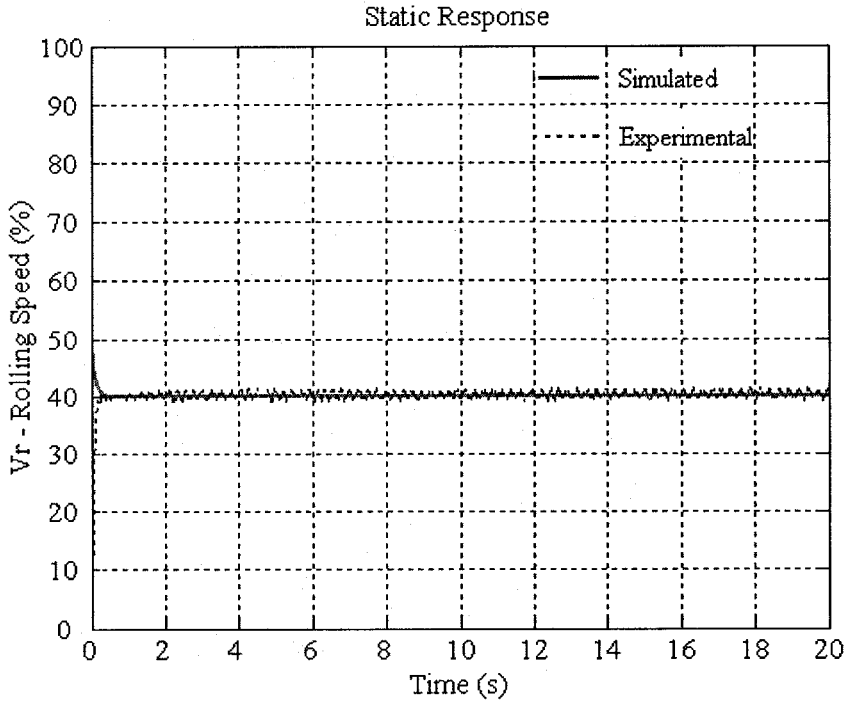

Figure 4.23 Measured rolling speed static response as compared with the simulation result

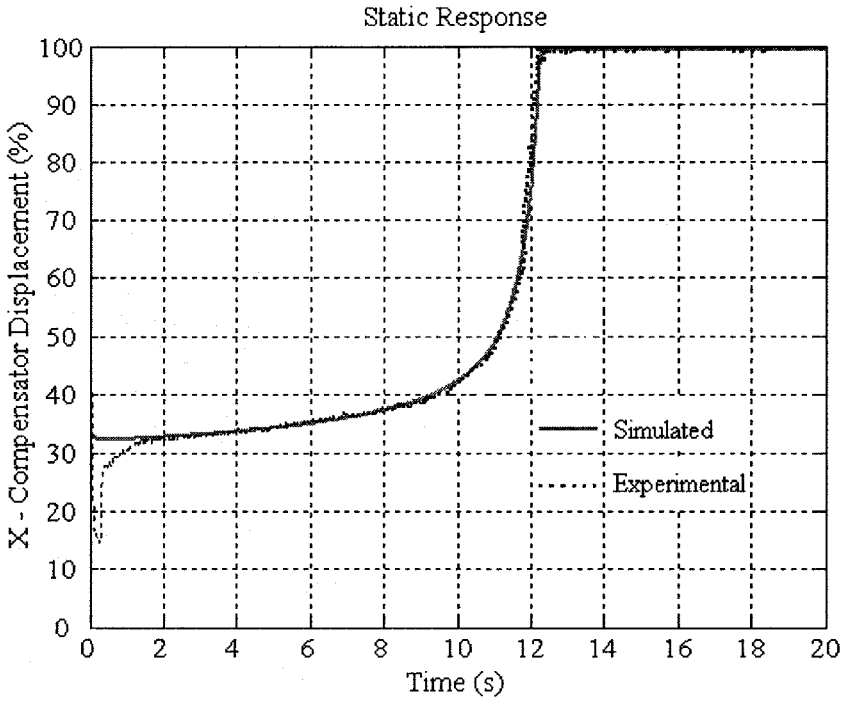

Figure 4.24 Measured displacement of spool static response as compared with the simulation result

4.4.3 Measurement of the Frequency Responses of the Hydraulic Control System due to the Harmonic Changes in the Rolling Torque

The same real time control module is also employed to measure the frequency response of the hydraulic control system. The command signal - the rolling torque - is changed in a harmonic manner. Sinusoidal signal, of 10% amplitude and 0.1 Hz to 3 Hz frequency, represents harmonic change of the rolling torque. After running the real time control system, the actual frequency responses can be measured and recorded. Figures 4.25 to 4.29 show the comparisons of rolling torque, rolling force, rolling speed and displacement of spool between the measured and simulated frequency responses of the control system at frequencies of 0.1 Hz, 0.5 Hz, 1 Hz, 2 Hz and 3 Hz. We can see that the measured results in steady state agree with the simulated results very well.

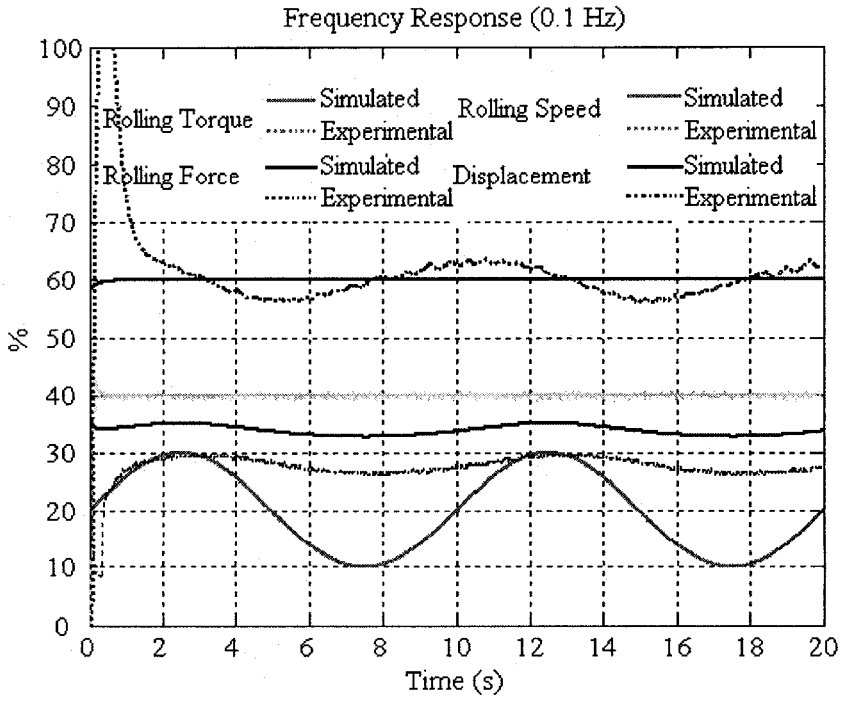

Figure 4.25 Measured frequency response as compared with the simulation result (0.1 Hz)

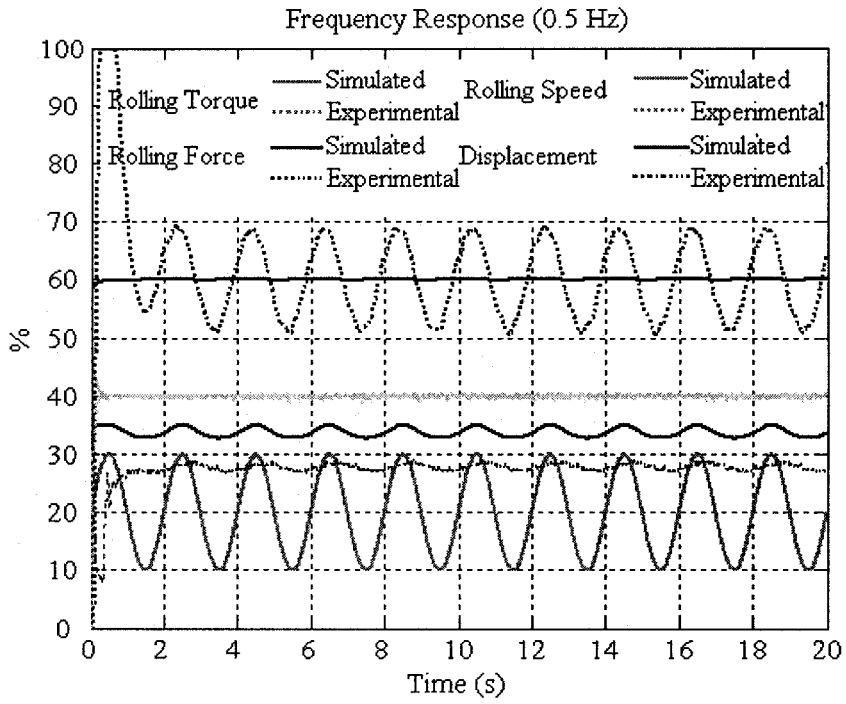

Figure 4.26 Measured frequency response as compared with the simulation result (0.5 Hz)

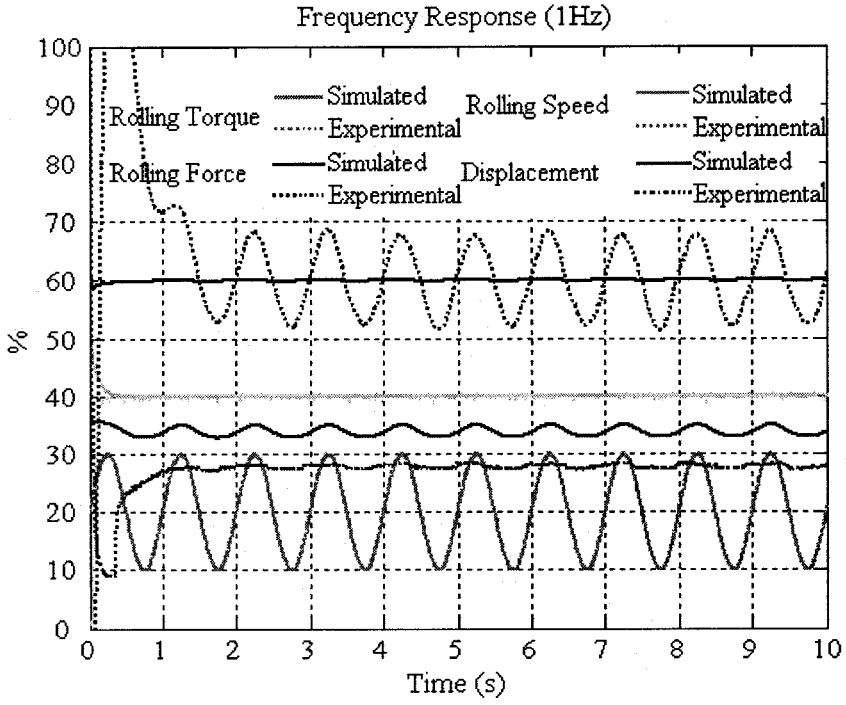

Figure 4.27 Measured frequency response as compared with the simulation result (1 Hz)

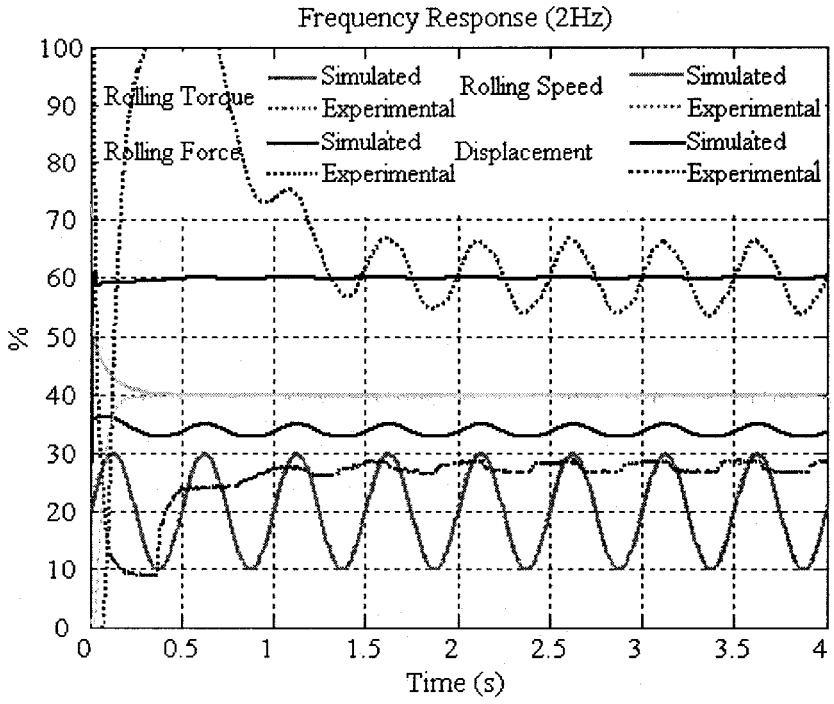

Figure 4.28 Measured frequency response as compared with the simulation result (2 Hz)

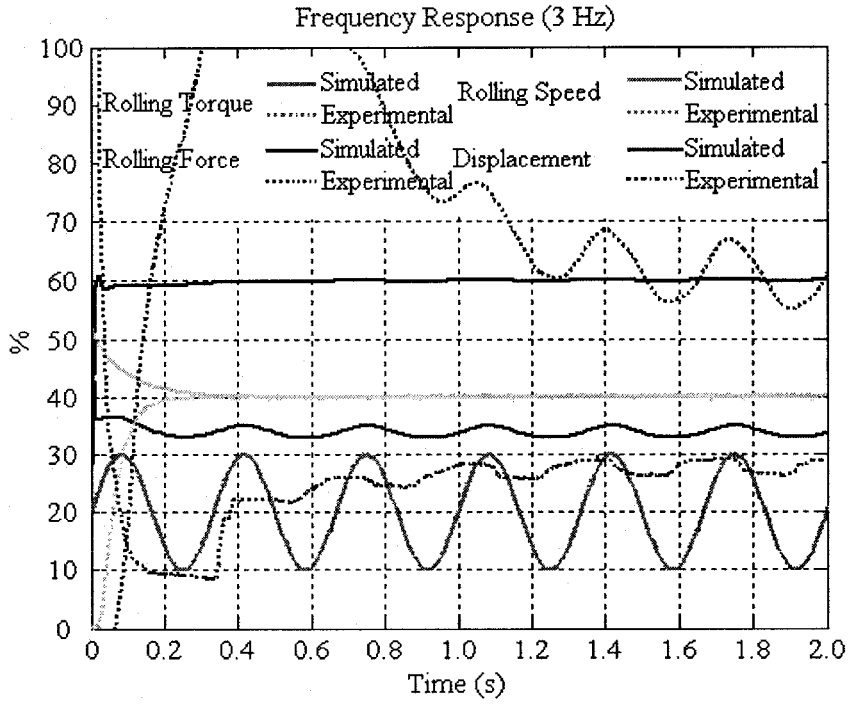

Figure 4.29 Measured frequency response as compared with the simulation result (3 Hz)

CHAPTER 5

CONCLUSIONS AND SUGGESTIONS FOR FUTURE WORK

Mathematical models have been developed to describe the performance of the swash plate axial piston pump with a conical cylinder block and the pressure compensator. These models have been utilized to simulate both the static and dynamic performance of the electro-hydraulic control system. The models have been validated on the basis of the satisfactory agreement between the simulation and experimentally measured results. In the following, a brief review of the study is given along with conclusions based on the results of the study.

5.1 Conclusions

This study is concerned with the development of an electro-hydraulic control system in order to control both rolling speed and rolling load with minimum number of components.

To start with, the classification of rolling mills and the brief description of the rolling process are rendered in order to know the basic concepts and principle of metal forming; in addition, the survey of the previous work is given in order to understand the previous achievements and to determine the objective of this research. Because the swash plate axial piston variable pump and the pressure compensator are the vital

components in this research, the mathematical models of the variable pump and pressure compensator are constructed; and then simulation programs based on Matlab-Simulink are developed to simulate both the static and the dynamic characteristics of the pump and the compensator.

As shown in Figure 3.8, the single negative feedback control scheme has been used to study the both static and dynamic characteristics of the pressure compensator. The simulation results show that the compensator has perfect linearity along the full range of the command signal.

The pump performance has been simulated using two control schemes as shown in Figure 3.20 and 3.21; the first one is a double negative feedback control loops and the other is a single negative feedback control loop.

The simulation results for the double feedback control loops reveal that the transient period has a nearly 80 ms settling time when the swiveling angle is increasing and 60 ms when the swiveling angle is decreasing. Both cases experience a 10 ms delay time. The results also show that the settling time is reduced on account of having a steady state swiveling angle vibration; in addition, the magnitude of the vibration is reduced to 1% instead of 3%.

Regarding the single feedback control loop, the simulation results indicate that the settling time is 200 ms, which is longer than that in double feedback control loops, and hence this control scheme is inconvenient for the constant power operation of the pump. On the other hand, this can be regarded as an advantage when the control

piston reaches the end of its stroke with nearly zero velocity, which reduces the impact on the piston.

Metal forming and rolling mills are highly dependent on the hydraulic power; in addition, in the rolling mills intermediate stages, both rolling speed and rolling load must be controlled. Consequently, an electro-hydraulic control system has been proposed and the modeling of the control system is built. The entire electrical control system is composed of two interacting control schemes. First one is to control the rolling speed and the other is to control the rolling load; each of them consists of double negative feedback control loops with PID or PD controllers. The simulation programs based on Matlab-Simulink are developed to simulate both the static and the dynamic characteristics of the control system. From the simulation results, the following characteristic features of the rolling mills can be obtained.

(i) With the assumption of constant internal leakage of the variable displacement pump and the hydraulic motor, the rolling speed is not affected by the change in the rolling torque.

(ii) In the view of static performance, rolling load is kept constant whenever the pressure difference across the compensator is more than 4% of the upstream pressure.

(iii) In the view of dynamic performance, rolling load experiences shocks at the transient periods of the stepwise change in the rolling torque.

(iv) The control system shows smooth controlling of both rolling speed and rolling load in accordance with the harmonic change of the rolling torque with specific harmonic fashion.

(v) Finally, an experimental setup composed of real time control software and a hydraulic test bed is constructed in order to validate the compensator mathematical model and verify the control system simulation modeling. The satisfactory agreement between the simulation and experimental results validates the model of the control system, which ensures that it can work properly. The maximum deviation is 5% at steady state, and the dynamic performance is not satisfied. However, we can improve it by increasing damping.

5.2 Main Contributions

The main contributions in this thesis is summarized as follows:

(i) The comprehensive mathematical models and simulation models for the pressure compensator and electro-hydraulic control system of rolling mill have been developed to investigate their static and dynamic performances.

(ii) The hydraulic test bed has been setup to validate the mathematical models and to verify the simulation results through the experiments.

(iii) In the proposed electro-hydraulic control system, the minimum hydraulic components have been employed, which would greatly reduce the cost.

(iv) The control system has very good flexibilities to various rolling mill requirements, and it is very convenient to adjust due to different variable load demands.

5.3 Suggestions for Future Work

Recommendations for future investigations are as follows.

(i) Reducing the transient period and putting an adequately sized accumulator on the upstream pressure line in order to minimize the rolling load shocks due to the stepwise change in the rolling torque.

(ii) In the present study, both rolling speed and rolling load reference values are assumed constant. In future investigations, different combinations of the working conditions must be assumed in order to study the capacity of the proposed control system to take care of various situations.

(iii) In the present work, the controllers used in the control system are PID or PD controllers. In the future study, fuzzy logic controllers can be used to develop the performances of the control system.

(iv) In the present research, the project is only concerned with the development of an electro-hydraulic control system in order to control both rolling speed and rolling load with minimum number of components. In future investigation,

we can study more applications of variable load than rolling mills, such as earth moving equipment, printing press, aerospace applications, etc.

(v) Forces and moments transmitted to bearing due to variable loads is another task for future work.

(vi) In the present work, the simulation results are represented by the graphics; in the future the simulation can use more efficient numerical solution schemes.

REFERENCES

[1] **S. Kalpakjian and S. R. Schmid, (2000),** *Manufacturing Engineering and Technology,* ISBN 0201361310, Prentice Hall.

[2] **W. L. Roberts, (1978),** *Cold Rolling Of Steel,* ISBN 0-8247-6780-2, Marcel Dekker, Inc., New York.

[3] **J. R. Nieb and V. T. Nicolas, (1991),** *Automated monitoring and control of vibration and chatter in rolling processes,* Iron and Steel Engineer, Vol. 68, No.7, pp. 33-42.

[4] **F. W. Paul, (1975),** *A mathematical model for evaluation of hydraulic controlled cold rolling mills,* Proceedings of 6th IFAC World Congr., pp. 53.4.1-53.4.9.

[5] **L. M. Pedersen, (1995),** *Modeling and identification of hot rolling mill,* Proceedings of American Control Conference, Vol. 5, pp. 3674–3678.

[6] **N. Venkata Reddy and G. Suryanarayana, (2001),** *A set-up model for tandem rolling mills,* Materials Processing Technology, Vol. 116, pp. 269-277.

[7] **V. B. Ginzburg, (1984),** *Dynamic characteristics of automatic control system with hydraulic actuators,* Iron and Steel Engineer, Vol. 61, No. 1, pp. 57-65.

[8] **R. M. Gou, (1991).** *Evaluation of dynamic characteristics of HAGC system, Iron* and Steel Engineer, Vol. 68, No. 7, pp. 52-61.

[9] **J. J. Ferguson** *et al,* **(1986).** *Modern hot-strip mill thickness control,* IEEE Transactions on Industry Applications, Vol. IA-22, No. 5, Sept./Oct., pp. 934-940.

[10] **H. Katori** *et al.* **(1992),** *Application of two-degree-of-freedom control system to automatic gauge control,* Proceedings of American Control Conference, pp. 806-810.

[11] **S. G. Choi, M. A. Johnson, and M. J. Grimble, (1994),** *Polynomial LQG control of back-up-roll eccentricity gauge variations in cold rolling mills,* Automatica, Vol. 30, No. 6, pp. 975–992.

[12] **L. M. Pedersen and B. Wittenmark, (1998),** *Multivariable Controller Design for a Hot Rolling Mill,* IEEE Transactions on Control Systems Technology, Vol. 6, No. 2, March, pp. 304-312.

[13] **M. J. Grimble and G. Hearns, (1998),** *LQG controllers for state-space systems with pure transport delays: Application to hot strip mills*, Automatica, Vol. 34, No. 10, pp. 1169–1184.

[14] **S. S. Garimella and K. (Cheena) Srinivasan, (1998),** *Application of Iterative Learning Control to Coil-to-Coil Control in Rolling,* IEEE Transactions on Control Systems Technology, Vol. 6, No. 2, March, pp. 281-293.

[15] **A. Kugi, W. Haas, K. Schlacher, A. Aistleitner, H. Frank, and G. W. Rigler, (2000),** *Active compensation of roll eccentricity in rolling mills,* IEEE Transactions on Industry Applications, Vol. 36, No. 2, Mar./Apr., pp. 625–632.

[16] **A. Kugi, K. Schlacher and R. Novak, (2001),** *Nonlinear Control in Rolling Mills: A New Perspective,* IEEE Transactions Industry Applications, Vol. 37, No. 5, Sept./Oct., pp. 1394-1402.

[17] **D. F. Zhu, A. M. Bai, C. B. Chen and Z. Zheng, (1992),** *Analysis on load condition of medium plate mill*, Iron and Steel (Peking), Vol. 27, n3, pp. 32-35.

[18] **K. Dasgupta, S. K. Mondal and A. Chattapadhyay, (2002),** *Modeling and dynamics of a load-sensing hydraulic system of heavy earth moving equipment*, Journal

of the Institution of Engineers (India): Mechanical Engineering Division, Vol. 83, n10, July, pp. 62-68.

[19] **B. Chen, Z. L. Wang, L. H. Qiu and B. J. Fei, (2000),** *General scheme of aircraft intelligent hydraulic pump system,* Beijing University of Aeronautics and Astronautics, Vol. 26, n 3, pp. 333-336.

[20] **M. K. Bahr, (2003),** *Performance Investigation of the Swash Plate Axial Piston Pumps With Conical Cylinder Block,* Ph.D. Thesis, Concordia University, Department of Mechanical & Industrial Engineering.

[21] **L. Meriovitch, (1970),** Methods *of analytical Dynamics,* McGraw-Hill.

[22] **P. Fitch, (2001),** *Hydraulic Components Design and Selection,* ISBN 0-9705922-3-X, Bardyne.

[23] **M. K. Bahr, V. Yurkevich, J. Svoboda and R. B. Bhat, (2002),** *Implementation of Single Feedback Control Loop for Constant Power Regulated Swash Plate Axial Piston Pumps,* International Journal of fluid Power, Vol. 3, No. 3, December 2002.

[24] **M. K. Bahr, J. Svoboda and R. B. Bhat, (2001),** *Response of Constant Power Regulated Swash Plate Axial Piston Pumps to Harmonic and Random Inputs,* Proceedings of the International Conference on Multidisciplinary Design in Engineering, CSME-MDE2001, Concordia University, Montreal, Canada.

[25] **M. K. Bahr, J. Svoboda and R. B. Bhat, (2002),** *Experimental Investigation On Swash Plate Axial Piston Pumps With Conical Cylinder Blocks Using Fuzzy Logic Control,* Proceedings of the International Mechanical Engineering Congress and Exposition ASME-ME2002, New Orleans, Louisiana, USA.

[26] **Rexroth Corporation, (1997).** *Electronic Control System for the Closed Loop Control of Variable Displacement Axial Piston Pumps Type A4VS with HS3 or HS Control,* Data Sheet RE 30 021/03.97.

[27] **R. Koziol and J. Sawicki, (1992),** *Some problems in analysis and synthesis of rolling mills control systems,* Materials Processing Technology, Vol. 34, pp. 541-545.

[28] **O. Wiklund, R. Korhonen, A. Nilsson and P. Sidestam, (2002),** *Hybrid modelling of the rolling force in a plate mill, Scandinavian* Journal of Metallurgy, Vol. 31, pp.153–160.

[29] **Y. Lee and B. Kim, (2002),** *Analytical model of pass-by-pass strain in bar rolling and its verification,* Scandinavian Journal of Metallurgy, Vol. 31, pp. 126–133.

[30] **K. Sawamiphakdi, P.M. Pauskar, D.Q. Jin and G.D. Lahoti, (2002),** *Ring rolling process modeling using explicit finite element analysis,* Advanced Technology of Plasticity, Vol. 1, pp. 859-863.

[31] **W. Y. D. Yuen, (2003),** *On-line and off-line models for the rolling process,* Scandinavian Journal of Metallurgy, Vol. 32, pp. 86–93.

[32] **J. Mischke and J. Jonca, (1992).** *Simulation of the roller straightening process,* Materials Processing Technology, Vol. 34, pp. 265-272.

[33] **P. Mäntylä, R. Korhonen and N-G Jonsson, (1992),** *Improved Thickness and Shape Accuracy with Advanced Pass Scheduling in Plate Rolling,* Materials Processing Technology, Vol. 34, pp. 255-263.

[34] **R. Dhaouadi et al, (1993),** *Two-degree-of –freedom robust speed controller for high-performance rolling mill drives,* IEEE Transactions on Industry Applications, Vol. 29, No. 5, Sept./Oct., pp. 919-925.

[35] **E. John M. Geddes and I. Postlethwaite, (1998),** *Improvements in product quality in tandem cold rolling using robust multivariable control,* IEEE Transactions on Control Systems Technology, Vol. 6, No. 2, March, pp. 257-269.

[36] **C. G. Haynes and J. S. Stancker, (1984),** *Optical measurement procedure to determine position of rolls and chocks in rolling mills*, Iron and Steel Engineer, Vol. 61, No. 1, pp. 35-38.

[37] **Z. Rdzawski and A. Sadkowski, (1992),** *New approach to developing a rolling technology*, Materials Processing Technology, Vol. 34, pp. 287-294.

[38] **W. L. Green and T. R. Crossley, (1971),** *An analysis of the Control Mechanism used in Variable Delivery Hydraulic Pump.* Proceedings of the Institution of the Mechanical Engineers, Vol. 185, pp. 63-72.

[39] **H. Zaki and A. Baz, (1979),** *On the Dynamics of Axial Piston Pumps*, Fluidic Quarterly, Vol. 11, No. 2, pp. 73-87.

[40] **A. Baz, (1983),** *Optimization of the Dynamics of Pressure-Compensated Axial Piston Pumps*, Journal of Fluid Control, Vol. 15, Issue 2, pp. 64-81.

[41] **Y. Atsushi, (1983),** *Cavitation in an Axial Piston Pump*, Bulletin of the JSME, Vol. 26, No. 211, pp. 72-78.

[42] **S. J. Lin, A. Akers and G. Zeiger, (1985),** *The Effect of Oil Entrapment in an Axial Piston Pumps.* Journal of Dynamic Systems, Measurement and Control, Vol. 107, pp. 246-251.

[43] **G. Zeiger and A. Akers, (1985),** *Torque on the Swash Plate of an Axial Piston Pump*, Journal of Dynamic Systems, Measurement and Control, Vol. 107, pp. 220-226.

[44] **G. Zeiger and A. Akers, (1986),** *Dynamic Analysis of an Axial Pump Swash Plate Control,* Proceedings of Institution of Mechanical Engineers, Vol. 200, No. C1, pp. 49-58.

[45] **K. A. Edge and J. Darling, (1986),** *Cylinder Pressure Transients in Oil Hydraulic Pumps with Sliding Plate Valves,* Proceedings of the Institution of Mechanical Engineers, Vol. 200, No. B1, pp. 45-54.

[46] **S. D. Kim, H. S. Cho and C. O. Lee, (1987),** *A Parameter Sensitivity Analysis for the Dynamic Model of d Variable Displacement Axial Piston Pump,* Proceedings of the Institution of Mechanical Engineers, Vol. 201, No. C4, pp. 235-243.

[47] **I. Kiyoshi and N. Masakasu, (1994),** *A Study of the Operating Moment of a Swash Plate Type Axial Piston Pump,* Journal of Fluid Control, Vol. 22, Issue 1, pp. 7-46.

[48] **A. Akers, and S. J. Lin, (1987),** *Control of an Axial Piston Pump Using Single-Stage Electro-hydraulic Servovalve,* Proceedings of American Control Conference, Vol. 3, pp. 1865-1870.

[49] **Z. You, (1989),** *Interactions Between Two Pressure Compensated Pumps in a Single Load Circuit,* Proceedings of the 2nd International Conference on Fluid Power Transmission and Control, China, pp. 569-571.

[50] **Y. Z. Lu, and Z. N. Chen, (1989),** *Measurement and Simulation Model Study of Cylinder Pressure Transition in An Axial Piston Pump,* Proceedings of the 2nd International Conference on fluid Power Transmission and Control, China, pp. 471-476.

[51] **K. A. Edje and J. Darling, (1989),** *The Pumping Dynamics of Swash Plate Piston Pumps,* Journal of Dynamic System, Measurement and Control, Vol. 111, pp. 307-12.

[52] **G. J. Schoenau, R. T. Burton and G. P. Kavanagh, (1990),** *Dynamic Analysis of a Variable Displacement Pump,* Journal of Dynamic System, Measurement and Control, Vol. 112, pp. 122-132.

[53] **P. Kaliafetis and TH. Costopoulos, (1995),** *Modeling and Simulation of an Axial Piston Variable Displacement Pump with Pressure Control,* Mechanism and Machine Theory, Vol. 30, No. 4, pp. 599-612.

[54] **R. M. Harris, K. A. Edge and D. G. Tilley, (1994),** *The Suction Dynamics of Positive Displacement Axial Piston Pumps,* Journal of Dynamic Systems, Measurement and Control, Vol. 116, pp. 281-287.

[55] **N. D. Manring and R. E. Johnson, (1994),** *Swivel Torque within a Variable-Displacement Pump,* Proceedings of the 46th National Conference on Fluid Power, pp. 13-24.

[56] **R. B. Gregory, (1994),** *Pressure Compensated Pump Control for Forestry Logic Skidders,* Proceedings of the 46th National Conference on Fluid Power, pp. 25 - 32.

[57] **N. D. Manring and R. E. Johnson, (1996),** *Modeling and Designing a Variable-Displacement Open-Loop Pump*, Journal of Dynamic Systems, Measurement, and Control. Vol. 118, pp. 267-271.

[58] **N. D. Manring, (1998),** *The Torque on the Input Shaft of an Axial Piston Swash Plate Type Hydrostatic Pump,* Journal of Dynamic Systems, Measurement, and Control, Vol. 120, pp. 57-62.

[59] **L. Olems, (2000),** *Investigations of the Temperature Behavior of the Piston Cylinder Assembly in Axial Piston Pumps,* International Journal of Fluid Power, Vol. 1, pp. 27-38.

[60] **S. A. Kassem and M. K. Bahr, (2000),** *Effect of Port Plate Silencing Grooves on Performance of Swash Plate Axial Piston Pump,* Current Advances in Mechanical Design and Production, Pergamon Press, VII, pp. 139-148.

[61] **S. A. Kassem and M. K. Bahr, (2000),** *On the Dynamics of Swash Plate Axial Piston Pumps with Conical Cylinder Blocks*, Proceedings of the 6th Terminal Symposium on Fluid Control, Measurement and Visualization, Sherbrooke, Canada

[62] **X. Zhang, J. Cho, S. S. Nair and N. D. Manring, (2001),** *New Swash Plate Damping Model for Hydraulic Axial-Piston Pumps,* Journal of Dynamic Systems, Measurement and Control, Vol. 123, pp. 463-470.

[63] **N. D. Manring and Y. Zhang, (2001),** *The Improved Volumetric-Efficiency of an Axial-Piston Pump Utilizing a Trapped-Volume Design,* Journal of Dynamic Systems, Measurement and Control. Vol. 123, pp. 479-487.

[64] **N. D. Manring and F. A. Damtew, (2001),** *The Control Torque on the Swash Plate of an Axial-Piston Pump Utilizing Piston-Bore Springs,* Journal of Dynamic Systems, Measurement and Control. Vol. 123, pp. 471-78.

[65] **M. K. Bahr, J. Svoboda and R. B. Bhat, (2002),** *Dynamic Loads on the Drive Shaft Bearings of Swash Plate Axial Piston Pumps with Conical Cylinder Blocks*, Proceedings of the CSME Forum2002, Queen's University, Toronto. Canada.

[66] **W. L. Roberts, (1983),** *Hot Rolling Of Steel,* ISBN 0-8247-1345-1, Marcel Dekker, Inc., New York.

[67] **W. L. Roberts, (1988),** *Flat Processing of Steel,* ISBN 0-8247-7780-8, Marcel Dekker, Inc., New York.

[68] **H. E. Merritt, (1967),** *Hydraulic Control Systems,* ISBN 0 471 59617 5, John Willey & Sons, Inc., New York.

[69] **A. Esposito, (2000),** *Fluid Power with Application,* ISBN 0-13-060899-8, Prentice Hall.

[70] **C. T. Chen, (1993),** Analog *and Digital Control System Design: Transfer- Function, State-Space, and Algebraic Methods,* ISBN 0-03-094070-2, Saunders College Publishing.

[71] **C. M. Close, D. K. Frederick & J. C. Newell, (2002),** *Modeling and Analysis of Dynamics Systems (Third Edition),* ISBN 0-471-39442-4, John Willey & Sons, Inc., New York.

[72] **Rexroth Corporation, (2000).** *4/2 and 4/3 proportional directional valves directly controlled, with electrical position feedback Types 4WRE and 4WREE,* Data Sheet RE 29 061/09.00.

APPENDIX A

CONSTRUCTIONAL AND OPERATIONAL PARAMETERS OF THE TEST PUMP

Symbol	Description	Value	Unit
A_{cp}	Area of the control piston	$8.1x10^{-4}$	m^2
A_p	Piston cross-section area	$2.27x10^{-4}$	m^2
B	Effective bulk modulus	$1x10^9$	Pa
C_d	Coefficient of discharge	0.611	-
D_1/R_1	Pitch circle diameter/radius of the cylinders' arrangement at the base of the cylinder block	0.07175/0.0359	m
D_2/R_2	Pitch circle diameter/radius of the cylinders' arrangement at the top of the cylinder block	0.0602/0.0301	m
f_v	Proportional valve viscous friction coefficient	90	N.s/m
f_α	Equivalent angular viscous friction coefficient	1.5	Nm/(rad/s)
I_e	Equivalent moment of inertia of the swash plate	0.0039	$kg.m^2$
k_i	Proportional solenoid force-current constant	2.5	N/A

k_v	Proportional valve spring stiffness	20000	N/m
k_α	Equivalent viscous friction coefficient of the swash plate	72	Nm/rad
L_1/L_2	Lengths, referred in Fig. 2.2	0.0766/0.0661	m
L_c	Cylinder length	0.0573	m
L_p	Piston length	0.0591	m
m_p	Piston mass	0.118	kg
m_v	Proportional valve spool mass	0.1	kg
N	Number of pistons	9	-
p_s	Pump suction pressure	$0.05x10^5$	Pa
p_T	Tank line pressure	$1x10^5$	Pa
R_L	Leakage resistance	$1x10^{13}$	$Pa/(m^3/s)$
r_s	Radius of swash plate swinging	0.055	m
$s_{v(max)}$	Proportional valve spool displacement (maximum)	(0.001)	m
V_{ci}	Initial control volume	$13x10^{-6}$	m^3
V_o	Additional piston chamber volume	$1x10^{-6}$	m^3
w	Proportional valve area factor	$4.8x10^{-3}$	m
$x_{cp(min, max)}$	Control piston displacement (minimum, maximum)	(0, 0.015)	m
β	Cylinder block cone angle	5	deg
ρ	Oil density	850	kg/m^3

APPENDIX B

M-FILE FOR THE SIMULATION OF THE ELECTRO-HYDRAULIC CONTROL SYSTEM

```
** Dynamic Model for Variable Displacement Pump model A4VSO40 **
********** Operational parameters **********
n=1500      RPM
********** Kinematical parameters **********
thodeg=0
********** Constructional parameters **********
R1=35.875      mm
R2=30.1        mm
L1=76.6        mm
L2=66.1        mm
Lp=59.1        mm
dp=17          mm
Lc=57.3        mm
k=1
z=9
mp=0.118       kg
Vo=1e-6        m^3
********** Oil parameters **********
density=850    kg/m^3
```

B=1.3e+9 Pa

********** Hydraulic parameters *********

cd=0.611

cdth=0.611

Ps=0.05e+5 Pa

RL=1e+13 Pa/(m^3/s)

********** Numerical **********

dtor=pi/180

rtod=180/pi

********** Parameters for control Piston **********

Rs=0.055 m

kcp=24e+3 N/m

Acp=8.1e-4 m^2

%Xcmin=0.0008 m

Xcmin=0

Xcmax=. 015 m

mr=2 kg

fcp=20 N.s/m

********** Proportional Valve **********

Xpvmax=1e-3 m

Pt=1e5 Pa

Vci=12.3e-6 m^3

Wov=4.8e-3 m

RLcp=1e+13 Pa/(m^3/s)

mv=0.1 kg

kv=20000 N/m

fv=10 N.s/m must be changed to be 90

ki=4.5 N/A

********** Pump **********

Vgmax=40 cc

********** Proportional Throttle **********

m=0.1; mass of the spool(kg)

x0=0.001; width of overlap(m)

Pt=100000; pressure after the port B(Pa)

Ro=900; mass density (kg/m^3)

V=0.0004; volume of the control oil(m^3)

B=1.3e9; bulk modulus(Pa)

Qs=60; flowrate(l/min)

Af=0.02; area constant

Cd=0.611; discharge coefficient

ki=5.3; current constant(N/Amp)

ks=4000; spring stiffness(N/m)

f=48; viscous constant

status = fclose('all')